Role of TLR2 in immune sensing of gut microbiota in RNA virus induced glomerulonephritis

Doctoral thesis

to obtain a doctorate (PhD)

from the Faculty of Medicine

of the University of Bonn

Sümeyye Ertugrul

Aydin, Turkey

Bonn, 2024

Written with authorization of

the Faculty of Medicine of the University of Bonn

First reviewer: Prof. Dr. Christian Kurts

Second reviewer: Prof. Dr. Jürgen Ruland

Day of oral examination: 03.05.2024

From the Institute of Molecular Medicine and Experimental Immunology

Director: Prof. Dr. Christian Kurts

Table of contents

List of abbreviations

Ab	Antibody
Acc	Acceleration
ACK	Ammonium–chloride–potassium
ANOVA	Analysis Of Variance
BCR	B cell receptor
BL6	C57BL6/J
BM	Bone marrow
bp	base pair
BUN	Blood urea nitrogen
cfDNA	circulating free DNA
citH3	citrulinated histon 3
CKD	Chronic kidney disease
DAPI	4',6-diamidino-2-phenylindole
DC	Dendritic cell
dCT	delta cycle threshold
ddCT	delta delta CT
ddH2O	deionized distilled water
Dec	deceleration
DEPC	Diethylpyrocarbonate
EDTA	Ethylenediaminetetraacetic acid
ELISA	Enzyme-linked immunosorbent assay
ELISPOT	Enzyme-linked immunosorbent spot
FABP2	Fatty Acid Binding Protein 2
FACS	Fluorescence-activated cell sorting
FCS	Fetal Calf Serum
GN	Gleoumerulinephrithis
HIV	Human Immunodeficiency Virus

i.v.	intra venous
Ig	Immunoglobulin
IL	Interleukin
KC	Kupffer Cell
KO	Knock out
LAL	limulus amoebocyte lysate
LBP	Lipopolysaccharide binding protein
LCMV	Lymphocytic choriomeningitis virus
LPS	Lipopolysaccharides
MPO	Myeloperoxidase
NFDM	Non-fat dry milk
O.D.	optical density
P/S	Penicillin/Streptomycin
PBS	Phosphate-buffered saline
PC	Plasma cell
PFA	Paraformaldehyde
PFU	plaque-forming unit
rpm	Revolutions per minute
RT	Room Temperature
RT-PCR	Reverse transcription polymerase chain reaction
s.c.	Subcutaneous
SA	strepdeavidin
sAb	Secondary antibody
TLRs	Toll-like receptors
Treg	Regulatory T cell
U/ml	Unit/mililiter
UI	Uninfected

1. Introduction

1.1 The immune system

The immune system serves as a sophisticated defense network comprising cells and coordinated processes to protect our body, including skin, respiratory passages and intestinal tract from infections and diseases. Our immune system can be categorized into two major groups: the innate and adaptive immunity. Innate immunity acts as an initial barrier against invading pathogens, responding rapidly without immunologic memory. It plays a vital role in attracting immune cells to the infection sites through the production of cytokines and chemokines. Adaptive immunity is reliant on specific antigens, involving a lengthier timeframe between exposure and a full-scale of response to generate immunological memory (Marshall et al., 2018). These two immune systems work together in harmony despite their distinct mechanisms. Any malfunction within these systems can result in inappropriate responses potentially leading to auto-inflammatory and autoimmune diseases.

1.1.1 Innate immunity

The innate immune system is composed of diverse types of immune cells, which recognizes a limited number of microorganisms via germline-encoded pattern-recognition receptors (PRRs). These PRRs can distinguish specific molecular markers on microbes, known as pathogen-associated molecular patterns (PAMPs) and also detect molecules released by damaged cells, referred as damage-associated molecules patterns (DAMPs) (Vivier and Malissen, 2005). Upon activation of these PRRs, a cascade of signaling molecules is triggered, including chemokines, pro-inflammatory cytokines and type I and type III interferons (IFNs). These interferons are closely associated stimulated genes (ISGs) and serve as direct defenses against viral infections. It is worth noting that the responses initiated by these mechanisms can vary across different cell types and are not limited to specific cellular lineages (Vivier and Malissen, 2005). The innate immune system includes a diverse array of immune cells including, phagocytic cells like neutrophils and

macrophages, dendritic cells (DCs), mast cells, basophils, eosinophils, natural killer (NK) cells and innate lymphoid cells (ILCs). Neutrophils, despite their short life, possess granules enzymatic pathways that contribute to the elimination of harmful microbes. In contrast, macrophages as long-lived cells, are not only engaged in phagocytosis but also play a pivotal role in presenting antigens to T cells (Turvey and Broide, 2010). DCs, in addition to phagocytotic functions, serve as antigen presenting cells (APCs), initiating the transition between innate and adaptive immunity. Natural killer (NK) cells play a major role in the rejection of tumours and elimination of virus infected cells. On the other hand, eosinophils combat larger parasites. And mast cells and basophils share essential features with each other, and are fundamental in initiating acute inflammatory responses, particularly in the context of allergy and asthma (Marshall et al., 2018).

Mammals possess a variety of distinct classes of PRRs which include Toll-like receptors (TLRs), RIG-I-like receptors (RLRs), Nodlike receptors (NLRs), AIM2-like receptors (ALRs), C-type lectin receptors (CLRs), and intracellular DNA sensors such as cGAS (Akira et al., 2006; Cai et al., 2014).

1.1.1.1 Toll-like receptors

Toll-like receptors (TLR) have an essential role in innate immunity during host defense by recognizing pathogen-associated molecular patterns derived from various microbes. They are expressed in innate immune cells like DCs and macrophages but also non-immune cells like epithelial cells and fibroblast cells. TLRs are a type of integral membrane glycoproteins with specific structural features. They possess extracellular domains that contain varying numbers of leucine-rich-repeat (LRR) motifs and they have a cytoplasmic signalling domain that is similar to the interleukin 1 receptor (IL-1R). This signalling domain known as Toll/IL-1R homology (TIR) domain (Bowie and O'Neill, 2000). When cells are exposed to TLR activator, they enlist an adaptor protein that possess a TIR domain, like myeloid differentiation factor 88 (MyD88). This adaptor protein is brough to the inner part of the TLR within the cell through a self-interaction of their TIR domains resulting in the generation of proinflammatory cytokines and chemokines (Akira et al., 2006).

TLRs can be classified mainly 2 subgroups based on their localization in cell surface TLRs and intracellular TLRs. Cell surface TLRs includes, TLR1, TLR2, TLR4, TLR5, TLR6 and TLR10 whereas intracellular TLRs are localized in the endosome and include TLR3, TLR7, TLR8, TLR9, TLR11, TLR12 and TLR13.

1.1.1.1.1 TLR2

TLR2 exhibits flexibility in forming heterodimers either with TLR1 or TLR6 depending on the specific molecule it encounters, which could be either triacyl and diacyl lipoproteins (Takeuchi and Akira, 2010). TLR2 functions as a versatile sensor, capable of detecting broad spectrum of PAMPs. These include lipoproteins, peptidoglycans, lipotechoic acids, zymosan, mannan, and tGPI-mucin. Furthermore, researchers have identified TLR2 endogenous ligands, known as “alarmins” such as heat shock proteins, human β-defensin-3, hyaluronan fragments and high mobility group box 1 (HMGB1) (Oliveira-Nascimento et al., 2012). The primary ligands for TLR2 that have been identified are lipoproteins. These lipoproteins are present in all bacteria and are prominently found in the outer membrane of Gram-positive bacteria. They have distinctive NH3-terminal lipo-amino acid, *N*-acyl-*S*-diacylglycerol cysteine and typically consist of three lipid chains (triacyl). However, in mycobacteria they can have two lipid chains (diacyl) (Babu et al., 2006). Regardless which of the two dimers is activated, the classical signaling pathway that is initiated remains the same (Farhat et al., 2008). After being stimulated by a ligand, TLR2 heterodimers generally kickstart an intracellular signaling pathway that relies on Myd88, the common feature shared by TLRs except TLR3. This pathway leads to the translocation of nuclear factor-B (NF-B) into the nucleus, where it regulates gene transcription. This results in the production of inflammatory cytokines such as IL1-β, IL-6, IL-8, IL-12, IL-17, TNF-α, IFN-γ, iNOS and ICAM-1.

The role of TLR2 has been investigated in various contexts, like infectious diseases, cancer or autoimmunity (Liu et al., 2014). The intricate interplay between the host immune system and invading microbes involves complex molecular and cellular mechanisms. Understanding of these interactions and their consequences is essential for developing effective strategies to combat infections.

1.1.1.1.2 TLR4

TLR4 recognizes different ligands such as, lipopolysaccharide (LPS), Taxol, viral glycoproteins, rSV fusion protein, as well as endogenous ligands like, necrotic cells, heat shock proteins, fibronectin, extracellular cell matrix (ECM) components, fatty acid, minimally oxidized low-density lipoprotein (mmLDL) and fibrogen together with myeloid differentiation factor (MD2) (Liu et al., 2014; Takeuchi and Akira, 2010). In the bloodstream, LPS initially forms a complex with LPS binding protein (LBP), which then facilitates the transfer of LPS to CD14. This binding process of LPS also requires the MD-2 protein, which interacts with the extracellular domain of TLR4 (Vaure and Liu, 2014). Upon attachment of a ligand to TLR4 at the cell surface, TLR4 receptors undergo homodimerization, wherein they pair up through within their intracellular TIR-domains. This molecular rearrangement leads to structural alterations in the TLR4 receptor. TLR4 initiates intracellular signaling by at least two significant pathways: first; there is the TIRAP–MyD88 pathway, responsible for orchestrating the early activation of NF-kB and production of inflammatory cytokines, including IL-12; and second; TRIF-TRAM pathway initiate and trigger the production of type I interferons (IFNs) and co-stimulatory molecules via interferon regulatory factor-3 (IRF3) transcription factor (Vaure and Liu, 2014). This complex process is observed not only in humans, but also in mice, as TLR4 expressed in various immune cells, such as monocytes, macrophages, microglia, myeloid DCs, granulocytes, naïve B cell and freshly isolated T cells.

1.1.1.1.3 TLR9

TLR9 localizes to the endosomal compartment, like TLR7, where it senses, unmethylated DNA with CpG motifs, indicative of DNA viruses such as HSV, MCMV, HCMV, pox viruses and HIV. In addition to the detection of DNA viruses, it was recently shown that TLR9 also has a role in the detection of RNA viruses such as dengue virus (DV). This is due to the release of mitochondrial DNA (mtDNA) from infected human DCs (Lai et al., 2018). And this recognition leads to activation of TBK1-IRF3 dependent pathway (Ishii et al., 2008). However, endogenous TLR9 ligands also exist such as, hypomethylated self-DNA within immune complexes, neutrophil extracellular traps, oxidized mitochondrial nucleoids or

other chromatin formats (Devarapu and Anders, 2018). TLR9 ligation is followed by type I IFN production by pDCs together with TLR7 (Kato et al., 2005).

1.1.1.2 cGAS/STING pathway

Cyclic GMP–AMP synthase (cGAS) has been proposed to function in the cytosol, although some studies suggested that, cGAS can be localized in both the nucleus and at the plasma membrane depending on certain contexts. Cytosolic cGAS is activated by foreign or self-DNA that gains access to this compartment and mediated by the downstream adaptor molecule stimulator of interferon genes (STING), which is an endoplasmic reticulum (ER)-localized adaptor (Motwani et al., 2019). Active cGAS converts GTP and ATP into cGAMP which is endogenous second messenger that binds to STING to form dimers, tetramers and higher-order oligomers. Upon activation STING translocates from ER to Golgi where it recruits kinases such as TANK- binding kinase 1 (TBK1) and IκB kinase (IKK), which phosphorylate interferon regulatory factor 3 (IRF3) and the nuclear factor-κB (NF-κB) inhibitor IκBα, respectively. Although any DNA, foreign or self, can cause cGAS activation, the length of the DNA is important (Motwani et al., 2019). Short DNAs of 20 bp can bind to cGAS, but longer dsDNA of >45 bp can form more stable ladder-like networks of cGAS dimers (Luecke et al., 2017). On the other hand, STING can be activated by cyclic dinucleotides, produced by bacteria directly, or viral liposomes independent of cGAS. But in general, cGAMP is thought to bind with higher affinity to STING than to bacterial cyclic dinucleotides, which suggest that STING is more strongly activated when the cGAS receptor is engaged (Motwani et al., 2019).

1.1.2 Adaptive immunity and role of B cells

The evolution of adaptive immunity is intricately tied to the functioning of innate immune system. When innate immune system proves inadequate in eradicating an infectious agent, adaptive immunity steps in to orchestrate highly specific responses. This type of immunity relies on specific antigens and memory capabilities, enabling the host to mount a rapid and more effective immune response upon subsequent encounters with the same

antigen (Marshall et al., 2018). This memory forms the foundation for immunity and is the fundamental principle of how vaccines function. The adaptive immune system comprises specialized cells, such as antigen-specific T cells, which activate and multiply under the influence of APCs. Upon contact to antigen, B cells undergo a process of differentiation, transforming into antibody-secreting plasma cells that are responsible for generating antibodies (Marshall et al., 2018). In essence, the collaboration of adaptive and innate immunity is paramount in combating infectious and provide long-term immunity.

B cells play a critical role in the adaptive immune system by differentiation into short-lived or long-lived plasma upon antigen encounter. Moreover, they contribute to the development of secondary and tertiary lymphoid tissues. The maturation of B cells is a multistep process. B cells originate from hematopoietic stem cells (HSCs) in the bone marrow (BM) or fetal liver. During B cell maturation, the B cell receptor (BCR) is created through intricate genomic rearrangements known as V(D)J recombination at the IgH and IgL loci. Immature or transitional B cells display distinct characteristics, such as $IgM^{+}CD24^{hi}CD38^{hi}$ expression in human and $IgM^{+}CD93^{+}IgD^{+}$ expression in mice. After their BCRs are correctly assembled, these cells complete their maturation by migrating to the spleen, where they can differentiate into naïve B cell subsets, including naïve, follicular or marginal zone (MZ) B cells. Notably, naïve follicular B cells can be identified by their $IgM^{+}GL7^{-}IgD^{+}CD138^{-}$ expression, while MZ B cells in mice characterized by $IgM^{+}CD93^{-}IgD^{low}CD23^{-}$ expression (Schultheiß et al., 2022).

Based on their phenotypic features, these mature B cells can then circulate in the blood and lymph vessels or populate the secondary lymphoid organs like spleen, lymph nodes, tonsils and Peyer’s patches ready for detection of antigens. Upon antigen encounter, activated B cells can rapidly expand in an extrafollicular response into short-lived plasmablasts (PB) or into germinal center (GC) B cells. While plasmablasts rapidly produce and secrete antibodies, GC B cells undergo affinity maturation. The germinal center reaction is a T cell-assisted BCR diversification process, which facilitates class-switch recombination (CSR) and increase of the BCR affinity via introduction of random point mutations (somatic hyper mutation, SHM) mediated by the enzyme AID. GC B cells

then differentiate into antibody-secreting plasma cells which can become long-lived or memory B cells (Oleinika et al., 2019; Sanz et al., 2019).

Plasma cells (PC) are long-lived, terminally differentiated, antibody-producing cells and characterized by $CD19^{+}CD138^{+}CD38^{low}CD98^{+}BLIMP1^{hi}$ expression in mouse. While plasmablasts are the short-lived proliferating counterparts of plasma cells and characterized by $CD19^{+}CD138^{low}CD38^{low}CD98^{+}BLIMP1^{int}$ expression in mouse (Delaloy et al., 2022; Oracki et al., 2010). These two cell types are collectively referred to as antibody-secreting cells (ASCs). Plasma cells home to the bone marrow, where they continuously produce antibodies to provide immediate protection to the host upon re-infection. Memory B cells are characterized by $CD19^{+}CD138^{-}CD38^{+/-}IgM^{-}$ expression in mouse and lose their IgM expression once they class switched to IgG or IgA. They can recirculate and after contact to antigen, they can be rapidly induced to differentiate into antibody-producing plasmablasts through interaction with cognate T cells. This memory response is typically more robust than the primary B cell response to antigen and generates high affinity, class-switched immunoglobulins (Mesin et al., 2016). This phenomenon plays a crucial in the effectiveness of vaccine strategies capitalize on long-lived memory B cell responses, and most successful vaccines rely on the mounting of a long-lasting protective antibody response (Plotkin, 2010).

1.2 Cell death types: Role of NETosis

Cell death is a fundamental biological process that plays a crucial role in maintain the overall balance within an organism by removing damaged or dysfunctional cells. It represents an irreversible outcome in the life of a cell, marking its final state. Cell death can be broadly classified into two main categories: programmed cell death (PCD) or non-PCD based on their reliance on specific cellular signals (Shen et al., 2023; Yan et al., 2020). PCD, is driven by intricate intracellular signaling pathways whereas non-PCD typically results from unexpected cellular injuries. Within PCD, there are further distinctions, notably apoptotic and non-apoptotic cell death. Apoptosis and anoikis are the examples for apoptotic cell death characterized by controlled cell membrane rupture and reliance on caspase-dependent mechanisms. In contrast, non-apoptotic cell death

involves caspase-independent membrane rupture and encompasses various mechanisms and phenotypes including, vacuole-presenting cell death (autophagy, entosis, methuosis and paraptosis), mitochondrial-dependent cell death (mitoptosis and parthanatos), iron-dependent cell death (ferroptosis), immune-reactive cell death (pyroptosis and NETosis), as well as other types, such as necroptosis. Additionally, necrosis represents a type of non-PCD.

In response to physiological or pathological signals, cells employ different types of cell death to uphold the host organisms normal functioning. Autophagy typically precedes apoptosis and can trigger a cascade of events. When apoptotic cells are not cleared in time, it will lead to programmed cell necrosis or cell necrosis (Shen et al., 2023). These various cell death processes can interact through the interconnected or overlapped signaling pathways, closely linked to the development of various diseases.

NETosis is non-apoptotic immune-reactive cell death type that is initiated by the pathogens or their components and mostly occurs in immune cells, like neutrophils. Once neutrophils recognize the pathogen, they undergo histone modification, chromatin recondensation and neutrophil extracellular traps (NETs) release and eventually leads to cell death. NETs contain initially 24 different proteins but subsequent studies have extended this list, suggesting that the composition of NETs varies depending on the stimulus (Papayannopoulos, 2018). Some of the proteins that are induced in NETs are, myeloperoxidase (MPO), neutrophil elastase (NE), cathepsin G, lysozyme and defensins (Klopf et al., 2021). NETs form via two pathways. The first is a cell death pathway termed NETosis that begins with nuclear delobulation and the disassembly of the nuclear envelope and continues with loss of cellular polarization, chromatin decondensation and plasma membrane rupture. The second is a non-lytic form of NETosis that can occur independently of cell death and involves the secreted expulsion of nuclear chromatin that is accompanied by the release of granule proteins through degranulation. These components assemble extracellularly and leave behind active anucleated cytoplasts that continue to ingest microorganisms (Papayannopoulos, 2018).

NETs are also associated with different diseases. Since neutrophils are the central cells of non-specific, innate immunity and they can actively fight against infection, their role in different disease conditions is crucially important. Cardiovascular diseases, viral infections, autoimmune diseases, metabolic diseases and cancer are the examples of the contribution of NETs. For instance, MPO-DNA complexes, citrullinated histones and neutrophil elastase are features of several systemic autoimmune diseases like SLE. Studies showed that, oxidized mitochondrial DNA (mtDNA) that is present in NETs and plasmcytoid dendritic cells (pDCs), contributes essentially to the dysregulation of interferon α, is critical in SLE patients (Lood et al., 2016; Wang et al., 2015). In case of rheumatoid arthritis, anti-citrullinated protein antibodies (ACPAs) are formed, which correlate with the activity of NETosis and neutrophil count. Taken together, NETs represent an important target for therapeutics.

1.3 Infections

Infections are environmental factors that can be caused by viruses, bacteria, parasites or other infectious agents (Jara et al., 2018). The invasion of human body with infectious pathogens, can affect different parts of the immune system.

1.3.1 Viral infections

Viral infections are classified as acute viral infections and chronic viral infections. Acute infections are unbalanced processes during which the host and virus change actively until the infection is resolved, the host is killed or the infection become chronic. Chronic infections are, dynamic processes in which virus and host balance each other and maintaining the chronic infection without killing the host (Carty et al., 2021; Virgin et al., 2009).

Chronic viral infections are characterized by three strategies: 1) continuous replication, 2) latency and reactivation and 3) invasion of the genome followed by vertical spread from generation to generation (Virgin et al., 2009). Some viruses rely on only one of these strategies but most of the viruses use more than one mechanism. For instance, human

immunodeficiency virus (HIV), hepatitis B virus (HBV) and hepatitis C virus (HCV) in humans, simian immunodeficiency virus (SIV) in nonhuman primates and lymphocytic choriomeningitis (LCMV) in mice use the first strategy. They replicate continuously despite ongoing antiviral immunity (Virgin et al., 2009). Epstein-Barr virus (EBV) utilizes three different latency gene expression programs and papillomaviruses latently infect epithelial stem cells and initiate different viral transcriptional programs. Moreover, mammalian genomes are chronically infected by a huge number of endogenous retroviral elements (ERVs) that spread vertically from one host generation to another. They have two effects on the immune system. First, they can encode for B or T cell antigens (Levisetti, 2003; Wang-Johanning et al., 2008) and second, ERV-encoded superantigens can shape the T cell repertoire (Meylan et al., 2005; Sutkowski et al., 2001).

Like mentioned above, some viruses can use multiple strategies to survive in host. One of the well-known examples of this group is the HIV infection. HIV effectively utilizes both continuous replication and establishment of latency and is able to survive in memory CD4 T cells in the proviral state without expressing any proteins that can be recognized by the immune system (Chun et al., 1997).

1.3.2 HIV and LCMV infections

HIV, a type of lentivirus can be subdivided into two groups HIV-1 and HIV-2 based on genetic variations (International Agency for Research on Cancer, 1996). It is characterized as a single-stranded RNA virus and its genetic material also known as proviral DNA, is formed through the reverse transcription of the viral RNA genome into DNA. This process involves the degradation of the RNA and the integration of double-stranded HIV DNA into the human genome (German Advisory Committee Blood (Arbeitskreis Blut), Subgroup ‘Assessment of Pathogens Transmissible by Blood’, 2016). HIV possesses structural proteins such as glycoproteins gp120 (surface protein SU) and gp41 (transmembrane protein, TM), along with regulatory proteins like Tat (transactivator protein), Rev (RNA splicing-regulator), Nef (negative regulating factor), Vpu (virus protein unique) and Vif (viral infectivity factor) (Sauter et al., 2012). Tat and Rev proteins play a crucial role in

initiating of HIV replication while other regulatory proteins like Nef, Vpu and Vif impact viral replication, virus budding and pathogenesis.

HIV can enter the body through intact mucosal membranes, injured skin, parenteral inoculation or even via breast milk (McIntyre, 2002). In case of sexual transmission, HIV attaches first dendritic cells (DCs) or monocytes/macrophages (German Advisory Committee Blood (Arbeitskreis Blut), Subgroup 'Assessment of Pathogens Transmissible by Blood', 2016). Furthermore, it targets CD4 T cells by interacting with surface glycoproteins and employs the coreceptors CCR5 and CXCR4 to gain entry into the cells (Altfeld and Gale Jr, 2015). Once inside the cell, the viral RNA undergoes reverse transcription mediated by a viral capsid (CA) associated reverse transcriptase, forming a cDNA copy. This cDNA copy integrates into the host cell's DNA, creating "provirus" dsDNA containing the HIV genome. The HIV enzyme integrase assists in this integration into host cell chromosome. Following integration, the proviral DNA is transcribed by the host RNA pol II, leading to the expression of HIV proteins. These viral proteins accumulate, are assembled and the two copies of HIV genome are packaged. Finally, HIV is released from the infected cell by budding from the plasma membrane (German Advisory Committee Blood (Arbeitskreis Blut), Subgroup 'Assessment of Pathogens Transmissible by Blood', 2016). This process is vital for HIV replication and its spread within the human body.

Global update on HIV showed that today, there are 39 million people living with HIV. 29,8 million of these infected individuals received life-saving treatment. By 2025, access to antiretroviral therapy is planned to expand 35 million people (World Health Organization (WHO), 2023, HIV and AIDS https://www.who.int/news-room/fact-sheets/detail/hiv-aids). In 2022, 630.000 people died from HIV-related causes and 1,3 million acquired HIV. Although combined antiretroviral therapy (cART) therapy helps the patients to suppress the viral load and to achieve manageable health conditions, there is no cure for HIV infection. Infected patients suffer from various diseases including, liver, cardiovascular and/or kidney diseases although they have been treated with cART (Fernando et al., 2008). Therefore, current research will help to move forward this field and will contribute to the development of new treatment avenues for especially patients with kidney diseases.

LCMV, a RNA virus like HIV and HCV and it is a member of the arenaviridae family that is carried and transmitted by mice. Humans can get infected with LCMV when they get in contact with the secretions of infected house mice (Zinkernagel et al., 2009). LCMV first isolated by Armstrong and Lillie in 1933 from cerebrospinal fluid of a woman who was suffering from St. Louis encephalitis (Armstrong and Lillie, 1934). Since then, there were numerous cases reported with mild symptoms including headache, myalgia, fever, anorexia, nausea, malaise and vomiting or severe central nervous system (CNS) diseases, predominantly aseptic meningitis or meningoencephalitis. When the virus is acquired postnatally by children or adults, the clinical manifestations are usually those of aseptic meningitis (Bonthius, 2012). But if it occurs prenatally, much more severe disease ensues.

LCMV has different strains that show extensive diversity and different pathogenicity in humans and experimental animals. These strains have been isolated from infected humans, experimental models and natural rodent reservoirs (Albariño et al., 2010). For instance, the E350 strain was cloned from the original LCMV strain isolated by Armstrong and Lillie in 1933. This strain is characterized by intense lymphocytic infiltration induced in the meninges and eyes of infected experimental mice and monkeys (Armstrong and Lillie, 1934). The clone13 (C13) strain is similar to E350, differing in only a few amino acids that contains single point mutation in the viral polymerase. This mutation leads to strong binding of C13 to dendritic cells (DCs) and to increased intracellular replication. The WE2.2 strain is phylogenetically distant from the C13 and E350 strains with many more mutations. It is non-immunosuppressant and uses a different receptor than C13 (Zhou et al., 2012). The Armstrong strain shares 88 % amino acid homology with WE strain and differs from C13 by only 5 out of 10,600 nucleotides (Zhou et al., 2012). This difference in the viral polymerase and glycoprotein genes respectively accounted for the biological phenotype of acute versus persistent infection. This shows the importance of the glycoproteins in attachment to the host cells like in HIV. The concept that single amino acid changes in a pathogen that can dramatically alter the in vivo persistence of a virus was fist clarified using LCMV (Zhou et al., 2012) but also has been further studied in other fields like HIV, hepatitis E virus and potentially autoimmune diseases (Tishon et al., 1991).

Various studies showed that, infection with these different LCMV strains can induce different biological effects in several model systems. For example, the WE-54 strain of LCMV causes a fatal hepatitis in rhesus macaques, while the Armstrong strain causes no disease in these animals (Lukashevich et al., 2004). On the other hand E350 destroys liver cells of adult mice but does not kill guineapigs while WE2.2 causes no significant liver injury in adult mice but is highly lethal to guineapigs (Bonthius, 2012). WE and Armstrong strains exhibits slow or intermediate replication kinetics via potent cytotoxic T-lymphocytes (CTL) whereas the Docile strain of LCMV shows rapid replicating kinetics via exhausted $CD8^+$ T cells and therefore, persists in multiple tissues (Zinkernagel et al., 2009).

Furthermore, Oldstone and Dixon discovered the association between circulating antibodies to nuclear DNA, immune complexes against viral antigen or self-antigen and deposition of immune complexes in the kidney during LCMV infection (Hotchin, 1971; Zhou et al., 2012). The absence of circulating antibodies was due to their accumulation as immune complexes in the glomeruli.

1.3.3 HIV associated kidney diseases

Untreated HIV infection may advance to acquired immunodeficiency syndrome (AIDS). Despite the beneficial effect of cART on immune function in HIV patients, it is not able to fully restore the overall health of cART-treated patients. These individuals face an elevated risk of cardiovascular, liver, kidney, bone and neurologic diseases. Notably, even with cART, 10-15 % of infected patients experience renal diseases (Fernando et al., 2008). Some studies showed direct connection between virus and renal conditions by direct infection of podocytes and renal epithelial cells (Rosenberg et al., 2015) while other research highlights that certain HIV medications, like tenofovir and atazanavir, can also induce nephrotoxicity (Benveniste et al., 1999; Foy et al., 2013). The risk of acute or chronic kidney diseases in these patients remains elevated, leading to increased mortality (Nobakht et al., 2016). Therefore, further research is necessary to explore the link between HIV infection and glomerular disorders.

Kidneys play a vital role in blood filtration, maintaining body water balance, regulating blood pressure and eliminating metabolic waste products such as, toxins and drugs (Tecklenborg et al., 2018). Consequently, kidneys are crucial for immune homeostasis especially in the late stage of renal diseases. HIV infection is associated with a wide range of renal conditions, such as HIV-associated nephropathy (HIVAN), HIV-associated immune complex kidney disease (HIVICD) and other glomerulonephritides. These diseases can be differentiated through histopathologic analyses, but may exhibit overlapping clinical characteristics (Weiner et al., 2003). HIVAN is characterized by focal glomerular sclerosis, often of the collapsing variant, and microcystic tubule dilation. It primarily affects patients of African descent and is believed to result from genetic, environmental and host factors (Kimmel et al., 2003). HIVICD, on one hand, involves immune complex deposition, leading to diverse renal histopathologies, including IgA nephropathy, lupus-like glomerulonephritis, post-infectious glomerulonephritis (PIGN) and membranoproliferative glomerulonephritis (MPGN). Before the introduction of cART, focal glomerular sclerosis (FGS) or HIVAN was the prevalent diagnosis for kidney issues in HIV patients. Over the past three decades, there has been a noticeable shift in certain patient groups from FGS to HIVICD (Kimmel et al., 2003; Nobakht et al., 2016). Hence, it has become imperative to conduct renal biopsies to differentiate between HIVICD and other forms of HIV-associated kidney diseases in order to provide appropriate treatment to the patients.

1.4 Autoimmune diseases

Autoimmunity is a complex phenomenon characterized by the immune system’s failure to distinguish between self or foreign antigens, leading to an immune response against the host’s own tissues and antigens. Activation of self-reactive B and T cells can led to tissue injury and progress the autoimmunity into various disorders collectively known autoimmune diseases (Hussein and Rahal, 2019). Autoimmune diseases affect nearly 5 % of the population in the world mainly of women (Jara et al., 2018). The link between the real cause and the disease still remains unclear. But studies showed that the combination of multiple factors such as genetics, age, environment, infections as well as immune

system dysregulation are associated with development of autoimmune diseases. Especially viral infections including, Epstein-Barr virus (EBV), influenza A virus, hepatitis C or cytomegalovirus have been found to be associated with multiple autoimmune diseases such as, rheumatoid arthritis (RA), Sjogren syndrome, systemic lupus erythematosus (SLE) and type 1 diabetes (T1D) (Smatti et al., 2019). These infections trigger the immune system and lead to overwhelmed immune regulatory mechanisms in which viral components share similarities with the host's own proteins, leading to an immune response against both the virus and self-antigens (Hussein and Rahal, 2019). This reaction becomes the antigen source for the generation of autoantibodies (Caza et al., 2014).

Well studied autoimmune diseases are systemic lupus erythematosus (SLE), rheumatoid arthritis (RA), Sjogren's syndrome, Guillain-Barré syndrome (GBS), multiple sclerosis (MS), Grave's disease, still's disease, inflammatory bowel disease (IBD), Hashimoto's disease, and psoriasis. Different viruses and bacteria were found to be associated with different autoimmune diseases. For instance, infective endocarditis is related with RA or SLE with elevated levels of acute phase reactants, anemia and circulating immune complexes (CIC) whereas, EBV affects SLE with positive association of various autoantibodies such as, anti-nuclear antibodies (ANAs) or anti-EBV antibodies (Smatti et al., 2019). Some viruses have been detected as triggers for central nervous system (CNS) autoimmune disorders, including EBV, measles virus and human T cell leukemia virus type 1 (HTVL-1) (Jara et al., 2018). Zika virus (ZIKV) has been associated with the development of GBS (Monsalve et al., 2017) and Varicella zoster virus has also been associated with MS (Brooks, 2017).

SLE is characterized by the dysfunction of both, the innate and the adaptive immune systems, which results in the increase of cytokine production, apoptosis of circulating cells and defect of clearing apoptotic bodies as well as overproduction of autoantibodies reactive to dsDNA (Rojas et al., 2018). It is known that double stranded (ds) DNA and nucleosomes are key autoantigens in the pathogenesis of SLE (Amoura et al., 1997). Based on these findings, a correlation between dsDNA and disease activity was found that can be used for new interventions and diagnosis strategies (Pacheco et al., 2017).

Moreover, infections can stimulate pro-inflammatory cell death programs including pyroptosis and NETosis, induce extracellular release of host nuclear antigens, and promote their recognition by activating innate and adaptive immune system. Release of bacterial DNA upon infection, associated with other bacterial molecules and complexes that can elicit autoimmunity and activate autoreactive B cells through molecular mimicry.

HIV infection was also related to SLE or Grave's disease with elevated levels of autoantibodies such as anti-dsDNA, anti-Sm (Smith antigen) or ANAs. Although the coexistence of SLE and HIV is rare, since 1976 to date, 76 patients with SLE and HIV infection have been described and this coexistence is called lupus-like syndrome (Vega and Espinoza, 2018). It is clear that, various infections are associated with SLE. Therefore, it is important to understand the pathological mechanisms associated with disease development.

1.5 Microbiome

The human body hosts a vast community of bacteria with approximately 10^{14} microorganisms, known as the gut microbiome. These microorganisms reside in different areas, including the skin's surface, the gastrointestinal, genitourinary, and respiratory tracts. Notably, the intestinal tract boasts the highest number of taxonomic units and genetic contents with approximately ten times more bacteria than human cells in the body (Azad et al., 2013). The number of bacteria changes in different parts of the human body, density of each bacterium is also different from organ to organ. For instance, the jejunum/ileum and large intestine harbours higher densities of bacteria compared to stomach and duodenum while, the colon has the highest bacterial density. The bacteria present in colon are mainly anaerobes due to the low concentration of oxygen present there (Villanueva-Millán et al., 2015).

The human microbiota is primarily composed of four major groups:, Bacteroidetes Firmicutes, Proteobacteria, and Actinobacteria (Morgan et al., 2013). Each of these groups serves distinct functions and alterations within each group can lead to various

health complications. For instance, in HIV patients, depletion of Lachnospiraceae, Ruminococceae, Bacteroides, and Rikenellaceae result in (Vujkovic-Cvijin and Somsouk, 2019) loss of diversity and this cannot be remedied with cART therapy (Dubourg et al., 2016). Additionally, specific species of Clostridia-related bacteria and Bacteroides fragilis, play a crucial role in promoting beneficial immune responses. They aid in the development of steady-state Th17 cells and the induction of regulatory T cells (Tregs). The loss of these cells can disrupt the homeostasis of intestinal immune system (Kamada and Núñez, 2013). Moreover, not only the microbiota but also microbial fermentation products, such as short chain fatty acids (SCFA) regulate the size and function of the colonic Treg pool. This regulation helps protect against colitis and impairment of these bacterial groups can lead to a breakdown in immune tolerance between immune cells and gut microbiota (Smith et al., 2013).

For a significant period, it was commonly believed that infant gastrointestinal tract was devoid of microorganisms. However, recent research has revealed that the fetal intestine may come into contact with microbes found in the amniotic fluid that. Is swallowed (DiGiulio et al., 2008). The composition of the newborn’s gut is subject to various influences, including the method of delivery (vaginal or caesarean), the choice diet (breast milk or formula), hygiene conditions, the use of antibiotics and supplementation of with prebiotics and/or probiotics (Rautava et al., 2012). This establishment of this early microbiota plays a pivotal role in shaping an adulthood life, as it can impact the susceptibility to several childhood diseases such as, asthma, allergic disorders, type 1 diabetes, obesity and eczema (Villanueva-Millán et al., 2015). As the microbiota establishes itself in the early years of life, the microbial composition undergoes an augmentation in both diversity and richness. Each person eventually reaches a state of homeostasis in their microbial composition, which is likely to remain relatively stable throughout most of their healthy adult life. However, in later stages of life, the microbiota composition once again become less diverse and more dynamic, characterized by an elevated Bacteroides to Firmicutes, an increase in Proteobacteria, and decrease in Bifidobacterium.

1.5.1 Gut-liver axis

The gut-liver axis highlights the relationship between gut and liver that links the diseases in both organs to the microbiome. The gut and liver connected via portal system, systemic circulation and biliary system (Duarte et al., 2023). Microbiome products are transported directly to the hepatic sinusoids via the portal vein and flows into the central vein. These microbiome products activate toll-like receptors (TLR) on hepatic stellate cells (HSC) and Kupffer cells (KC), causing inflammatory responses and hepatocyte injury. Gut-liver interaction is not only a one-way path from gut to the liver but the liver also directly communicates with the gut via biliary system. In the liver, hepatocytes synthesize and secrete bile, a complex solution containing components like IgA, bicarbonate, antimicrobial molecules and bile acids. Bile acids have multiple functions, such as facilitating the digestion and absorption of lipids and lipid-soluble vitamins, and shape the gut microbial composition (Hsu and Schnabl, 2023). Dysregulation of this interaction, can be observed in many diseases like, alcohol-related liver disease (ALD), non-alcoholic fatty liver disease (NAFLD), cirrhosis and viral infections like HIV and HCV (Hsu and Schnabl, 2023). The new field that is investigating the connection between gut and liver in HIV infection showed that, there are different methods to treat bacterial translocation in HIV patients. While fecal microbiota transplant and probiotics allows colonization of commensal microbiota, Rifaximin and targeted therapies reduce pathobionts (Duarte et al., 2023).

Overall, the growing recognition of gut microbiota and liver in the pathogenesis and progression of many diseases opens up a new inside for microbiome-based tools to effectively diagnose and treat patients.

1.5.2 Leaky gut in HIV

Mucosal dysfunction in HIV infection is a major factor contributing to the persistent inflammation and characterized by drastic immunological alterations, breaches in the epithelial barrier, translocation of microbial products into circulation and microbiome dysbiosis. This phenomenon is also called “leaky gut” (Cohen, 2008). These bacterial products induce a significant increase in proinflammatory cytokine production via toll-like receptors (TLRs), contributing to immune activation and inflammation (Miedema et al., 2013). The loss of permeability of the gut results in depletion of $CD4^+$ T cells and Th17 cells within the gastrointestinal tract. $CD4^+$ Th17 cells, generate a rapid response to microbial pathogens at mucosal sites (including the intestinal mucosa), inducing chemokine expression for recruitment of neutrophils, monocytes and lymphocytes. The consequences of Th17 cell depletion include dysbiosis in the intestinal flora, reduced number and activity of neutrophils which may contribute to defects in preventing bacterial dissemination and impairment of secreting proinflammatory cytokines which my play an important role in the production of antimicrobial peptides that in turn control microbial replication at the luminal surface of the intestine (Márquez, 2016). Numbers of other immune cells are also altered in HIV infection. Increased turnover, cell activation, apoptosis and altered functions of cytotoxic $CD8^+$ T cells, natural killer cells (NK cells), innate lymphoid cells and B cells have been reported (Taiwo et al., 2013).

In HIV patients, enrichment of Erysipelotrichaceae, Enterobacteriaceae, Desulfovibrionaceae, and Fusobacteria and a depletion of Lachnospiraceae, Ruminococceae, Bacteroides, and Rikenellaceae were found (Vujkovic-Cvijin and Somsouk, 2019). One study showed that, the intestine of HIV patients is enriched in aerotolerant species and harbours reduced species that are intolerant to oxygen such as Faecalibacterium prausnitsii or members of the Ruminococcus genus. This loss of diversity in HIV patients is not restored with cART therapy (Dubourg et al., 2016). Novel therapies to restore gut ecology and function are necessary to reduce inflammation and improve prognosis of cART treated HIV-infected individuals.

In addition, there are also systemic consequences of the bacterial translocation in HIV-infected patients. Increased Lipopolysaccharide (LPS), bacterial DNA, bacterial flagellin, Lipopolysaccharide Binding Protein (LBP), sCD14, IL-6, Fatty Acid Binding Proteins (FABP) and EndocAb are correlated with the disease progression and known to be leaky gut markers (Márquez, 2016). Systemic immune activation with high levels of $CD4^+$ and $CD8^+$ T cells, high levels of circulating proinflammatory cytokines and chemokines concomitant with polyclonal B-cell activation were found to be associated with HIV-related immune-senescence (Márquez, 2016).

1.6 Aims of the project

HIV, can chronically infect up to 1 % of the world's population and despite successful anti-retroviral therapy, autoimmune diseases and renal disease affect 10–15 % of infected patients. On the other hand, due to virus-induced breakdown of intestinal barrier function, these patients also suffer from leaky gut. In chronic HIV infection, autoantibodies, immune complex (IC) formation, chronic inflammation and IC-induced glomerulonephritis (IC-GN) are frequently observed. But due to the lack of appropriate *in vivo* animal models, the underlying cellular and molecular mechanisms remains unclear.

To address these problems, we first aimed to developed a murine model of neonatal chronic infection with WE strain of the lymphocytic choriomeningitis virus (neoLCMV). Using this mouse model, we aimed to detect autoantibody formation, circulating IC, type I interferon (IFN-I) and TNF signatures and IC-GN, the features of patients with HIV nephropathy.

Second, we aimed to define the role of TLR2 and TLR4 which are known to sense translocated gut microbiota, in the production of IFN-I and inflammatory cytokines. To this end, we employed in the neoLCMV model in mice lacking the above-mentioned TLRs.

Third, we wished to understand the role of self-DNA sensing in RNA virus-induced GN. Here, we aimed to clarify whether NETs formation and sensing its DNA content by cGAS/STING or TLR9 is important for autoantibody formation and the development of GN in the neoLCMV infection. To this end, we employed in the neoLCMV model in mice lacking the above-mentioned TLRs.

And lastly, we correlate IFN I, autoantibody formation and GN in patients with chronic RNA virus infection by examining a large cohort of HIV patients in the University Hospital Bonn to verify the mechanisms determined in the neoLCMV model studies in above-mentioned aims.

2. Materials and Methods

2.1 Materials

2.1.1 Technical equipment

Equipments	Company
Autoclave	Miele
BVC professional	Vacuubrand
Centrifuge 5417R	Eppendorf GmbH
Centrifuge 5430R	Eppendorf GmbH
Centrifuge 5810R	Eppendorf GmbH
Confocal microscopy Leica SP8	Leica-microsystems
Dissection instruments	Fine Science Tools
EasySep™ Magnet	Stemcell
Flexmap 3D	Luminex A DiaSorin company
Freezers	Liebherr
Fridges	Liebherr
GM500 IVC green line and blue line mouse cages	Tecniplast
Haemocytometer Neubauer	Novoglas AG
HERAsafe	Heraeus
Ice boxes	Neolab
ImmunoSpot reader	Immunopst by C.T.L
Leica CM3050 cryostat	Leica-biosystems
Light cycler 480 II	Roche
LSR Fortessa	BD Biosciences
MaxQ 4450 (Orbital Shaker)	Thermo Fisher Scientific
MCO-170AICUVH CO2	PHCbi
Metabolic cages	Tecniplast
Metal cell strainers (Custom)	Universit of Bonn
MF26 (ice machine)	Scotsman
Multichannel pipettes	ErgoOne Starlabs
Multipipette M4	Eppendorf AG
Nanodrop 2000	Thermo Fisher Scientific
peqSTAR	VWR Peqlab
Pipetboy	Integra Bioscience GmbH
Pipettes Research plus	Eppendorf AG

Practum224-1S (Analytical balance)	Sartorius
Precision balance MS6002TS/00	Mettler Toledo
Safire 2 Multi-Detection Plate Reader	Tecan Group Ltd
ScanLaf Mars	Labogene
Smartflow mouse cage fan unit	Tecniplast
Spark microplate reader	Tecan Group Ltd
Sprout Mini Centrifuge	Heathrow Scientific
Star-count (STC 100)	VWR International
Thermomixer compact	Eppendorf AG
Titramax 1000 (Platform shaker)	Heidolph
TW8 (water bath)	Julabo
Vortex-Genie 2	Scientific Industries
Vortexer	VWR International
Water purification system Nanopure Diamond	Barnstead Werner

2.1.2 Consumables

Consumables	Company
75 cm2 and 150 cm^2 cell culture flasks	TPP
96 well V-bottom cell culture microplates, PS	Greiner Bio-One
C-Chip disposable haemocytometer	NanoEntek
Cellstar tubes (15 ml, 50 ml)	Greiner Bio-One
Cole-Parmer Transportable Dewar Flasks	Cole-Parmer Instrument Company
Cover Glass (24 x 50 mm)	VWR International
Deep well plates	VWR International
ELISA plate sealers	R&D Systems
ELISA-plate, microlon 96W Flat-Bott., High binding	Greiner Bio-One
FastPrep®-24™	MP BIOMEDICALS
Feather surgical blades	pfmmedical ag
Filter tips (0.1-10 µl, 1-200 µl, 10-100 µl, 100-1250 µl)	Greiner Bio-One
Filter tips (2.5 µl)	Sarstedt AG & Co.
LPS-free tubes	Eppendorf AG
Mediware tuberculin syringes (1 ml)	Servoprax GmbH
Micro haematocrit capillaries, heparinized	Brand GmbH & Co. KG
Micro tubes (0.2 ml, 0.5 ml, 1.5 ml, 2 ml, 5 ml)	Sarstedt AG & Co.

Microplate, 96well, PS, F-Bottom (Chimney Well) clear, Black, Med. binding	Greiner Bio-One
Multiscreen Filter plates HA, 0,45 µm, Clear, Mixed cellulose Esters	Merck Milipore Ltd
Non-woven swabs (5 cm x 5 cm)	Medicomp
Paper filter	Hawach Scientific
Parafilm M	Pechney Plastic Packaging
Peha-soft nitrile gloves	Paul Hartmann AG
Petri dishes (94/16 mm)	Greiner Bio-One
Pipette tips type Eppendorf	Greiner Bio-One GmbH
ProLong™ Diamond Antifade Mountant	Thermo Fisher Scientific
qPCR adhesive sealing sheets	Thermo Fisher Scientific
RNase & DNase-free tubes	Eppendorf AG
Serological pipettes	Corning
Single use cannulas (0.80 x 120 mm, 21G x 4/3/4)	B. Braun
Single use cannulas (26G x 1, 27G x 1, 23G x 1)	B. Braun
Single use syringes (2-20 ml)	BD Biosciences
SuperFrost Plus (Adhesion Slides) 75 x 25 mm	VWR International
SW22 Shaking water bath	JULABO GmbH
Thin brush	
Tissue culture cover slips 13mm (Plastic)	Sarstedt AG & Co.
Tissue culture test plates	TPP
Tissue-Tek Cryomold Intermediate (15 mm x 15 mm x 5 mm)	Sakura® Finetek
Transfer pipettes 3.5 ml	Sarstedt AG & Co.
Tubes 5 ml, 75 x 12 mm, PS	Sarstedt AG & Co.
Venofix® A, 0,65 x 20 mm, 30 cm Schlauchlänge, G 23 blau	B. Braun
VWR Cell strainers (100 µm, 70 µm, 40 µm)	VWR International
VWR Reagent Reservoirs	VWR International

2.1.3 Reagents and chemicals

Reagents	Company
0.01 % poly-L lysine solution	Sigma-Aldrich
100 % Acetic acid	PanReac AppliChem
2-Mercaptoethanol, 50 mM	gibco

3-Amino-9-ethylcarbazole tablet	Sigma-Aldrich
3,3',5,5'-Tetramethylbenzidine dihydrochloride tablet	Sigma-Aldrich
Bovine serum Albumin, V	PAN Biotech
Chloroform, ACS, (99.8+%)	Alfa Aesar
Collagenase IV	Merck KGaA
Crystal violet (C.I. 42555)	Merck KGaA
D-(+)-glucose	Sigma-Aldrich
DAPI	Biolegend
DNase I	Merck KGaA
EDTA	Merck KGaA
Ethanol	Carl Roth
Fetal calf serum	ThermoFisher Scientific
Fixable Viability Dye eFluor 780	ThermoFisher Scientific
Fluoromont G	ThermoFisher Scientific
Formaldehyde solution	Sigma-Aldrich
Gelatin from cold water fish skin	Sigma-Aldrich
Hydrochloric acid	Sigma-Aldrich
Hydrogen peroxide	Sigma-Aldrich
L-Glutamine 200 mM	gibco
Methanol	Carl Roth
Methyl cellulose	Sigma-Aldrich
N,N-Dimethyl-Formad, (99 %)	Sigma-Aldrich
Near-IR fluoresence reactive dye	ThermoFisher Scientific
Nonfat dried milk powder	PanReac AppliChem
Normal Donkey Serum	Abcam
Normal Rat Serum	Abcam
O.C.T. Compound contaning	Sakura® Finetek
Paraformaldehyde	Merck KGaA
PBS Tablets	ThermoFisher Scientific
Pen Strep	gibco
Percoll	Cytiva
Phorbol myristate acetate	Merck KGaA
Sodium Azide	PanReac AppliChem
Sodium Bicarbonate	gibco
Sodium Chloride	Sigma-Aldrich
Sodium Pryruvate 100 mM	gibco
StemCell magnet	
Streptavidin Peroxidase	Sigma-Aldrich
Sucrose, (99 %)	Alfa Aesar
TRIS-hydrochlorid	Carl Roth
Triton X-100	Sigma-Aldrich

TRIzol reagent	Ambion, Life Technologies
Trypan blue	Merck KGaA
Trypsin-EDTA Solution	Sigma-Aldrich
Tween 20	Sigma-Aldrich

2.1.4 Kits

Kits	Company
Cytofix/Cytoperm Fixation/Permeabilization Solution Kit	BD Biosciences
Foxp3/Transcription Factor Staining Buffer Set	ThermoFisher Scientific
High-Capacity cDNA Reverse Transcription Kit	ThermoFisher Scientific
Human LBP	Hycult Biotech
Mouse Albumin ELISA Kit	Bethyl
Mouse CIC (Circulating Immune Complexes)	MyBioSource
Mouse Claudin 2 ELISA Kit	abbexa
Mouse FABP2 ELISA Kit	abbexa
Mouse LBP ELISA Kit	abcam
ProcartaPlex Assay	ThermoFisher Scientific
Quant-iT™ PicoGreen™ dsDNA Reagent and Kit	ThermoFisher Scientific
RNeasy Plus Micro Kit	Qiagen
RNeasy Plus Mini Kit	Qiagen
SYBR Green PCR Master Mix	ThermoFisher Scientific

2.1.5 Buffers and Mediums

Mediums	Company
Cell culture medium	DMEM Medium + 10 % FCS + 1 % P/S
DMEM (10X)	PAN Biotech
DMEM (1X) (+ L-Glutamine, -Pyruvate)	PAN Biotech
DPBS (1X) (- Ca, -Mg)	gibco
ELISPOT medium	500 ml X-VIVO medium + 50 ml FCS + 5.5 ml P/S + 5.5 ml Mercaptoethanol

RPMI 1640 (1X) (+ L-Glutamine, +Pyruvate)	gibco
RPMI 1640 (1X) without L-Glutamine	gibco
X-VIVO medium	Lonza

Buffers	Composition
ACK Lysing Buffer (1X)	Lonza
AEC buffer	Disolve 1 AEC tablet in 2.5 ml DMF
Blocking buffer	PBS + 0.1 % BSA
Ca-Deprived buffer	0.1 mM L-Aspartic acid + 0.2 mM L-Threonine + 0.3 mM L-Serine + 0.5 mM Glycine + 0.6 mM L-Alanine + 0.9 mM L-Glutamine acid + 0.9 mM Glutamine + 20 mM D(+) Glucose + 20 mM Fructose + 197 mM Sucrose + 3 mM KCL + 0.7 mM Na2H2PO4H2O + 0.5 mM MgCl2 + 10 mM HEPES + 24 mM NaHCO3 --> in 2 L Ca- medium and adjust pH to 7.4
Coating buffer	500 ml PBS + 50 mM $NaHCO_3$ pH: 8.2
Digestion buffer 1	500 ml RPMI1640 + 1 % FCS + 1 mg/ml collagenase + 100 µg/ml DNase I
Digestion buffer 2	100 ml PBS + 1 % FCS + 400 µl collagenase + 100 µl DNase I
ELISPOT wash buffer	PBS + 0.1 % Tween
FACS buffer	PBS + 0.1 % FCS + 0.1 % NaN3
FACS fix	500 ml PBS + 1 % Formaldehyde + 0.02 % NaN3 + 2 % D-(+)-glucose
Fix and stain solution	0.2 % Crystal violet + 11 % Formaldehyde + 2% EtOH
Immunofluorescence blocking buffer	PBS + 5 % BSA + 0.5 % Triton + 0.1 % NaN3
Perfusion buffer 1	300 ml 0.9 % NaCl + 1.11 g EDTA + 1% P/S
Perfusion buffer 2	100 ml Ca-Deprived Buffer + 500µl collagenase
PFA Fixation buffer	PBS + 2 % PFA

Phosphate-Citrate buffer	25.7 ml 0.2 M Na2HPO4 + 24.3 ml 0.1 M citric acid + 50 ml ddH2O pH: 5
Sodium-acetate buffer	PBS + 0.1 % sodium-acetate
TMB subsrate	Disolve 1 TMB tablet in 10 ml of 0.05 M Phosphate-Citrate Buffer + 2 µl of fresh 30 % hdyrogen peroxide per 10 ml subsrate solution
Virus buffer	PBS + 2% FCS+ 1% P/S

2.1.6 Mouse antibodies

2.1.6.1 Flow cytometry

Antigen	Fluorophore	Clone	Company
B220	BUV737	RA3-6B2	BD Bioscience
Bcl6	PerCP Cy5-5	K112-91	BD Bioscience
CD11b	AF488, BV786	M1/70	Biolegend
CD11c	BUV737	HL3	BD Bioscience
CD138	PECy7	281-2	Biolegend
CD146 (LSEC)	FITC	-	Miltenyi Biotec
CD184 (CXCR4)	eF450	2B11	ThermoFisher Scientific
CD19	PE, APC Cy7, BV785	6D5	Biolegend
CD25	APC	PC61	Biolegend
CD278 (ICOS)	PE	C398.4A	Biolegend
CD3	FITC	145-2C11	ThermoFisher Scientific
CD3	BUV395	145-2C11	BD Bioscience
CD3	APC Cy7	145-2C11	Biolegend
CD38	PE	90	Biolegend
CD4	BV650, BV785	RM4-5	Biolegend

CD62L	BV605	MEL-14	Biolegend
CD8	Percepy5.5	53-6,7	Biolegend
CD95	BV605	SA367H8	Biolegend
CD98	BUV395	RL388	BD Bioscience
CXCR3	BV605	CXCR3-173	Biolegend
CXCR5	Biotin	-	BD Bioscience
F4/80	PB, PE	BM8	Biolegend
Foxp3	AF488	MF-14	Biolegend
GL7	PB	GL7	Biolegend
HLA-DR (MHC-II)	BV510, APC	M5/14.15.2	Biolegend
IgA	APC	mA-6E1	eBioscience
IgD	BUV395, BV711, FITC	11-26c.2a	BD Bioscience
IgG	PerCP Cy5-5	Poly4053	Biolegend
IgM	BV510	RMM-1	Biolegend
IgM	PE-Cy7	R6-60.2	BD Bioscience
Ly6C	Percepy5.5	HK1.4	Biolegend
Ly6G	APC, PB	1A.8	Biolegend
PD1	PE-Cy7	RMP1-30	Biolegend
SA	BV510	-	Biolegend
Tim4	PECy7	RMT4-54	Biolegend

2.1.6.2 Immunofluorescence

Antibody	Fluorophore	Host	Company
Biotin-SP-conjugated AffiniPure Goat Anti-mouse IgG (H+L)	Biotin		Jackson Immuno Research Ltd.
Peroxidase AffiniPure Goat Anti-Mouse IgG (H+L)			Jackson Immuno Research Ltd.
donkey anti-goat IgG antibodies conjugated (Secondary Antibody)	Alexa Fluor 488	Donkey	Invitrogen
donkey anti-rabbit IgG (H+L) Highly cross-adsorbed (Secondary Antibody)	Alexa Fluor 568	Donkey	Invitrogen

goat anti-mouse antibodies directed against MPO (Primary Antibody)	-	Mouse	R&D systems
rabbit anti-mouse antibodies directed against citrullinated histone H3 (Primary Antibody)	-	Mouse	Abcam

2.1.7 Others

Reagents	Company
Calf - thymus Nucleosome (Antigen)	Arotec diagnostics
Calf - thymus RNP - Sm (Antigen)	Arotec diagnostics
Calf - thymus DNA (Antigen)	Calbiochem®
clone13 (C13) - LCMV (Virus)	Generated in house, DE
CountBright absolute Counting Beads	ThermoFisher Scientific
DNA sodium salt from Calf-thymus	Sigma-Aldrich
OneComp eBeads	ThermoFisher Scientific
WE - LCMV (Virus)	Generated in house, DE

2.1.8 Cell lines

Line	Description
L13K (L929)	Tissue Fibroblast: Established from the normal subcutaneous areolar and adipose tissue of a male C3H/An mouse; used in virus studies
Vero	Interferon-deficient kidney epithelial cell line: Isolated from kidney epithelial cells extracted from an African green Monkey - Verda Reno (Vero). Also used in virus studies

2.1.9 Primers

Gene	Sequence	Company
β-actin	Unknown	Qiagen
CXCL1	Unknown	Qiagen
CXCL2	Unknown	Qiagen

CXCL9	Unknown	Qiagen
CXCL10	Unknown	Qiagen
IL-6	Unknown	Qiagen
IL-4	Unknown	Qiagen

2.1.10 Mice

All mice that were used in this thesis were purchased at Jackson Laboratories, Charles River or Janvier, and maintained under special pathogen free (SFP) conditions at the House of Experimental Therapy, the central animal facility of the University Clinic Bonn. For experimental procedures the animals were moved to and maintained at the animal facility of the Institute of Experimental Immunology.

Mice	Background	Official name
cGAS-/-	BL/6	B6(C)-*Cgas*$^{tm1d(EUCOMM)Hmgu}$/J
STING-/-	BL/6	B6(Cg)-*Sting1*$^{tm1.2Camb}$/J
TLR2-/-	BL/6	(B6.129- *Tlr2*^{tm1Kir} /J)
TLR4-/-	BL/6	B6(Cg)-*Tlr4*$^{tm1.2Karp}$/J
TLR9-/-	BL/6	C57BL/6-*Tlr9*$^{em1.1Ldm}$ /J

2.1.11 Softwares

Name	Source
Biorender	https://www.biorender.com
FACS Diva 8.0.1	BD Bioscience
Fiji Image J	https://imagej.net/software/fiji/ (free software)
FlowJo 10	Tree star Inc

GraphPad Prism9	GraphPad Software
Immunospot 5.0 Pro DC	Immunopst by C.T.L
iWork	Apple
Microsoft office 2019	Microsoft
SP8 software	Leica-microsystems
Zotero	https://www.zotero.org (free software)

2.2 Methods

2.2.1 *In vivo* experimental set-up

All mice experiments in this thesis were conducted using the same experimental set-up. Newborn mice were infected subcutaneously (s.c.) with $2x10^6$ PFU WE-LCMV in a volume of 10 µl within 24 hours after birth in order to trigger a chronic infection. This group of mice called “neoLCMV” in following experiments. The control group for chronic infection were infected intravenously (i.v.) with $2x10^6$ PFU C13-LCMV in a volume of 50 µl at 5-week-old age. And mice of the uninfected (UI) control group were injected with 10 µl of PBS. This set-up was used for the experiments including comparison UI, neoLCMV and C13-LCMV by using WT (BL/6) mice. For knock out (KO) experiments, same experimental strategy used. Both KO and WT (BL/6) mice were infected subcutaneously (s.c.) with $2x10^6$ PFU WE-LCMV. In this thesis, WT mice refers BL/6.

In order to determine the virus titer in the infected mice, 5 days before the end of the experiment 32 µl of blood was taken by puncturing the facial vein (lower jaw area). One day before the end of the experiment, the mice were placed in metabolic cages for 16 hours to obtain urine (see Fig. 2.1).

On the experiment day, the mice were killed in deep isoflurane anesthesia and continued with perfusion of the mice using perfusion buffer 1 or perfusion buffer 2 (see 2.1.5). Mice were bled from the heart with 2mM EDTA Mediware tuberculin syringes.

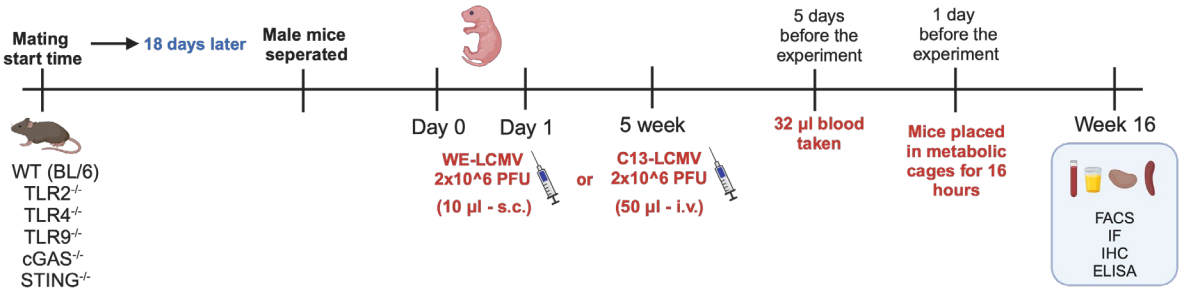

Fig. 1: Experimental set-up for neoLCMV and C13-LCMV infection (created by BioRender).

2.2.2 Organ preparation

2.2.2.1 Isolation of splenocytes

Mice were killed in deep isoflurane anesthesia. Afterwards, we continued with perfusion of the mice with perfusion buffer 1. Spleens were collected in 24 well/plate containing RPMI 1640 medium until further usage. For lymphocyte isolation, collected spleens were meshed through the a 100 µm filter and centrifuged at 1500 rpm for 5 min at 4°C. Supernatant was discarded and the pellet was resuspended in 1 ml ACK lysis buffer for 3 min at RT to remove red blood cells. After 3 min of incubation, the lysis reaction was stopped with 3 ml of RPMI 1640 medium and cells were washed for 5 min at 1500 rpm at 4°C. Cells were resuspended in FACS buffer for surface staining and/or intracellular staining and kept on ice until further usage. For myeloid cell isolation, spleens were digested with 2 ml digestion buffer 1 in 24 well/plate and incubated in MaxQ 4450 (Orbital Shaker) at 37°C for 30 min. After incubation, cells were filtered through a 100 µm filter and centrifuged for 5 min at 1500 rpm 4°C. Supernatant was removed and the pellet was resuspended in 1 ml ACK lysis buffer for 3 min at RT to remove red blood cells. After 3 min of incubation, the lysis reaction was stopped with 3 ml of RPMI 1640 medium and washed for 5 min. at 1500 rpm 4°C. Cells were resuspended in FACS buffer for surface staining and/or intracellular staining and kept on ice until further usage.

2.2.2.2 Isolation of immune cells from kidney

Upon killing, kidneys were collected in 24 well/plate with RPMI 1640 medium until the usage. First, capsules of kidneys were removed and then digested with 1,5 ml digestion buffer 1 in 24 well/plate and incubated in MaxQ 4450 (Orbital Shaker) at 37°C for 40 min. After incubation, cells were filtered through a 70 µm filter and centrifuged for 5 min at 1500 rpm at 4°C. Supernatant was removed and the pellet was resuspended in 1 ml ACK lysis buffer for 3 min at RT to remove red blood cells. After incubation, the lysis reaction was stopped with 3 ml of RPMI 1640 medium and washed for 5 min. at 1500 rpm 4°C. Then, cells were resuspended in 1 ml of RPMI 1640 medium and filter through a 40 µm filter to remove any large undigested cellular aggregates and centrifuged for 2 min at x50g at 4°C. After centrifugation, supernatant collected and transferred into new 15 ml falcon tubes and centrifuged for 5 min at 1500 rpm at 4°C. Supernatant was removed and the pellet was resuspended in FACS buffer for surface staining and/or intracellular staining and kept on ice until further usage.

2.2.2.3 Isolation of lymphocytes from Liver

For lymphocyte isolation in liver, mice were perfused with perfusion buffer 1 via the portal vein for at least 30 seconds until the liver became pale by using Venofix® A G 23 needle. After that, samples were kept in PBS on ice until further usage. Collected samples were meshed with large steel filters in petri dishes on ice together with 10 ml RPMI 1640 medium to get a single cell suspension. Then, cells were transferred into 15 ml falcon tubes and incubated for 2-3 min on ice to remove hepatocytes. This step was also done by centrifugation for 2 min at x50g, followed by the and collection of supernatant but not the pellet. After removing hepatocytes, 12-13 ml of supernatant was collected into new 15 ml falcon tubes and centrifuged for 5 min at 1500 rpm at 4°C. Supernatant was removed and pellet was washed 1x with PBS by centrifugation with the same speed and time. After the washing step, the pellet was resuspended in 4 ml of 40 % percoll at RT and underylayed with 3 ml 80 % percoll with single use cannulas (0.80 x 120 mm, 21G x 4/3/4). Samples were centrifuged for 20 min x800g (or 2000 rpm) with no break (Acc 7, Dec 1) at RT. After centrifugation, the interphase layer was collected in a new 15 ml falcon tube and

filled it up to 15 ml with RPMI 1640 medium to wash at 1500 rpm at 4°C for 10 min. Cells were resuspended in PBS for further stainings.

2.2.2.4 Isolation of myeloid cells from Liver

For myeloid cells isolation from liver, mice were perfused with pre-warmed perfusion buffer 2 via the portal vein for at least 30 seconds until liver gets pale by using Venofix® A G 23 needle. Perfused livers were collected in 50 ml falcon tubes with 5 ml Ca-deprived buffer. Livers were collected in petri dishes then; the buffer was removed from petri dish with a vacuum pump. Sliced liver pieces were transferred were in to the same 50 ml falcon tube and 2.5 ml digestion buffer 2 was added. Samples were incubated in a shaking bath with aspeed of 250 rpm for 17 min. After incubation, the cell suspension was passed through the metal filter into a petri dish and mashed with a syringe and then the metal filter was cleaned up with PBS until everything collected. Then, samples were centrifuged at x50g at 4^{o}C for 2 min. Supernatant was collected into a new 50 ml falcon tube and centrifuged at x800g at 4^{o}C for 10 min. In parallel, 20 ml 25 % percoll was added in a new 50 ml falcon and on top slowly 15 ml 50 % percoll was added with glass pipette. After centrifugation, supernatant was removed and pellet was resuspended with 10 ml PBS and layered them on top of two-step percoll gradient. Samples were centrifuged for 30 min at x1350g at 4^{o}C without break (Acc 7, Dec 1). After centrifuge, interphase layer was collected in new 15 ml falcon tube and filled it up to 15 ml with PBS to wash at 1500 rpm at 4^{o}C for 10 min. Cells were resuspended in PBS for further stainings.

2.2.2.5 Isolation immune cells from bone marrow

Femur and tibia bones were collected from mice and flushed with PBS by using single use cannula 26G, through a 70 µm filter and centrifuged at 1500 rpm for 5 min at 4°C. Supernatant was discarded and pellet was resuspended in 1 ml ACK lysis buffer for 3 min. at RT to remove red blood cells. Following the incubation, the lysis reaction was stopped with 3 ml of RPMI 1640 medium and washed for 5 min. at 1500 rpm at 4°C. Cells were resuspended in desired buffer or medium for further usage.

2.2.3 Flow cytometry

All samples for flow cytometry were measured on a BD LSR Fortessa and analyzed by using FlowJo software.

2.2.3.1 Surface staining

Previously prepared cell suspensions (see 2.2.2.1-5) were pipetted into 96 well/plats and spun down for 3 min at 1500 rpm at 4°C. Supernatant was discarded and pellet was resuspended in 100 µl surface Ab master mix. Cells were incubated for 20 min at 4°C. After incubation, cells were washed with PBS for 3 min at 1500 rpm at 4°C and the pellet was resuspended either in FACS Fix or continued with sAb staining and/or intracellular staining.

2.2.3.2 Secondary antibody and intracellular staining

Cells were stained in their surface staining continued with first, sAb staining upon last washing step from surface staining protocol and incubated with sAb master mix for 20 min at 4°C. After incubation, cells were washed with PBS for 5 min at 1500 rpm at 4°C and continued with intracellular staining with Foxp3/transcription factor staining buffer kit (eBioscience). Washed cells were resuspended in 200 µl of freshly prepared fixation buffer for 15 min at RT on a plate shaker (Titramax 1000). After fixation, cells were spun down for 5 mi. at x400g at 4°C and supernatant discarded. The pellet was resuspended with 200 µl permeabilization buffer and centrifuged for 5 min at x400g at 4°C. After that, 100 µl of transcription factor master mix was added and incubated for 30 min at RT on a plate shaker (Titramax 1000). After incubation, cells were washed with 200 µl permeabilization buffer and centrifuged for 5 min at x400g at 4°C. Cells were resuspended in FACS Fix and kept at 4°C until the measurement. For the determination of absolute cell numbers, CountBright absolute Counting Beads were added to each sample and calculated back to the total cell numbers per organ. At the same time, compensation beads were also prepared with OneComp ebeads for each measurement to be able to adjust the lasers in the BD LSR Fortessa.

2.2.4 Mouse and human plasma preparation

For mice, 32 µl of blood was taken by puncturing the facial vein (lower jaw area) 5 days before the experiment in order to perform virus titration. After collecting blood with heparin-coated capillaries, it was transferred into PBS + 1 % FCS + 2 mM EDTA and centrifuged at 5000 rpm for 10 min. Collected plasma was stored at -80^{o}C until further analysis. For further serological analysis, blood from heart was collected on the respective experimental day with 2mM EDTA Mediware tuberculin syringes and single use canula (26 G). First, samples were kept on ice and then centrifuged at 5000 rpm for 10 min. After plasma carefully separated from the pellet, kept at -80^{o}C until further analysis. For plasma preparation from human samples, 8 ml of blood was collected from HIV patients with kidney disease (CKD^{+}) and without kidney disease (CKD^{-}) and this cohort matched with healthy donors. Whole blood sample centrifuged at x800g for 5 min at RT. Plasma was transferred into two small 1.5 ml micro tube and centrifuged for 20 min at x2000g (Acc 9, Dec 9) to get rid of remaining cells, cell debris and apoptotic bodies. Plasma distributed in LPS-free tubes and RNase & DNase-free tubes to avoid thawing and freezing multiple times. Collected plasma was stored at -20^{o}C until further analysis.

Collection of human blood samples were approved by ethics (see 2.2.15).

2.2.5 Urine collection

One day before the end of the experiment, the mice were placed in metabolic cages for 16 hours to obtain urine (see Fig. 2.1). Collected urine volume was measured and aliquoted for further analysis and kept at -80^{o}C. 100 µl of urine (1:2 dilution of urine with water) was sent to central laboratory in University Clinic of Bonn to analyze urine parameters such as proteinuria, creatinine and urea. In parallel, 1 or 2 µl of urine (1:500 dilution) was used for albuminuria ELISA according to manufacturer’s instructions.

2.2.6 ELISA analysis

All ELISAs that were used in this project were pre coated sandwich-based assay. This assay, measures the amount of antigen between two layers of antibodies (capture and detection antibody). Except detection of albuminuria, for all other ELISAs plasma samples were used.

LBP, FABP2, Claudin 2 and CIC were detected with LBP ELISA, FABP2 ELISA, Claudin 2 ELISA and CIC ELISA respectively. Albuminuria was detected in urine of each mouse by using albuminuria ELISA kit.

Briefly, all reagents were brought to RT before use. 100 µl of standards, samples or controls were added to the appropriate wells in duplicates and incubated at 37°C, for 60 to 90 min. Plate content was discarded and without washing step 100 µl of biotinylated antibody added into all wells and incubated at 37°C for 1 hour. After incubation, each well was washed 3 times with 1X PBS. 100 µl of detection reagent solution was added and incubated at 37°C for 30 min. Each well was washed 5 times with 1X PBS and 90 µl of prepared TMB colour developing agent was added to each well and incubated at 37°C, for 10-20 min in the dark. Reaction stopped with 100 µl of TMB stop solution and read absorbance at 450 nm within 30 min.

2.2.7 Measurement of circulating free DNA in mouse plasma

Mouse plasma was prepared like previously described (see 2.2.5) and Quant-iT™ PicoGreen™ dsDNA Reagent and Kit were used for detection of circulating free DNA (cfDNA). Briefly, reagents were prepared according to the manufacturer's instructions. Plasma samples were diluted 1:30 with DEPC water. In parallel, 1X TE buffer were prepared by using 0.75 ml of the 20X stock and 14.25 ml water. Pico green solution was diluted 1:200 with 1X TE buffer. Next, DNA Lambda^{hi} standard was prepared through a dilution in 1X TE buffer to reach the end concentration of 400 ng/ml. Series of dilutions were prepared by 1:2 dilution steps. 50 µl of standards and samples were added to the 96 well/plate in duplicates. As a blank control, 50 µl of samples were added to the end of

plate. Standards and samples were incubated with 50 µl of pico green solution and samples kept as blank control incubated with 50 µl of 1X TE buffer. Fluorescence was measured immediately at excitation 480 nm and emission 525 nm. Results were analysed by first generating standard curve. Then, blank control fluorescence values subtracted from all data points, including standards, samples. Concentrations for samples and controls were calculated based on the standard curve. Values were obtained for samples multiplied by the appropriate factor to correct for the sample dilution.

2.2.8 Detection of autoantibodies in mouse plasma

For quantitation of antigen-specific IgG titers against nucleosome, DNA or RNA, high binding 96 well/ELISA-plates were coated with 50 µl/well of 0.01 % poly-L lysine for 1 hour at RT. After incubation, plates were washed 3 times with 1X PBS and each plate coated with different antigen such as, 50 µl of 1 µg/ml Calf - thymus Nucleosome, 50 µl of 10 µg/ml Calf - thymus DNA or 50 µl of 10 µg/ml Calf - thymus RNP–Sm (see 2.1.7). After coating with antigens, plates were incubated overnight at 4°C. Next day, plates were washed 3 times with 1X PBS and 200 µl of 4 % Non-fat dried milk powder (NFDM) in PBS was added into each well for 3 hours at RT. After incubation, plates were washed 1 time with 1X PBS and 50 µl of samples and standards were added in duplicates for overnight incubation at 4°C. Samples were diluted in PBS (1:20) and standards were chosen from animals that are positive for anti-DNA or anti-nuc. Next day, plates were washed 3 times with 1 % Non-fat dried milk powder (NFDM) in PBS and added 50 µl of goat anti-mouse IgG-Horse Radish-conjugated antibody was added to each well and incubated for 1 hour at RT. Antibody was diluted 1:1000 in 1% NFDM in PBS. After incubation, plates were washed 3 times with 1 % Non-fat dried milk powder (NFDM) in PBS and added 100 µl of TMB substrate (see 2.1.5) was added to each well and incubated for 10-15 min. The reaction was stopped with 100 µl of 1 % HCl. Absorbance read at 450 nm. O.D. at the lowest serum dilution was arbitrarily set to a value of 100 U/ml. Standard curve was plotted as O.D at 450 nm versus antigen concentration (U/ml). Relative IgG titers of samples were calculated using the strait-line equation and multiplied with the dilution factor.

2.2.9 ELISPOT analysis

Multiscreen Filter plates (HA, 0,45 µm, Clear, Mixed cellulose Esters) were coated with antigens such as, 50 µl of 100 µg/ml Calf-thymus DNA or 50 µl of 10 µg/ml Calf-thymus Nucleosome together with coating buffer (see 2.1.5). pH of coating buffer was carefully adjusted to 8.2 before the usage. Coated plates were incubated overnight at 4°C. Next day, solution was removed from the plate and directly 200 µl of blocking buffer was added into each well and incubated for 2-3 hours at RT. During incubation, splenocytes and BM cells were isolated as previously described (see 2.2.2.5 and 2.2.2.1). Cells were resuspended in ELISPOT medium (see 2.1.5) and counted with C-Chip disposable haemocytometer. Cell numbers were adjusted to 10 million cells in 200 µl. After incubation, plates were washed one time with 200 µl of 1X PBS and 200 µl of isolated splenocytes and BM cells were added to the first well and continued with 1:2 serial dilution until 125.000 cells in the last well. Cells were incubated for 4 hours at 37°C. After incubation, plates were washed 3 times with 200 µl of ELISPOT wash buffer (see 2.1.5) and 50 µl of anti-mouse IgG-Biotin was added into each well and incubated overnight at 4°C. Antibody was diluted 1:10000 in blocking buffer. Next day, plates were washed 3 times with 200 µl of ELISPOT wash buffer and 50 µl of POX was added into each well and incubated for 1 hour at RT. POX was diluted 1:5000 in blocking buffer. During incubation, 525 µl of AEC Buffer (see 2.1.5) in 10 ml 0.1 M sodium-acetate buffer (see 2.1.5) prepared. After mixed the buffer for 10 min the solution was filtered with paper filter to a new tube and finally 1 µl H_2O_2 per 1 ml. was added. After incubation, 50 µl of prepared buffer was added to each well and incubated 15-20 min at RT. This step followed carefully until red spots were visible. As soon as spots were observed, solution discarded and membrane removed from plates and let it dried for at least one day. Plates were first scanned and counted with an ImmunoSpot reader and continued with quality control with Immunospot 5.0 Pro DC software. In all plates, spot size and intensity range were adjusted according to blank wells. Total number of spots were calculated back to 10 million splenocytes.

2.2.10 RNA isolation, cDNA synthesis and RT-PCR

Kidney, spleen and liver were collected in 1.5 ml micro tube during the experiment and were immediately shock frozen with liquid nitrogen in Cole-Parmer Transportable Dewar Flasks. Samples were kept at -80ºC until further analysis. Thawed samples were placed in tubes that were prefilled with 1.4 mm ceramic beads and 300µl of RLT lysing buffer (provided in RNeasy Plus Micro and Mini Kits) and 10 µl of β-mercaptoethanol and homogenized with FastPrep®-24™ homogenizer for 50s seconds. After that, total RNA was purified using the RNeasy Plus Micro and Mini Kits according to manufacturer's instructions. Isolated RNA was resuspended in 20 µl of RNAse free water and concentration of RNA for each sample was measured with Nanodrop 2000. Samples kept at -80ºC until further usage. Before continuing with RT-PCR, cDNA synthesis was performed from isolated RNA samples using High-Capacity cDNA Reverse Transcription Kit (Applied Biosystems) and SYBR Green PCR Master Mix (Applied Biosystems) according to the manufacturers.

For one reaction, the following master mix was prepared:

Component	Volume
RNase inhibitor	1 µl
25x dNTPs	0.8 µl
10x reverse transcriptase	1 µl
10x RT ranadom primers	2 µl
10x RT buffer	2 µl
DEPC water	13.2 µl
RNA	200 ng

After the master mix was prepared for each sample, samples were placed in the peqSTAR Thermocycler using the following program:

Step	Temperature	Time
Step 1	25^0C	10 min
Step 2	37^0C	120 min
Step 3	85^0C	5 min
Step 4	4^0C	∞

Finally, cDNA samples were stored at -20ºC until further analysis.

To proceed with RT-PCR, the following master mix was prepared:

Component	Volume
cDNA (diluted 1:2)	1 µl
forward and reverse primer (10 µM)	0.2 µl
SYBR Green PCR Master Mix	5 µl
DEPC water	3.8 µl

The primers that were used in this project were purchased from Qiagen and provided as a combination of forward and reverse primers. For this reason, the volume of master mixes was adjusted by increasing DEPC water to have 10 µl per sample in total. β-actin was used as a housekeeping gene for normalization. After the master mix was prepared for each sample, it was added to 384 well plates in triplicates. Then, plates were sealed with an adhesive sealing sheets and spun down for 3 min at 1500 rpm at 4°C. Plates were run with following program in the Light cycler 480 II:

Step	Temperature	Time	Number of cycles
Initial denaturation	95 °C	10 min	1
Denaturation	95 °C	15 sec	45 - 60
Amplification	60 °C	1 min	
Melting (step 1)	50 °C	1 sec	1
Melting (step 2)	95 °C	0,11 °C/sec	1
Cooling	40 °C	∞	1

RT-PCR results were analyzed by first calculating the average CT values of triplicates for each sample. Then, dCT values were calculated by subtracting the average of CT value of β-actin from the average CT value of each triplicate. By subtracting average CTs of WT UI from each sample, ddCT values were collected. ddCT values were then further normalized to determine the fold change.

2.2.11 Analysis of ProcartaPlex assay

For procartaplex assay, plasma of neoLCMV mouse was used (see 2.2.5). ProcartaPlex multiplex assay kits were performed similar to ELISAs. The steps were similar, with the exception that antibody-coated beads are used to capture the analyte, instead of having capture antibodies attached directly to the plate. Each kit provides standards of known concentration so that a standard curve can be established. After incubation on a shaker, the beads were washed by putting the 96-well plate on a flat magnet for 30 seconds, after which the fluid was discarded by flicking the wells or by using an automated plate washer. The magnet was removed, and the beads are resuspended in the detection antibody. Another incubation and wash were followed by the addition of streptavidin–R-phycoerythrin (SAPE). The beads were then washed and analyzed with Flexmap 3D machine.

2.2.12 Virus generation and titration

C13-LCMV and WE-LCMV virus pools were generated in house. Vero cell line was used for C13 strain of virus and L13K cell line was used for WE strain of virus. Cell lines were freshly thawed after every 20 passages. Cell lines were kept in 75 cm^2 cell culture flask and splitted every second day. $5x10^4$ PFU in 1.5 ml of C13-LCMV or WE-LCMV virus added to each cell culture flask and incubated for 30 min at 37°C and shook every 5 min to allow infection of all the cells. After incubation, 8.5 ml cell culture medium added and incubated for 72 hours. After 72 hours, supernatant was collected and centrifuged for 10 min at 1500 rpm. 100 µl of aliquot was prepared and stored at -80. After virus pools were prepared, virus titration was performed in order to detect concentration of the stocks. Viral titers of plasma samples that were infected with WE or C13 strain of LCMV virus were also detected with this method. By this, viral load in the plasma of each mouse was calculated. The following protocol was applied:

L13K cells for WE-LCMV virus and Vero cells for C13-LCMV were treated with pre-warmed 5 ml trypsin for 5 min at 37°C to dissociate the cells from cell culture flask. Incubation was stopped with 10 ml cell culture medium and centrifuged for 5 min at x400g.

Supernatant discarded and pellet were resuspended in 5 ml cell culture medium. Cells were counted and numbers were adjusted to 1.215 x 10^5 cells/ml.

Cells were plated in 6 well/plate and distributed into each well by making an “8 movement” and incubated overnight at 37°C. Next day, 2X medium prepared as described in the following table:

Table 1: 2X Medium preparation

2X-medium	For 100 ml
20 % 10X DMEM	20 ml
2 % Pyruvate	2 ml
197.5 ml/L Natriumcarbonate	19.75 ml
2 % Glutamine	2 ml
2 % P/S	2 ml
10 % FCS	10 ml
ddH_2O	44.75 ml

In parallel, methylcellulose solution was prepared. First, 1 liter H_2O was warmed up to 60-80°C and 18 g methylcellulose added. This solution was mixed on magnet and then cooled down to RT. Solution was stored overnight to completely dissolved and next day autoclaved for further usage.

After 2X medium was prepared, it was mixed with Methylcellulose in 1:1 dilution. Due to the viscosity of methylcellulose, 10% more of methylcellulose was added to the mixture. Mixed vigorously and placed in a water bath to remove air bubbles. Then, virus stocks were prepared by using serial dilutions from 1:10^2 to 1:10^8 with virus buffer. Medium was aspirated from 6 well/plate until half-moon shape appeared and 100 µl of diluted samples were added in duplicates. Then, cells were incubated for 30 min at 37°C and shook every 5 min. After 30 min incubation, pre-warmed 2 ml 2X medium was mixed with methylcellulose carefully added into each well and incubated at 37°C for 2 days. After 2 days incubation, cells were feeded with 1.5 ml cell culture medium and incubated another 1 day. After that, medium was removed and 1.5 ml fix and stain solution was added for 15

min and then dried for another day. After fixation step, plaques were counted with Star-count (STC 100) and calculated back for total stock concentration. For negative control virus buffer used. PFU calculation performed as follows:

$$\frac{PFU}{ml} = \frac{number\ of\ plaque}{dilution\ \times\ volume\ of\ diluted\ virus\ [ml]}$$

2.2.13 Histological stainings

On the experiment day after perfusing, organs like liver and kidney were collected in 14 ml of 4 % PFA for further analysis. Samples were kept on roller for at least 6 hours at 4°C. Then, they were washed with 1X PBS and refilled immediately with fresh PBS again then transferred into 30 % sucrose solution for overnight incubation at 4°C. Next day, sucrose was discarded and tissues were dried on napkins before transferring into mounting cassette. Then, tissues were placed carefully in the middle of mounting cassette (Tissue-Tek Cryomold Intermediate, 15 mm x 15 mm x 5 mm) and O.C.T compound applied on top until entire tissue covered. Mounting cassette was immediately placed on ice cold ethanol until samples were completely dried. Samples stored at -80. Mounted samples were then continued for cutting step in cryostat (Leica CM3050 cryostat). Cryostat temperature was set to -17°C. First, few trimming steps done by using 30-35 µm. Then, liver tissues were cut with 30 µm thickness and placed in 24 well/plate with PBS. Next, PBS was removed from plates with transfer pipette and tissues washed with 1.5 ml of 0.1 % Triton. Washing solution was discarded and 300 µl of IF blocking buffer was added into each well and incubated at plate rotator for 1 hour at RT. After blocking step, we continued with staining.

2.2.13.1 Immunofluorescence staining

For IF staining of liver tissues, after the blocking step, we first continued with primary Ab staining. For this, blocking buffer was removed from each well and 300 µl of primary Ab master mix was added to each well. As primary Ab, goat anti-mouse MPO and rabbit anti-mouse citrullinated histone H3 (citH3) were used in 1:100 dilution. Tissues were incubated for overnight at 4°C. On next day, pAb master mix was removed from wells and washed with 1.5 ml 0.1 % Triton for 15 min. This washing step was repeated for 5 times. After the washing step, tissues were incubated with 300 µl of secondary Ab master mix on a plate rotator for 2 hours at RT. As secondary Ab, donkey anti-goat IgG AF488 and donkey anti-rabbit IgG AF568 were used in 1:1000 dilution. In this master mix, 1:1000 DAPI was also added for nucleus staining. Some tissues stained only with secondary Ab but not with primary Ab to have baseline for back ground signals. After incubation, tissues were washed with 1.5 ml 0.1 % Triton for 15 min. This washing step was repeated for 5 times. After the washing step, tissues were placed on SuperFrost microscope slides (75 x 25 mm) using a thin brush in PBS bath. And 3 drops of ProLong™ Diamond Antifade Mounting gel added on slides and covered with a coverslip (24 x 50 mm) and stored at 4°C in the dark until the analyses. For analysis, random multi-stack confocal images were acquired in Leica SP8. All images were exported as (lif.) file and imported to Leica SP8 software to obtain merged pictures. MPO^+ $citH3^+$ double positive cells were determined as NETosis-positive and to calculate fluorescence intensity of MPO^+ $citH3^+$ cells, Image J analysis software was used.

2.2.13.2 Immunohistochemistry staining of IgG and C3c

Mouse kidney immunohistochemistry staining (IHC) of IgG and C3c stainings were performed by Patrick Droste and Prof. Dr. Peter Boor from the laboratory of nephropathology at the University Clinic of Aachen. Samples were collected by me and sent to Aachen for staining. Briefly, ½ kidney was collected in 4 % PFA (see 2.1.5) on the experimental day and kept in these solutions for overnight at 4°C. Next day, tissues were

transferred to PBS and sent to Aachen for further analysis. The staining was performed as follows: Tissue sections were rehydrated and antigen retrieval was performed with Proteinase K (Dako, S3020). Slides were incubated with the following antibodies: Rabbit Anti-Human C3c (Dako, F0201) followed by biotinylated Goat anti-Rabbit IgG (Vector, BA-1000-1.5) or only biotinylated Horse Anti-Mouse IgG (Vector, BA-2001). Staining was developed with Vector DAB Substrate (3,3'-diaminobenzidine) (SK-4100) enhanced by previous use of VECTASTAIN Elite ABC-HRP Kit (PK-6100). Further counter staining was performed with Methylgreen. Negative controls remained negative. Slides were digitalized using Aperio Versa200 whole slide scanner (Leica Biosystems). Using Aperio ImageScope (Leica Biosystems), all glomeruli available on a section were evaluated for the presence of immune complex depositions and their severity. The following score was used for this purpose: No deposits (0), mild deposits (1), moderate deposits (2), and marked deposits (3). All tissue evaluations were performed in a blinded manner by a single investigator.

Human kidney IgG and C3c stainings were done by Vivette D D'Agati from Columbia University, Department of Pathology and Cell Biology, New York. HIV patient samples were collected in this department and 5 patient cases were analysed in this project.

2.2.14 Statistical analysis

All data were analyzed by GraphPad Prism 9 software and represented as mean ± standard error of meaning (SEM). Statistical differences between groups were analyzed using unpaired Mann-Whitney *t*-test (two groups) and one-way ANOVA with ordinary multiple comparisons test (there and more groups). Significance was set at *p<0.05, **p<0.01, ***p<0.001, ****p<0.001.

2.2.15 Animal and human ethics

All animal experiments were conducted according to the German Animal Welfare Act. Specific animals were approved by the State Office for Nature, Environment and consumer Protection (LANUV) from North Rhine Westphalia, Germany. The file number of approved animal ethic application is: TVA-81-02.04.2020.A447.

Human samples in this study were conducted in collaboration with Dr. med. Carolynn Schwarte-Zander and Prof. Dr. med. Jürgen Rockstroh from University clinic of Bonn with ethic approval number: 279/14.

HIV patients in this project were collected from both gender (female and male) and different age and they were all under ART therapy. Healthy donors were matched with this group. These patients were separated into two groups based on parameters mentioned below:

Table 2: Classification of HIV patients with and without kidney disease

	Healthy	CKD^{-} HIV^{+}	CKD^{+} HIV^{+}
Proteinuria/serum creatinine	<50	<200	>200
Kidney Insufficiency Score	0	0	1-3
HAV, HBV, HCV co-infections	No	No	No

3. Results

3.1 Hallmarks of HIV-associated nephropathy

HIV-associated nephropathy (HIVAN) covers a wide range of renal diseases such as, HIV-associated immune complex kidney disease (HIVICD), IgA nephropathy, lupus-like glomerulonephritis and classic focal segmental glomerulosclerosis (FSGS). Although, the infection is well controlled in these patients, renal diseases remain a common consequence in 10 to 15 % of HIV infected individuals (Nobakht et al., 2016). To further characterize the immunological features of HIV patients, we conducted a clinical study on HIV patients with (CKD^+ HIV^+) and without kidney disease group (CKD^- HIV^+), accompanied with healthy donors (see table 2).

3.1.1 Pathological features of HIV patients

HIV patients featured circulating autoantibodies and a Type I interferon and TNF signature, if they developed signs of nephritis. However, biopsies from such patients with or without IC-GN are difficult to obtain, because early antiviral treatment in Germany precludes this complication, and if it occurs, renal biopsies are rarely performed. We overcame this problem by establishing a collaboration with Vivette D D'Agati from Columbia University, Department of Pathology and Cell Biology, New York, who maintains the largest collection of such biopsies. Kidneys of HIV patients were stained for heavy chains of immunoglobulins like IgG, IgM and IgA and also for different immunoglobulin light chains like κ (kappa) and λ (lambda) together with complement stainings for C3c and C1q by our collaboration partners.

Five HIV patient cases showed higher IgG and IgM deposits but less IgA deposits (Fig 2 A) accompanied with higher C3c deposits (Fig 2 B). And no restriction found to κ (kappa) or λ (lambda) light chains of immunoglobulins (Fig 2 C).

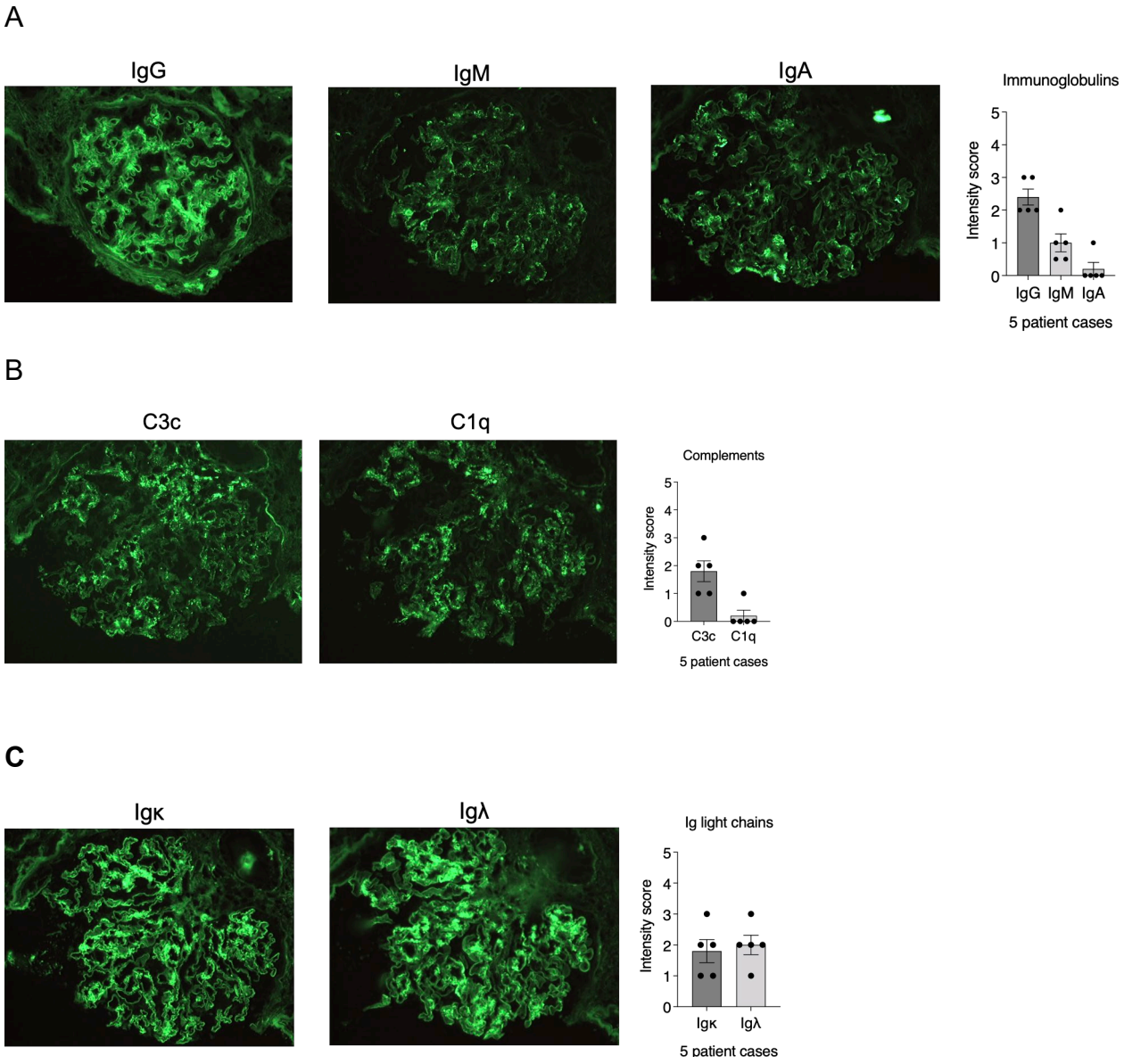

Fig 2: Increased immunoglobulin and complement deposits observed in the kidney of HIV patients.

(A) Representative immunofluorescence (IF) images of IgG, IgM and IgA stainings. (B) IF images of C3c and C1q staining. (C) Representative IF images of Igκ and Igλ staining. Bar charts on the right side: Mean ± SEM is shown. Each dot represents one patient (n=5). Tissues were embedded in formalin-fixed paraffin (FFPE) and cut 3 microns.

Analysis of these biopsies shows HIV patients have mostly IgG and IgM deposits together with C3c deposition in their kidney. And both lambda and gamma chains of immunoglobulins found in similar levels meaning no restriction was observed any of this light chains.

These stainings were performed by our collaboration partners from Columbia University, Department of Pathology and Cell Biology, New York.

3.1.2 Auto-immune features of HIV patients

Previous studies have described high prevalences of autoantibodies in HIV patients (Baranova et al., 2020; Lackner et al., 2010; Wang et al., 2020). In line with this, data provided by our collaboration partner PD Dr. med. Carolynne Schwarze-Zander from Studienambulanz Immunologie, University Hospital Bonn, showed elevated anti-DNA and anti-nucleosome levels in plasma of HIV patients. As shown in Fig. 3A, HIV patients with kidney disease group (CKD^+ HIV^+) showed higher anti-DNA and anti-nucleosome levels compare to the HIV patients without kidney disease group (CKD^- HIV^+) and healthy donors (Fig 3 A). In line with this, we also observed higher cell free DNA (cfDNA) in both HIV patient group compared to healthy donor but no significant difference observed within the HIV group (Fig 3 B). Surprisingly, we did not observe any significant differences in CIC levels in both groups compare to healthy donors (Fig 3 C). Moreover, based on previous findings, a significant increase observed in IFNAR-stimulated genes (ISGs) such as MX1, IFIT1, ISG15, IRF3 and IRF7 as well as slight increase in pro inflammatory cytokines IL1β, Tnfα, IL17, CCL18 although not significant (Konstantinos Symeonidis, 2019).

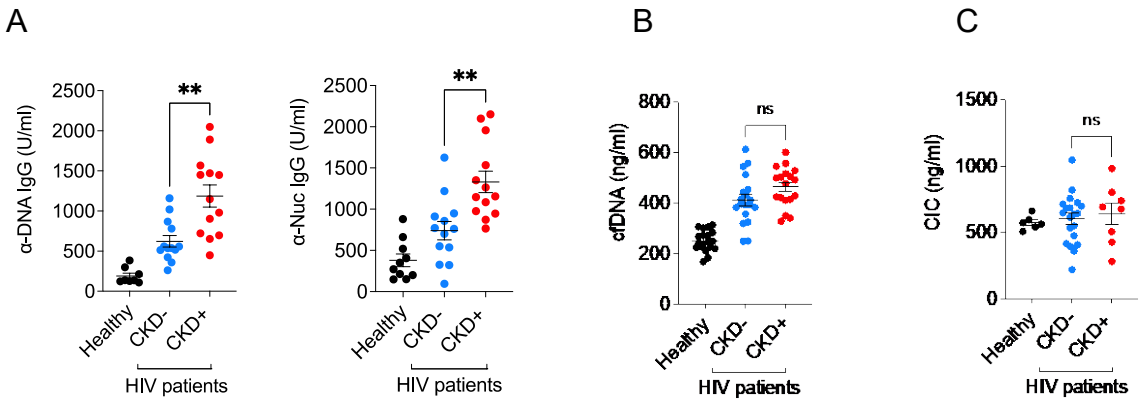

Fig 3: Elevated levels of autoantibodies and cfDNA in CKD⁺ HIV⁺ patients.

(A) Quantification of anti-DNA and anti-nucleosome antibodies by ELISA and B) cfDNA determined by Pico green assay in the plasma of healthy individuals (n=8-10), HIV patients with CKD (n=8-13) or without CKD (n=10-13). (C) circulating immune complexes (CIC) in the plasma of healthy individuals (n=8-10), HIV patients with CKD (n=8-13) or without CKD (n=10-13) by ELISA. Statistics were assessed by unpaired *t*-test, ns not significant, *p<0.05, **p<0.01, ***p<0.001, ****p<0.001.

Collectively, these results indicated the development of auto-immune disease in HIV patients with CKD (CKD⁺ HIV⁺). Data in Fig 3 A were provided by PD Dr. med. Carolynne Schwarze-Zander from Studienambulanz Immunologie, University Hospital Bonn.

These experiments (Fig 3 B-C) were equally performed and analyzed together with Christabel Celia Kho (PhD student in the laboratory of Prof. Dr. Zeinab Abdullah from IMMEI, University of Bonn).

3.2 Characterization of the neoLCMV mouse model

Many studies have shown that HIV/HCV infections have substantial health implications and can cause complications such as the development of autoimmunity (Zandman-Goddard and Shoenfeld, 2002). Additionally, the translocation of gut microbiota, elevated levels of inflammatory cytokines and NETosis are complications that have been described in these patients. However, due to the absence of suitable rodent models to study association of HIV infection with kidney disease the evaluation of underlying mechanisms remained a big challenge. As a result, it is not clear how and which factors lead to progression of kidney disease in chronic HIV and HCV infection. Therefore, it is crucial to study the role of the immune system and its contributing factors during the development of kidney disease. To this end, we aimed to established a mouse model in which we infected the neonates of BL6 mice with the WE strain of LCMV within the first 24 hours after birth in order to trigger chronic infection results in GN (assigned here as neoLCMV). Like HIV and HCV, lymphocytic choriomeningitis virus (LCMV) is a single stranded RNA virus that is sensed by Toll-like and RIG-I-like receptors. Injection of C13 LCMV into the adult BL/6 mice (5-week-old) does not result in the development of GN. The reason of choosing these time points for infection was because if the neonates infected with C13 strain, they do not survive and if the BL/6 mice infected with WE strain of LCMV at 5-week-old age, they do not develop chronic kidney disease (see table 3). Therefore, we established a model in which we could induce a chronic infection that leads to CKD and additionally, we infected the mice with C13-LCMV to trigger chronic infection that do not develop CKD. Using the neoLCMV group, we aimed to mimic CKD^{+} HIV^{+} and with the C13 infected group we could mimic CKD^{-} HIV^{+}. We also observed manifestations of the kidney disease first at the 10-week-old time point which further progresses with age. But the full blown of disease features were observed in 16- to 18-week-old age. Therefore, we focused on the 16-to-18-week p.i time points in our experiments.

Table 3: Infection strategy of LCMV strains in BL/6 mouse

Strain	Age		Outcome	Complications	Mimics in human
Armstrong	adult	→	acute infection	no GN	
	neonate	→	lethal		
Clone 13 (C13)	adult	→	chronic infection	no GN	CKD^{-} HIV^{+}
	neonate	→	lethal		
WE	adult	→	acute infection	no GN	
	neonate	→	chronic infection	GN	CKD^{+} HIV^{+}

3.2.1 Pathological features of neoLCMV mouse

Using different strains of LCMV, (i.e., C13 or WE), we confirmed that C13-infected mice showed only mild histological alternations meaning similar to UI and less deposition of IgG and C3c compare to neoLCMV (Fig 4A) whereas neoLCMV infected mice showed significantly higher glomerular deposition of IgG together with C3c at 16-to-18-week post infection (p.i). neoLCMV mice showed also increased Ki67 positive cells in the glomerular tuft (Fig 4B) and increased glomerulomegaly and immune cell infiltration by CD45 staining (Fig 4C-D). At this time point, kidneys were shrunken and reduced kidney weight (Fig 4E). In line with this, neoLCMV mice showed increased albuminuria compared to C13 infected group (Fig 4F).

A

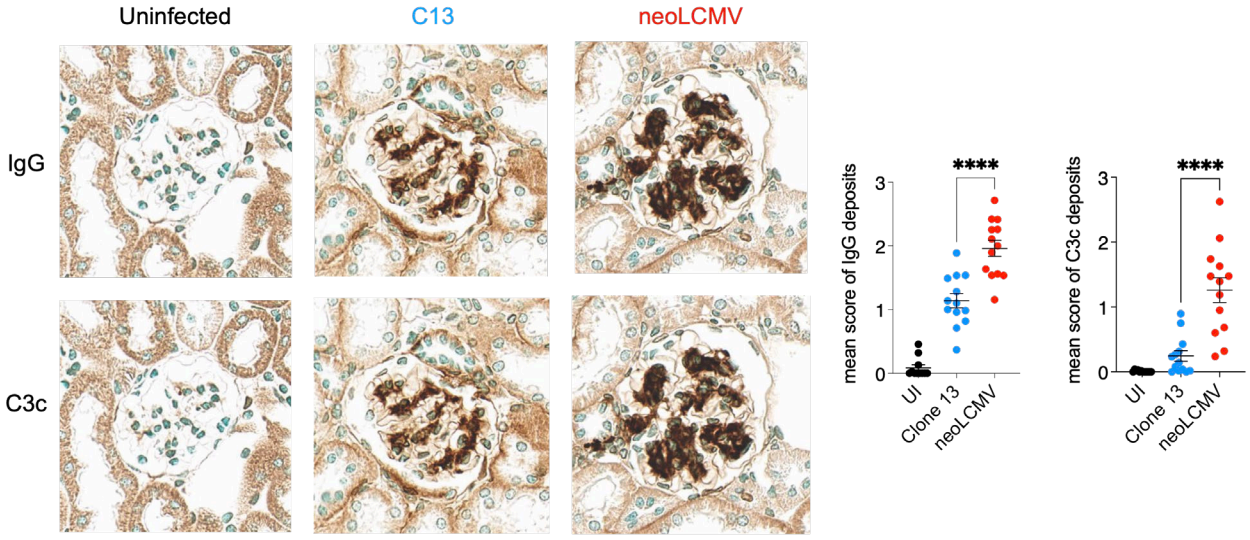
Uninfected
C13
neoLCMV
IgG
C3c
mean score of IgG deposits
mean score of C3c deposits
****
****
UI
Clone 13
neoLCMV

B

C

D

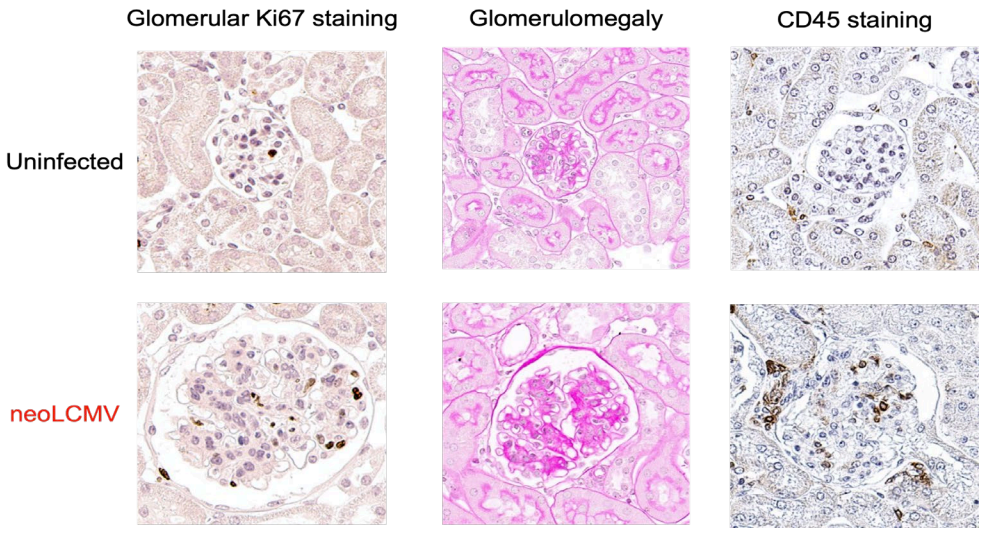
Glomerular Ki67 staining
Glomerulomegaly
CD45 staining
Uninfected
neoLCMV

E

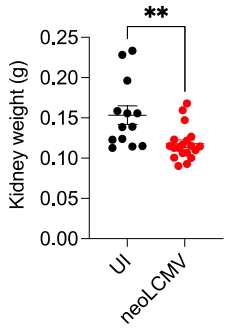
Kidney weight (g)
**
UI
neoLCMV

F

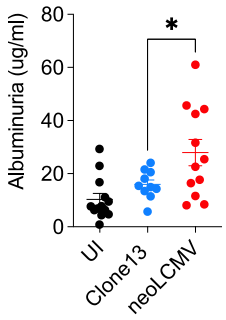
Albuminuria (ug/ml)
*
UI
Clone13
neoLCMV

Fig 4: Kidney pathology of the neoLCMV mice.

(A) IHC staining of immunoglobulin and complement staining of uninfected (UI) (n=3-11), C13 (n=5-13) and neoLCMV (n=6-13) mice at 16–18-week p.i. (B) Glomerular Ki67 staining of kidneys from uninfected (UI) and neoLCMV mice at 16–18-week p.i (C) PAS staining of uninfected (UI) and neoLCMV mice at 16–18-week p.i. (D) CD45 staining of uninfected (UI) and neoLCMV mice at 16–18-week p.i. (E) Kidney weight of uninfected (UI) (n=13) and neoLCMV (n=19) mice at 16–18-week p.i. (F) Albuminuria measurement in urine of uninfected (UI) (n=13), C13 (n=10) and neoLCMV (n=12) mice at 16–18-week p.i. by ELISA. Statistics were assessed by unpaired *t*-test (two groups), ns not significant, *p<0.05, **p<0.01, ***p<0.001, ****p<0.001.

Mouse kidney immunohistochemistry staining (IHC) and PAS staining of these figures were performed by Patrick Droste and Prof. Dr. Peter Boor from the laboratory of nephropathology at the University Clinic of Aachen. Samples were collected by me and Christabel Celia Kho (PhD student in the laboratory of Prof. Dr. Zeinab Abdullah from IMMEI, University of Bonn) and sent to Aachen for staining.

3.2.2 Auto-immune features of the neoLCMV mouse

To address if our neoLCMV mouse model also features the high prevalence of autoantibodies observed in chronic HIV infection in humans, we determined levels of anti-DNA and anti-nucleosome in the plasma. Indeed, neoLCMV mice showed significantly increased anti-DNA and anti-nucleosome antibodies compared to the C13 infected group (Fig 5 A). Moreover, we observed higher cfDNA in neoLCMV mice compared to C13 infected mice (Fig 5 B). Circulating immune complexes (CIC) levels also did not show significant differences (Fig 5 C). Although it was not significant, there is a trend towards increased levels of proinflammatory cytokines in the plasma of neoLCMV mice compared to the C13 infected group (Fig 5 D). In line with this, neoLCMV mice showed increased levels of IFNAR-stimulated genes (ISGs) such as ifi44, MX1 and CXCL10 in spleen and liver compare to C13 infected group (Fig 5 E). Although CXCL10 and MX1 were not significantly different in spleen, there is a trend towards increased levels. In the kidney, MX1 and CXCL10 were significantly higher compared to the C13 infected group (Fig 5 F).

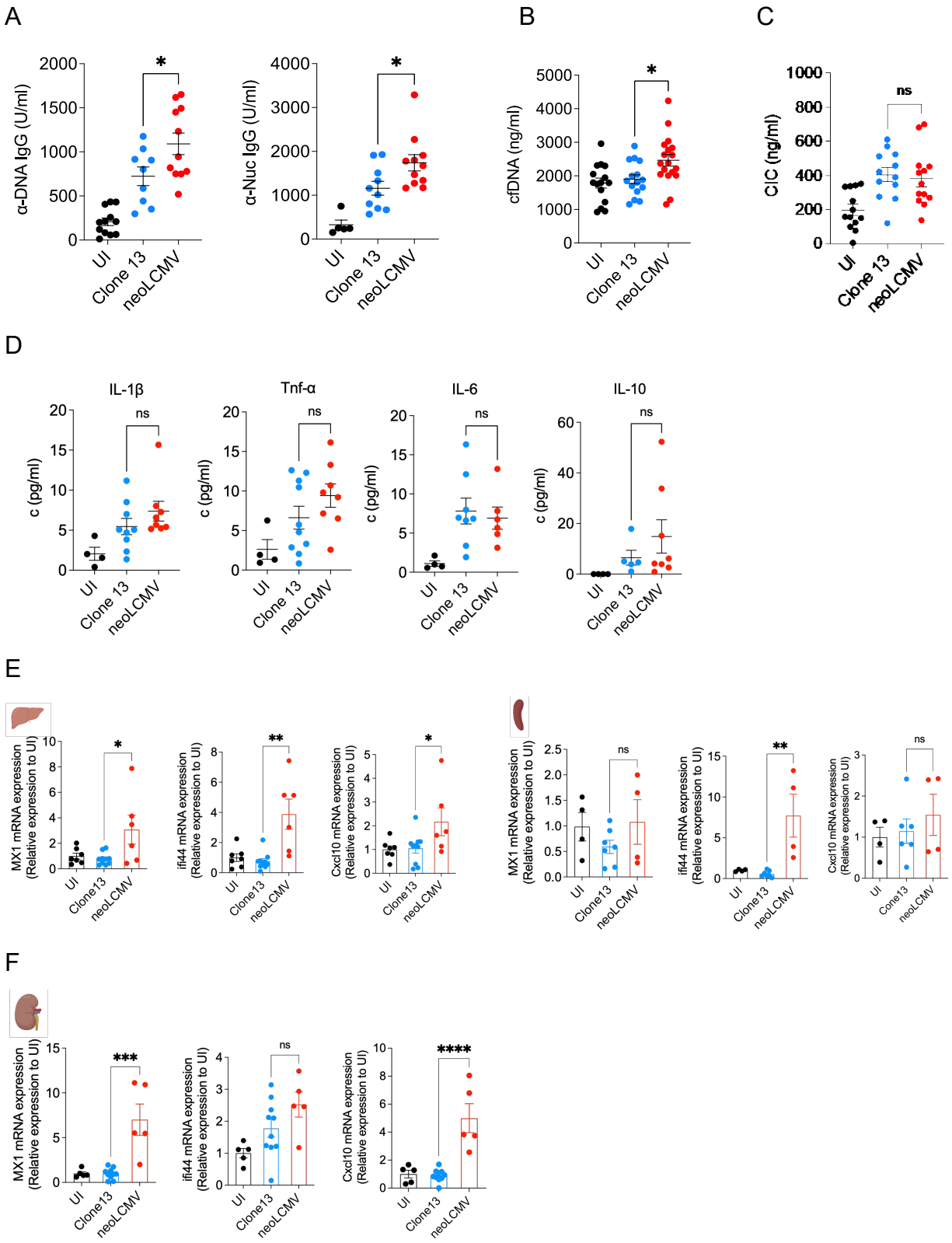
A
α-DNA IgG (U/ml)
α-Nuc IgG (U/ml)
B
cfDNA (ng/ml)
C
CIC (ng/ml)
ns
D
IL-1β
Tnf-α
IL-6
IL-10
c (pg/ml)
E
MX1 mRNA expression (Relative expression to UI)
ifi44 mRNA expression (Relative expression to UI)
Cxcl10 mRNA expression (Relative expression to UI)
F
UI
Clone 13
Clone13
Cone13
neoLCMV

Fig 5: The neoLCMV mice develop signs of autoimmunity.

(A) Quantification of anti-DNA and anti-nucleosome in uninfected (UI) (n=5-12), neoLCMV (n=11) and C13 infected mice (n=9-10) at 16–18-week p.i. by ELISA. (B) cfDNA determined by Pico green assay in the plasma of uninfected (UI) (n=12), neoLCMV (n=14) and C13 infected mice (n=15) at 16–18-week p.i. (C) circulating immune complexes (CIC) in uninfected (UI) (n=13), neoLCMV (n=13) and C13 (n=12) infected mice at 16–18-week p.i. by ELISA. (D) Measurement of cytokines in plasma of uninfected (UI) (n=8-9), neoLCMV (n=12-13) and C13 (n=4-5) infected mice at 16–18-week p.i. by procartaplex. (E-F) mRNA expression of ISGs measured in kidney, liver and spleen of uninfected (UI) (n=4-8), neoLCMV (n=4-6) and C13 (n=5-8) infected mice at 16–18-week p.i. by qPCR. Statistics were assessed by unpaired *t*-test (two groups) or one-way ANOVA with ordinary multiple comparisons test (three and more groups), ns not significant, *p<0.05, **p<0.01, ***p<0.001, ****p<0.001.

Altogether, the chronic neoLCMV mouse model mirrors key hallmarks of CKD in HIV patients and can therefore, be used as a model to address underlying cellular and molecular mechanisms of this disease in humans. Moreover, serological analysis showed that, the disease is mainly driven by autoantibodies rather than immune complexes which is in line with the autoimmune phenotype called “lupus like” mesangioproliferative glomerulonephritis consistent with “HIV-like” GN.

Of note, these analyses (Fig 5 A-D) were equally performed together with Christabel Celia Kho (PhD student in the laboratory of Prof. Dr. Zeinab Abdullah from IMMEI, University of Bonn). Experiments in Fig 5 E-F were performed by Dr. rer. medic. Hella Luksch from TUD Dresden University of Technology, Department of Pediatrics, Faculty of Medicine and University Hospital Carl Gustav Carus.

3.3 Features of leaky gut in HIV patients and neoLCMV mice

It is known that HIV infection targets and destroys $CD4^+$ T cells and causes immune activation by destroying Th17 cells, that are a subset of $CD4^+$ T cells that secrete interleukin 17 (IL-17) and resides in the gut. This results in a leaky gut and allows the gut microbes and parts of them to enter the blood stream (Vujkovic-Cvijin and Somsouk, 2019). This systemic inflammation contributes to the morbidity and mortality in untreated

and antiretroviral-treated HIV patients (Deeks et al., 2013). Therefore, we first aimed to show markers indicative of a leaky gut in the plasma of our HIV cohort and also in neoLCMV mice to verify bacterial translocation.

3.3.1 neoLCMV mice mimic leaky gut-like found in human HIV infection

Lipopolysaccharide (LPS) is an outer membrane components of gram negative-bacteria and essential for the both the shape and function of the outer membrane. High levels of LPS in the bloodstream are associated with many infections including HIV and are considered to be a major marker of microbial translocation (Márquez, 2016).

Lipopolysaccharide Binding Protein (LBP) is a soluble 60-kDa glycoprotein that recognizes and binds to LPS and is produced by gastrointestinal and hepatic epithelial cells in response to LPS stimulation (Márquez, 2016). Increased plasma concentration of LPS and LBP together with sCD14 and IL-6 are indicatives of the leaky gut (Al-Ayadhi et al., 2021). Therefore, we measured LPS and LBP in the plasma of HIV patients. The HIV-infected group showed increased levels of LPS and LBP compare to health donors but no significancy was observed between HIV infected group (Fig 6 A).

LPS levels in the plasma of neoLCMV mice was not in the range. Therefore, we measured another leaky gut marker, the fatty acid binding protein 2 (FABP2), which is known to be secreted by structurally damaged intestinal epithelial cells and can be detected in blood (Al-Ayadhi et al., 2021). NeoLCMV mice also showed increased levels of FABP2 and LBP compared to the C13 infected group (Fig 6 B). We further assessed the dysfunction of the gut barrier by Claudin 2 measurement in the plasma of neoLCMV mice. Claudin 2 is one of the tight junction proteins that is known to regulate the barrier function and is typically expressed in leaky epithelia and the small intestine (Luettig et al., 2015). Indeed, neoLCMV mice also showed increased levels of Claudin 2 compared to the C13 infected group (Fig 6 C).

It is known that, once microbial products have passed through the mucosa, they disseminate via the portal vein into liver. Sensing these microbial products by hepatocytes, hepatic stellate cells and Kupffer cells (KC) within the liver activates pro-inflammatory and profibrotic pathways. And although the underlying mechanisms are not yet known, HIV can reduce the number of KC and impairs hepatic function thus reducing the capacity of the liver to mitigate the consequences of microbial translocation (Deeks et al., 2013).
This combined loss of mucosal immune surveillance and hepatic impairment allows microbial products to access the peripheral circulation. We therefore checked KC numbers in the liver of neoLCMV mice. Although the count of KC was not changed between neoLCMV and the C13 infected group, the frequency of KC was significantly decreased in neoLCMV infected mice (Fig 6 D).

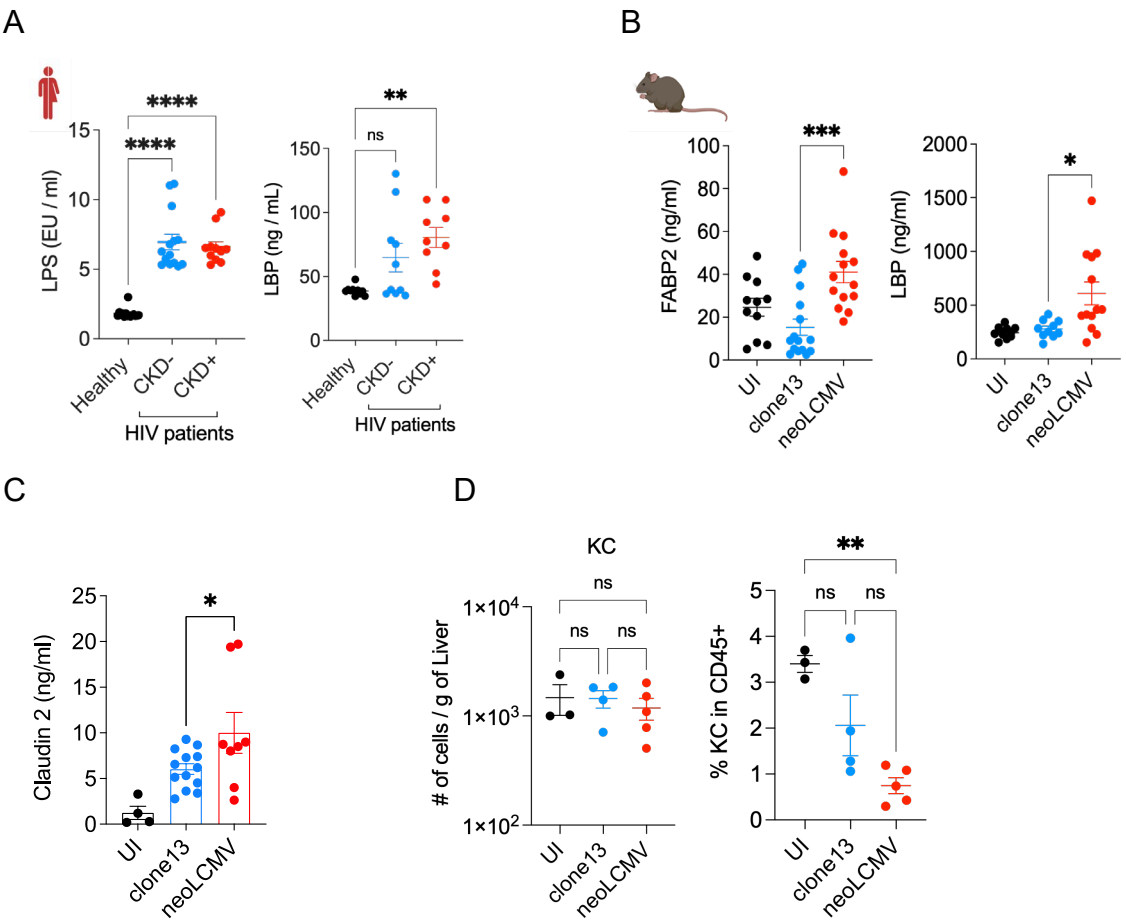

Fig 6: Enhanced leaky gut markers in plasma of humans and neoLCMV mouse.

(A) ELISA measurements of LPS and LBP in the plasma of healthy individuals (n=10-11), HIV patients with CKD (n=9-11) or without CKD (n=10-14). (B) ELISA measurements of LPS and FABP2 in the plasma of uninfected (UI) (n=11), neoLCMV (n=13-14) and C13 infected mice (n=10-11) at 16–18-week p.i. (C) ELISA measurement of Claudin 2 in the plasma of uninfected (UI) (n=4), neoLCMV (n=8) and C13 infected mice (n=13) at 16–18-week p.i. (D) Staining of Kupffer cell (KC) in the liver of uninfected (UI) (n=3), neoLCMV (n=5) and C13 (n=4) infected mice at 16–18-week p.i. by FACS. On the left, cell counts are calculated per gram of liver and on the right side, frequencies of KC showed within the living cell population. Samples were gated on $CD45^+$ LD^- $F4/80^+$ $Tim4^+$. Statistics were assessed by unpaired *t*-test (two groups) or one-way ANOVA with ordinary multiple comparisons test (three and more groups), ns not significant, *p<0.05, **p<0.01, ***p<0.001, ****p<0.001.

These results confirmed the presence of increased systemic inflammation and enhanced leaky gut makers in our HIV cohort as wells as leaky gut. In neoLCMV mice, we observed higher FABP2, LBP and Claudin 2 levels as well as decreased KC compared to the C13 infected group. Thus, neoLCMV mice but not C13 infected mice are a suitable model to mimic bacterial translocation found in HIV infected individuals. With these results, we could confirm bacterial translocation in the neoLCMV model and therefore, we used this set-up for further analyses to understand the underlying mechanisms of “lupus like” mesangioproliferative glomerulonephritis consistent with “HIV-like” GN.

3.4 Role of DNA sensing in the development of glomerulonephritis

After establishing a mouse model that can mimic the leaky gut-like phenotype in HIV patients, we then aimed to investigate the molecular and cellular mechanisms that might play a role in disease development. Patients suffering from chronic HIV infection show a broad spectrum of co-morbidities such as microbial translocation, excessive NETosis, immune signaling and autoantibody production, leading to the formation of immune complexes and subsequently the development of GN. Pathogen-derived RNA is sensed by RIG-I (retinoic acid-inducible gene 1) and MDA5 (melanoma differentiation associated protein 5), but the main cytosolic DNA sensor is cyclic GMP-AMP (cGAMP) synthase

(cGAS). Upon DNA binding, cGAS synthesizes cGAMP, that subsequently binds to STING (stimulator of interferon genes). This turn leads to the activation of the kinase TBK1 (TANK binding kinase 1), which uses STING as a scaffold to phosphorylate and activate the transcription factor IRF3 (interferon regulatory factor 3), thus eventually inducing IFN expression (Motwani et al., 2019). Based on the findings that IFN expression can be induced by a ‚leaky gut', and both in CKD^{+} HIV patients as well as neoLCMV mice showed increased cfDNA in their plasma, it is important to know how the cGAS-STING pathway affects the development of GN during HIV infection. To elucidate the complex immune mechanisms that play a role during chronic HIV infection, we first applied neoLCMV model in mice lacking cGAS or STING. Hence, we applied our neoLCMV model in cGAS-deficient and STING-deficient as well as in WT control mice. We combined this experiment in order to reduce the utilization of control group wild type BL/6 and uninfected mice.

3.4.1 cGAS/STING pathway plays no major role in the development of GN

Kidney histology of $cGAS^{-/-}$ (cGAS KO) and $STING^{-/-}$ (STING KO) mice showed that, deletion of either cGAS or STING did not protect these mice from GN upon infection, meaning similar levels of IgG and C3c deposition in kidney compare to WT (Fig 7 A). Although no significant differences were observed between the two knock out (KO) mouse lines and WT mice regarding the mean score of IgG and the percentage of glomeruli with IgG deposits, autoantibody levels in the plasma of $cGAS^{-/-}$ mice showed slight but not significant decrease compared to WT mice (Fig 7 B). In contrast to autoantibody levels in $cGAS^{-/-}$ mice, cfDNA levels were slightly but not significantly increased whereas $STING^{-/-}$ mice showed similar levels compared to WT mice (Fig 7 C). CIC levels in both KO groups were not altered compared to WT mice (Fig 7 D). To better understand of the kidney function in GN, we also measured albuminuria and ureacreatinine in urine of all mice. However, we did not observe any changes in both KO mice compared to WT mice, which is in line with the kidney histology which revealed that cGAS and STING KO mice develop similar levels of GN like WT mice (Fig 7 E). Moreover, viral titers in the plasma of both KO mouse lines showed similar levels to WT mice (Fig 7 F).

A

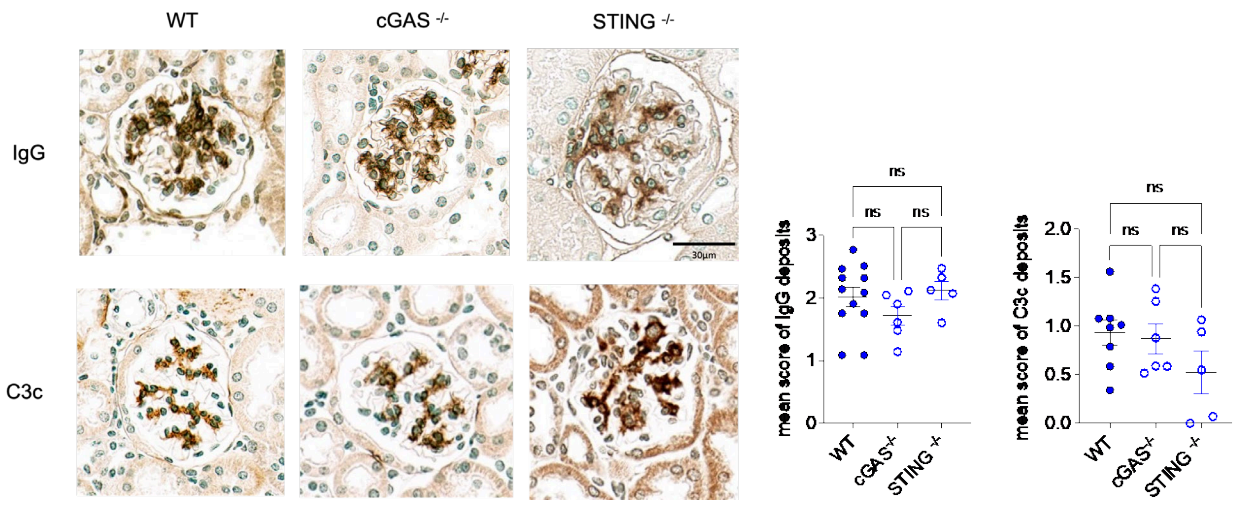
WT
cGAS -/-
STING -/-
IgG
C3c
30µm
mean score of IgG deposits
mean score of C3c deposits
ns
WT
cGAS-/-
STING -/-

B

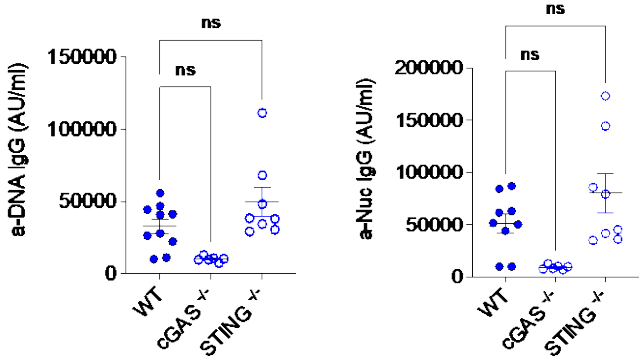
a-DNA IgG (AU/ml)
a-Nuc IgG (AU/ml)
ns
WT
cGAS -/-
STING -/-

C

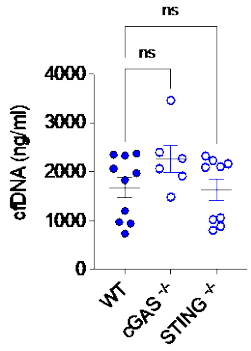
cfDNA (ng/ml)
ns
WT
cGAS -/-
STING -/-

D

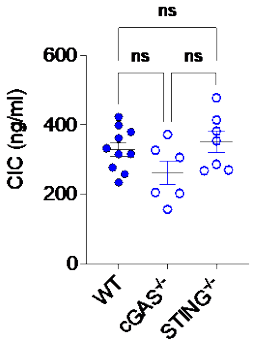
CIC (ng/ml)
ns
WT
cGAS-/-
STING-/-

E

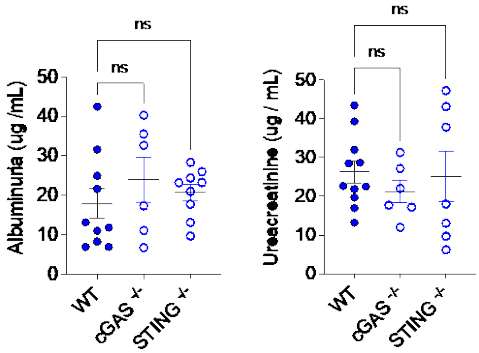
Albuminuria (ug /mL)
Urecreatinine (ug / mL)
ns
WT
cGAS -/-
STING -/-

F

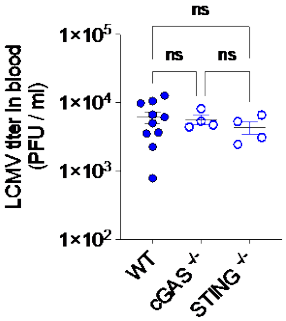
LCMV titer in blood (PFU / ml)
ns
WT
cGAS -/-
STING -/-

Fig 7: No protection from GN observed in neoLCMV infected cGAS$^{-/-}$ and STING$^{-/-}$ mice.

(A) IHC staining of IgG and C3c staining of kidney sections in WT neoLCMV (n=8-13), neoLCMV cGAS$^{-/-}$ (n=6) and neoLCMV STING$^{-/-}$ (n=5) mice at 16–18-week p.i. (B) Quantification of anti-DNA and anti-nucleosome in in WT neoLCMV (n=9-10), neoLCMV cGAS$^{-/-}$ (n=6) and neoLCMV STING$^{-/-}$ (n=8) mice at 16–18-week p.i. by ELISA. (C) cfDNA determined by Pico green assay in the plasma of in WT neoLCMV (n=10), neoLCMV cGAS$^{-/-}$ (n=6) and neoLCMV STING$^{-/-}$ (n=9) mice at 16–18-week p.i (D) circulating immune complexes (CIC) in in WT neoLCMV (n=10), neoLCMV cGAS$^{-/-}$ (n=6) and neoLCMV STING$^{-/-}$ (n=7) mice at 16–18-week p.i. by ELISA. (E) Measurement of albuminuria and ureacreatinine in urine of WT neoLCMV (n=10-11), neoLCMV cGAS$^{-/-}$ (n=6) and neoLCMV STING$^{-/-}$ (n=7-9) mice at 16–18-week p.i. by ELISA. (F) Titration of LCMV virus in the plasma of WT neoLCMV (n=10), neoLCMV cGAS$^{-/-}$ (n=4) and neoLCMV STING$^{-/-}$ (n=4) mice at 16–18-week p.i. Statistics were assessed by unpaired *t*-test (two groups) or one-way ANOVA with ordinary multiple comparisons test (three and more groups), ns not significant, *p<0.05, **p<0.01, ***p<0.001, ****p<0.001.

These results showed that, although there is a slight decrease in autoantibody levels and ureacreatinine in neoLCMV infected cGAS$^{-/-}$ mice, both cGAS$^{-/-}$ and STING$^{-/-}$ mice did not show protection from GN which indicates that the cGAS/STING pathway is not play a major role in development of GN in our neoLCMV model.

3.5 Role of TLRs in glomerulonephritis

Besides circulating free DNA or bacterial DNA in HIV patients and in our neoLCMV mouse model, there are also other cell damages or bacterial products that are released into circulation during chronic HIV/LCMV infection (Márquez, 2016). Upon bacterial translocation, increased leakage of bacterial components such as lipoteichoic acid (LTA), lipopolysaccharide (LPS) or bacterial flagellin can be sensed by toll-like receptors (TLRs). TLRs are known to recognize pathogen associated molecules that are derives from various microbes (Takeuchi and Akira, 2010). For instance, TLR9 recognizes unmethylated DNA with CpG motifs whereas TLR4 and TLR2 recognizes bacterial wall components such as LPS and LTA, respectively. Since it is known that HIV patients display the leaky gut syndrome, we therefore aimed to elucidate the role of different TLRs

by using single TLR KO mouse models. Therefore, we applied our neoLCMV infection model in TLR9$^{-/-}$, TLR4$^{-/-}$ and TLR2$^{-/-}$ mice.

3.5.1 TLR2 but not TLR4 or TLR9 showed partial protection from GN

Applying the neoLCMV infection model in TLR2$^{-/-}$ mice showed partial protection from GN, with significantly less IgG and C3c deposits observed in the kidney of these mice compared to WT mice. In neoLCMV TLR4 and TLR9 KO mice, similar levels of IgG and C3c deposits were detected compared to WT (Fig 8 A). For this reason, we focused in out further studies only on neoLCMV TLR2$^{-/-}$ mice compared to WT to understand the underlying mechanisms in the development of GN. Decreased anti-DNA, anti-nucleosome and anti-smRNP levels in neoLCMV TLR2$^{-/-}$ mice showed that, neoLCMV TLR2 is playing a role in autoantibody production (Fig 8 B). Interestingly, cfDNA and CIC levels remained similar to WT mice (Fig 8 C-D). We then tittered viral load in the plasma of both neoLCVM TLR2 and WT mice to ensure that the protection from disease was not due to the differences in LCMV clearing. Indeed, the viral load in the plasma of neoLCMV TLR2$^{-/-}$ and WT mice was similar (Fig 8 E). We then detected kidney damage by monitoring albuminuria, ureacreatinine and proteinuria in the urine of neoLCMV TLR2$^{-/-}$ and WT mice. Lack of TLR2 in neoLCMV TLR2 KO mice resulted in improved kidney function compared to WT neoLCMV mice (Fig 8 F-H).

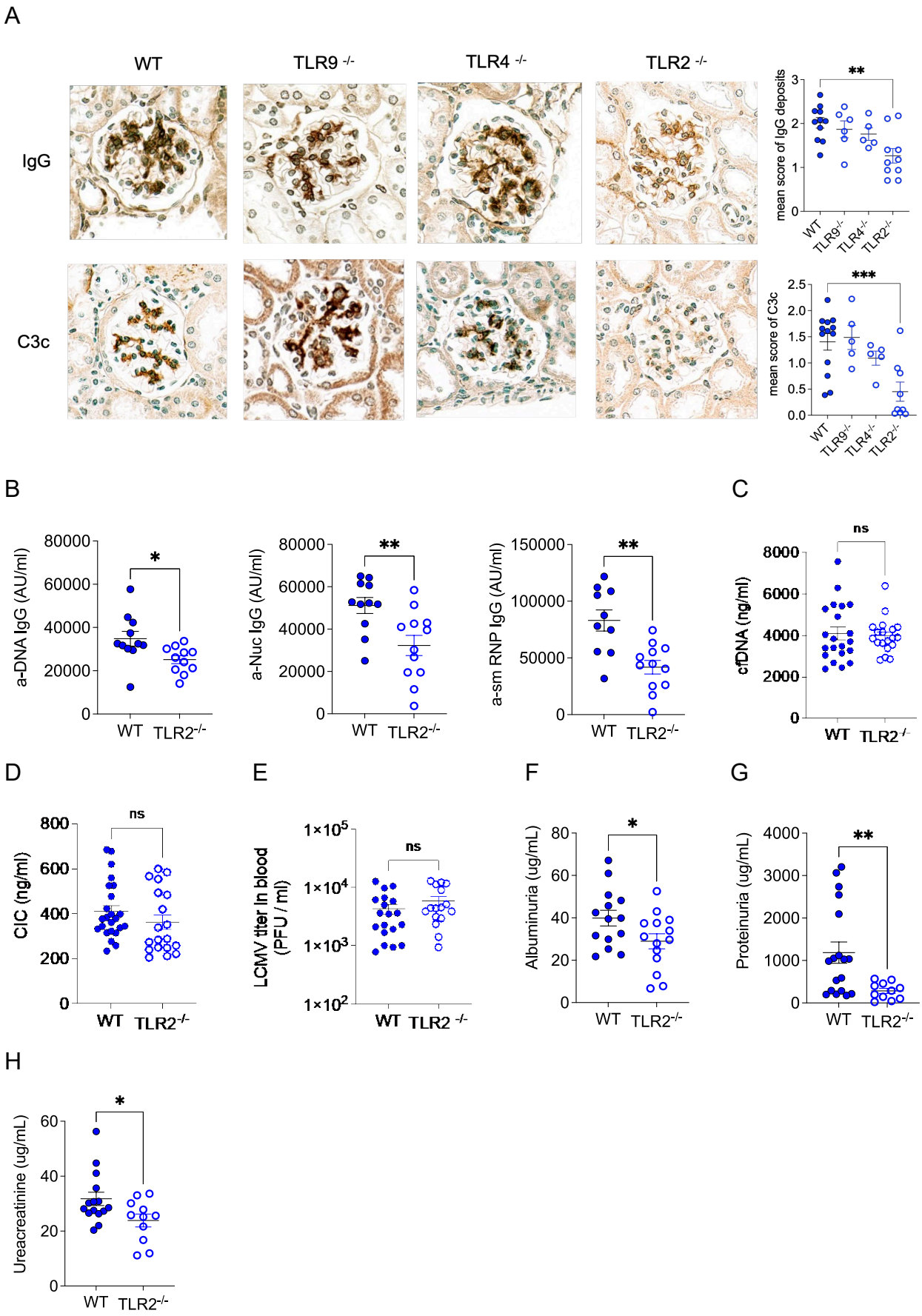
A
WT
TLR9 -/-
TLR4 -/-
TLR2 -/-
IgG
C3c
mean score of IgG deposits
mean score of C3c
**
***
WT
TLR9-/-
TLR4-/-
TLR2-/-
B
a-DNA IgG (AU/ml)
a-Nuc IgG (AU/ml)
a-sm RNP IgG (AU/ml)
*
**
WT
TLR2-/-
C
cfDNA (ng/ml)
ns
D
CIC (ng/ml)
E
LCMV titer in blood (PFU / ml)
F
Albuminuria (ug/mL)
G
Proteinuria (ug/mL)
H
Ureacreatinine (ug/mL)

Fig 8: TLR2$^{-/-}$ mice were partially protected from GN after neoLCMV infection.

(A) IHC staining of IgG and C3c staining of kidney sections in WT neoLCMV (n=12), neoLCMV cGAS$^{-/-}$ (n=5) and neoLCMV STING$^{-/-}$ (n=5) mice at 16–18-week p.i. (B) Quantification of anti-DNA, anti-Nucleosome and anti-smRNP in WT neoLCMV (n=10-11), neoLCMV TLR2$^{-/-}$ (n=11-12) mice at 16–18-week p.i. by ELISA. (C) cfDNA determined by Pico green assay in the plasma of in WT neoLCMV (n=21), neoLCMV TLR2$^{-/-}$ (n=20) mice at 16–18-week p.i (D) circulating immune complexes (CIC) in in WT neoLCMV (n=24) and neoLCMV TLR2$^{-/-}$ (n=19) mice at 16–18-week p.i. by ELISA. (E) Titration of LCMV virus in plasma of WT neoLCMV (n=19) and neoLCMV TLR2$^{-/-}$ (n=15) mice at 16–18-week p.i. (F) Measurement of albuminuria, (G) proteinuria and (H) ureacreatinine in urine of WT neoLCMV (n=14-18) and neoLCMV TLR2$^{-/-}$ (n=11-14) mice at 16–18-week p.i. by ELISA. Statistics were assessed by unpaired *t*-test (two groups) or one-way ANOVA with ordinary multiple comparisons test (three and more groups), ns not significant, *p<0.05, **p<0.01, ***p<0.001, ****p<0.001.

Collectively, these results indicated that lack of TLR2 resulted in improved kidney function and an important role of TLR2 in autoantibody production.

3.6 NETosis in HIV patients and the neoLCMV mouse model

In chronic HIV infection, the main source of the antigen is the leaky gut (Brenchley et al., 2006). In addition to that, increased levels of cfDNA in the plasma of HIV patients but also in our neoLCMV mouse model gave us a hint to focus on investigating the source of DNA in GN. Sources of increased cfDNA in plasma are apoptosis, necrosis or NETosis (Celec et al., 2018). It is known that in HIV infection but also in other autoimmune diseases such as systemic lupus erythematosus (SLE), inflammatory bowel disease (IBD), multiple sclerosis (MS), Type 1 diabetes mellitus, NETosis is playing a crucial role in disease pathogenesis (Joshi et al., 2016; Rother et al., 2017; Silvestre-Roig et al., 2016; Wong et al., 2015). NETosis is a type of programmed cells death and the neutrophil extracellular traps (NETs) formed as a consequence are composed of genomic DNA, associated with histones, antimicrobial proteins and enzymes that are released into the extracellular space and contribute to the killing and elimination of extracellular microorganisms (Kenny et al., 2017). Therefore, we hypothesized that enhanced NETosis can lead to increased

availability of host DNA and other self-antigens in the circulation further promoting the production of autoantibodies, contributing to the development of “lupus like” mesangioproliferative glomerulonephritis consistent with “HIV-like” GN.

To determine whether increased NETosis can be detected in our HIV patient cohort, spontaneous NETosis assays performed by Christabel Celia Kho. Healthy neutrophils isolated from donors and incubated them with the plasma of CKD^{+} HIV or CKD^{-} HIV patients. And indeed, the CKD^{+} HIV group showed elevated levels of NETosis as measured by DNA and neutrophil elastase (NE) staining (Christabel Celia Kho, 2019).

These results then validated in neoLCMV mouse model. Therefore, neutrophils isolated from neoLCMV in WT and $TLR2^{-/-}$ mice at 16- to 18-week-old mice by Christabel Celia Kho. As a positive control PMA stimulation was used (Rother et al., 2017). Neutrophils from $TLR2^{-/-}$ neoLCMV mice showed significantly decreased NETosis compared to WT neoLCMV mice (Christabel Celia Kho, 2019).

3.6.1 TLR2 signaling induces NETosis in the liver during chronic virus infection

Based on the pre-liminary findings from Christabel Celia Kho, that TLR2 signaling is implicated in neutrophils to induce NETosis, we then wanted to investigate the localization of NETosis. The first hypothesis was to check NETosis in the kidney as it is a kidney disease related infection. When we stained kidney sections of WT and $TLR2^{-/-}$ neoLCMV mice for NETosis with MPO and citH3, we did not observe colocalization of MPO and citH3 (Fig 9 A). Although WT neoLCMV mice showed increased MPO in tubular epithelium and also weak signals in the bowmans capsule in projection to the glomerular tuft. This might be due to the increased number of monocytes in kidneys of neoLCMV mice compared to the UI group (Fig 9 B). In this context, it has been showed that MPO can be released not only by neutrophils but also by monocytes and macrophages at the side of infection (Khan et al., 2018).

Surprisingly, neutrophil numbers in kidney did not change between C13 and neoLCMV infected group but slightly increased in neoLCMV infected group compare to uninfected (UI) group. Therefore, neutrophils might also contribute to MPO release. NeoLCMV TLR2$^{-/-}$ mice did not show significant difference compared to the WT neoLCMV group (Fig 9 C).

MPO alone is not indicative of NETosis. NETosis considered colocalization of MPO and citH3 and/or NE signals in IF staining. Since neoLCMV mice and CKD^{+} HIV patients showed increased leaky gut symptoms and translocation of microbial products occurs from the gut to the liver we then changed our hypothesis and we investigated NETosis in liver. And indeed, we observed significantly increased MPO^{+} citH3^{+} NETs in the liver of neoLCMV mice compare to C13 (Fig 9 D). When then investigated whether TLR2 signaling plays a role in inducing NETosis also in liver. MPO and citH3 stained liver tissues of TLR2$^{-/-}$ mice showed significantly decreased MPO^{+} citH3^{+} NETs compare to WT neoLCMV mice (Fig 9 E). We ensured that decreased NETosis in neoLCMV TLR2$^{-/-}$ mice was not caused by decreased neutrophil numbers in the of this mouse (Fig 9 F). We then further revealed that, NETosis occurs in liver only via TLR2 signaling but not TLR4 or TLR9 (Fig 9 G).

A

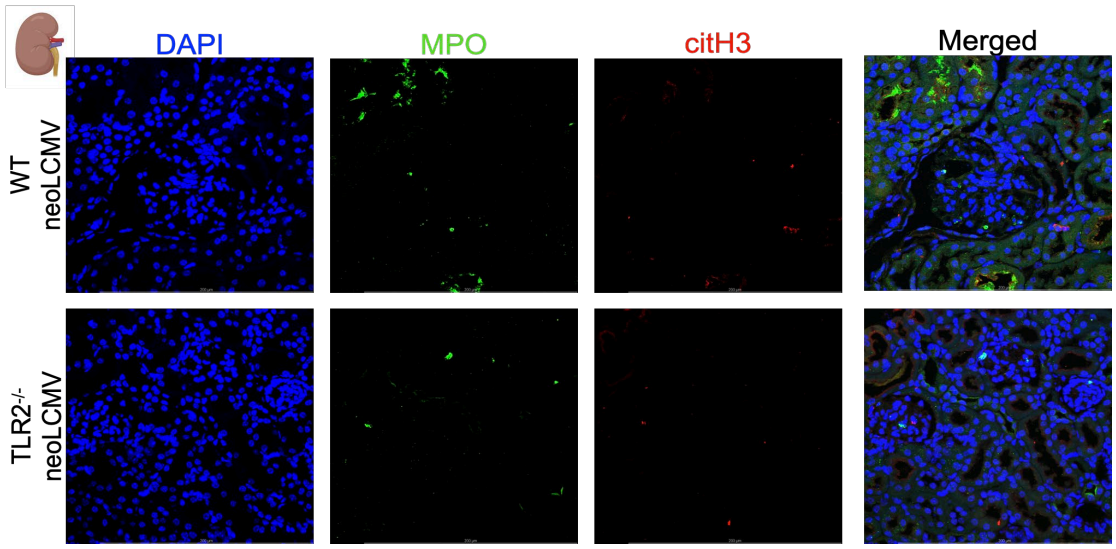
DAPI
MPO
citH3
Merged
WT neoLCMV
TLR2-/- neoLCMV

B

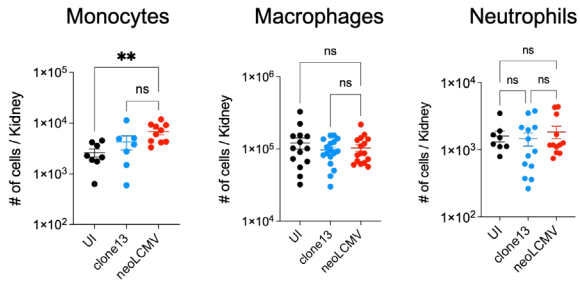
Monocytes
Macrophages
Neutrophils
# of cells / Kidney
UI
clone13
neoLCMV
**
ns

C

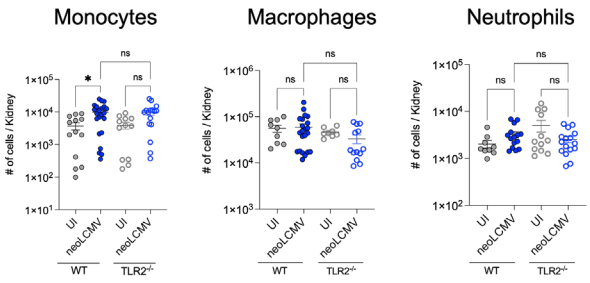
Monocytes
Macrophages
Neutrophils
# of cells / Kidney
UI
neoLCMV
WT
TLR2-/-
*
ns

D

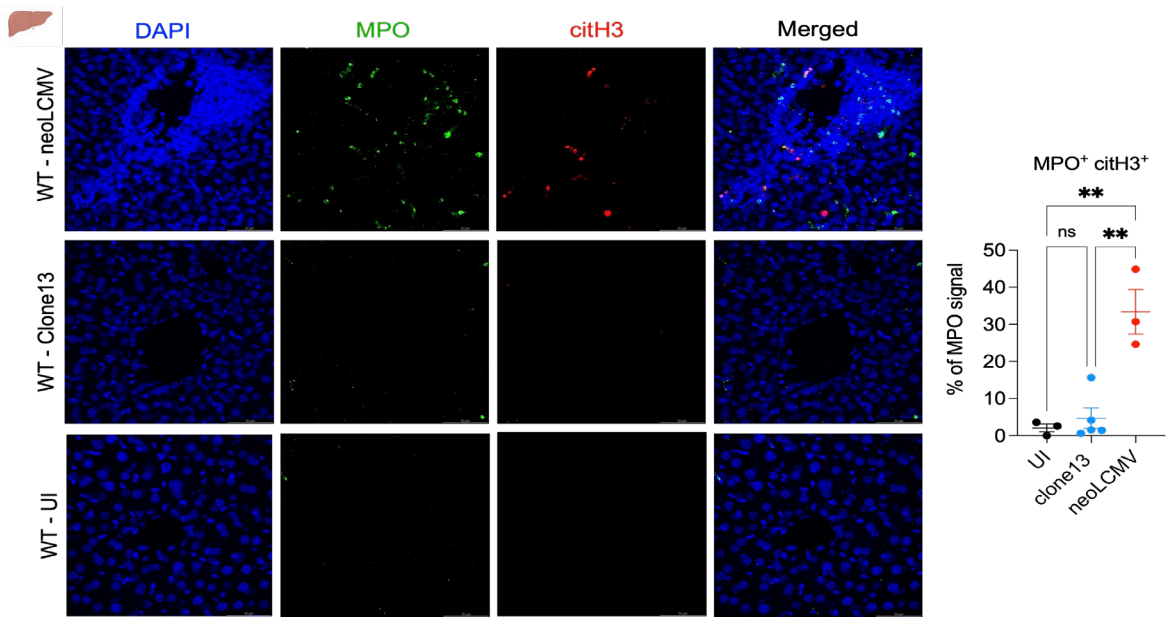
DAPI
MPO
citH3
Merged
WT - neoLCMV
WT - Clone13
WT - UI
MPO+ citH3+
% of MPO signal
UI
clone13
neoLCMV
**
ns

E

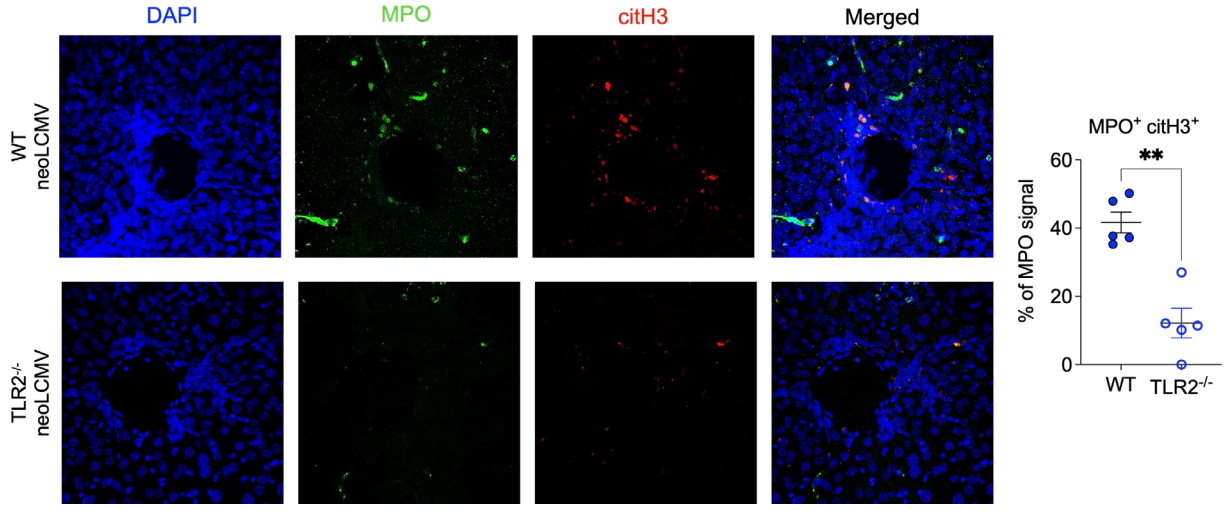
DAPI
MPO
citH3
Merged
WT neoLCMV
TLR2-/- neoLCMV
MPO+ citH3+
**
% of MPO signal
60
40
20
0
WT
TLR2-/-

F

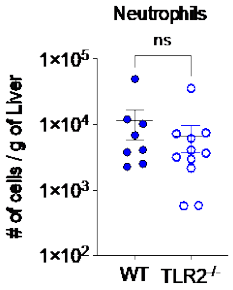
Neutrophils
ns
# of cells / g of Liver
1×10^5
1×10^4
1×10^3
1×10^2
WT
TLR2-/-

G

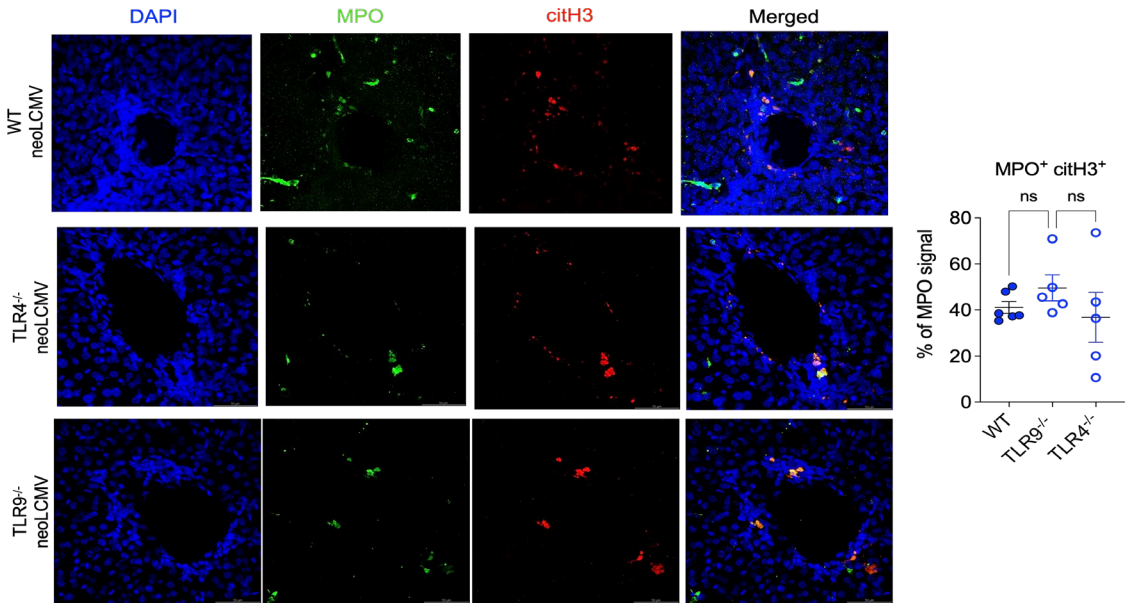
DAPI
MPO
citH3
Merged
WT neoLCMV
TLR4-/- neoLCMV
TLR9-/- neoLCMV
MPO+ citH3+
ns
ns
% of MPO signal
80
60
40
20
0
WT
TLR9-/-
TLR4-/-

Fig 9: TLR2 signaling in neutrophils induces NETosis in the liver.

(A) IF staining of DAPI, MPO and citH3 in kidney sections in WT neoLCMV (n=4) and neoLCMV TLR2$^{-/-}$ (n=5) mice at 16–18-week p.i. (B-C) Staining of monocytes (CD11b^{+}, Ly6C^{+}), macrophages (CD11b^{+}, F4/80^{+}) and neutrophils (CD11b^{+}, Ly6G^{+}) in the kidney of WT UI (n=8-14), C13 (n=7-17) and WT neoLCMV (n=10-16) mice and also WT UI (n=9-13), WT neoLCMV (n=15-22), TLR2$^{-/-}$ UI (n=8-12) and TLR2$^{-/-}$ neoLCMV (n=15-16) mice at 16–18-week p.i by flow cytometry. Samples were pre gated on CD45^{+} LD^{-}. (D) IF staining of liver tissues with DAPI, MPO and citH3 for NETosis. Pictures captured with Leica SP8. WT UI (n=3), C13 (n=5) and WT neoLCMV (n=3) mice at 16–18-week p.i (E) IF staining of liver tissues with DAPI, MPO and citH3 for NETosis. Pictures captured with Leica SP8. WT neoLCMV (n=5) and neoLCMV TLR2$^{-/-}$ (n=5) mice at 16–18-week p.i. (F) Detection of neutrophils in the liver of WT neoLCMV (n=8) and TLR2$^{-/-}$ neoLCMV (n=11) mice at 16–18-week p.i by flow cytometry. (G) IF staining of liver tissues with DAPI, MPO and citH3 for NETosis. Pictures captured with Leica SP8. WT neoLCMV (n=6), neoLCMV TLR4$^{-/-}$ (n=5) and neoLCMV TLR9$^{-/-}$ (n=5) mice at 16–18-week p.i. Statistics were assessed by unpaired *t*-test (two groups) or one-way ANOVA with ordinary multiple comparisons test (three and more groups), ns not significant, *p<0.05, **p<0.01, ***p<0.001, ****p<0.001.

All together, these findings suggest that, TLR2 signaling mediates NETosis and this cell death type occurs in the liver but not in the kidney during neoLCMV infection.

3.7 Loss of TLR2 lead decreased antibody production in spleen

It is known that infection leads to the activation of immune system. This sensing is mediated by TLRs activates downstream pathways and results in the elimination of pathogens and infected cells (Takeuchi and Akira, 2010). To understand more the role of TLR2 signaling in disease development in more detail, we aimed to investigate immune cells in different organs of neoLCMV TLR2$^{-/-}$ mice. As we observed that TLR2 signaling in neutrophils leads to NETosis, we first assessed neutrophil numbers in kidney, spleen and liver of WT neoLCMV and TLR2$^{-/-}$ neoLCMV mice. However, we could not observe any significant differences between the two mouse groups (Fig 10 A) suggesting that the affect that we observed in TLR2$^{-/-}$ mice was not due to the differences in neutrophil numbers.

We then looked at B cell subsets in the spleen of these mice by flow cytometry, since they are known as antibody producers. Plasma cells were defined by $CD19^{+}CD138^{+}CD38^{low}CD98^{+}$ expression and memory B cells are characterized by $CD19^{+}CD138^{-}CD38^{+/-}IgM^{-}$ expression. Although we did not observe significant difference in total B cell numbers (Fig 10 B) and also memory B cell numbers (Fig 10 C), we could observe significantly less plasma cells that are known to produce antibodies, in the spleen of $TLR2^{-/-}$ neoLCMV mice both in cell counts and frequency (Fig 10 D). These PCs produced IgA and IgG antibodies (Fig 10 E). In line with this finding, we also observed significantly less antigen specific B cell such as anti-DNA and anti-nucleosome IgG in spleen and BM of $TLR2^{-/-}$ mice (Fig 10 F).

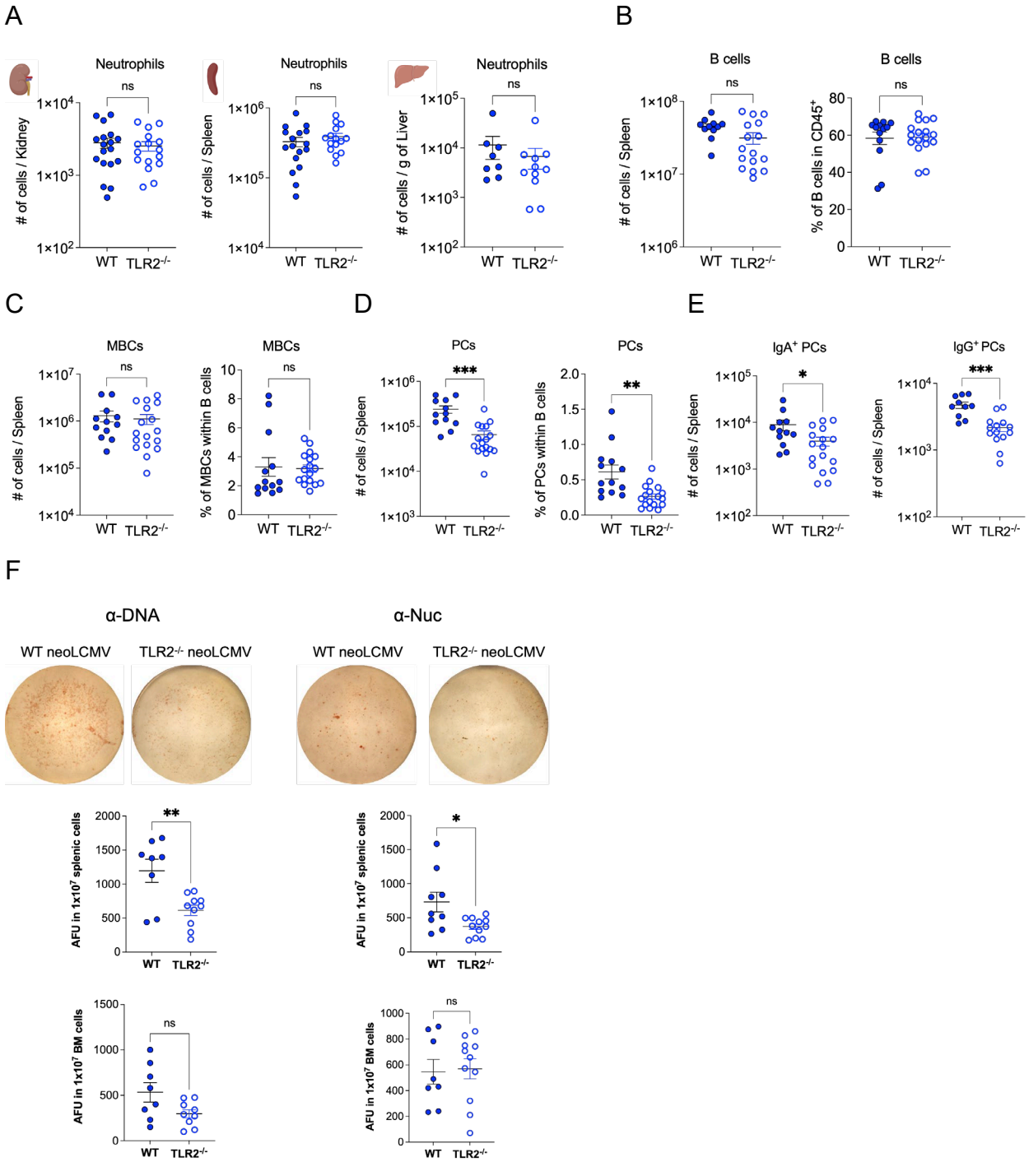
A
Neutrophils
# of cells / Kidney
# of cells / Spleen
# of cells / g of Liver
ns
WT
TLR2-/-
B
B cells
# of cells / Spleen
% of B cells in CD45+
C
MBCs
# of cells / Spleen
% of MBCs within B cells
D
PCs
# of cells / Spleen
% of PCs within B cells
E
IgA+ PCs
IgG+ PCs
F
α-DNA
α-Nuc
WT neoLCMV
TLR2-/- neoLCMV
AFU in 1x10^7 splenic cells
AFU in 1x10^7 BM cells

Fig 10: Decreased autoantibody production in absence of TLR2 during chronic neoLCMV infection.

(A) Surface staining of neutrophils ($CD11b^+Ly6G^+$) in kidney WT neoLCMV (n=11) and neoLCMV $TLR2^{-/-}$ (n=17), spleen WT neoLCMV (n=19) and neoLCMV $TLR2^{-/-}$ (n=14) and liver of WT neoLCMV (n=8) and neoLCMV $TLR2^{-/-}$ (n=11) mice at 16–18-week p.i by flow cytometry. (B) Surface staining of B cells ($CD19^+$ $B220^+$) in spleen WT neoLCMV (n=11) and neoLCMV $TLR2^{-/-}$ (n=16) mice at 16–18-week p.i by flow cytometry. (C) Surface staining of MBCs ($CD19^+B220^+IgM^-CD38^+CD138^-CD95^-IgD^-$), in the spleen of WT neoLCMV (n=13) and neoLCMV $TLR2^{-/-}$ (n=17) mice at 16–18-week p.i by flow cytometry. (D) Staining of PCs ($CD19^+B220^+CD38^{low}CD138^+CD98^+$) in spleen of WT neoLCMV (n=12) and neoLCMV $TLR2^{-/-}$ (n=17) mice at 16–18-week p.i by flow cytometry. (E) Staining of antigen specific PCs ($CD19^+B220^+CD138^+CD98^+IgG^+$ or IgA^+) in spleen of WT neoLCMV (n=10-12) and neoLCMV $TLR2^{-/-}$ (n=14-17) mice at 16–18-week p.i by flow cytometry. (F) IgG producing spots against DNA or nucleosome measured by ELISPOT assay from spleen and BM of WT neoLCMV (n=8-10) and neoLCMV $TLR2^{-/-}$ (n=9-11) mice at 16–18-week p.i. All cell populations pre gated on LD-CD45+. Cell counts per organ and frequency of B cells within $CD45^+$ cells calculated. Statistics were assessed by unpaired *t*-test (two groups) or one-way ANOVA with ordinary multiple comparisons test (three and more groups), ns not significant, *p<0.05, **p<0.01, ***p<0.001, ****p<0.001.

3.8 TLR2 signaling involved in Th2 response during neoLCMV infection

TLR2 signaling induces the production of different types of proinflammatory cytokines, primarily involved in Th1 immune responses but also Th2 responses (Schaub et al., 2007; Takeuchi and Akira, 2010). IL-12 triggers the differentiation of Th1 cells that are primarily responsible for cell mediated immunity, while IL-6 can be produced by macrophages, DCs or monocytes and is able to polarize naïve $CD4^+$ T cells to effector Th2 cells which are producing IL-4 and responsible for humoral immunity, supporting the activation of immunoglobulin secreting cells in different types of autoimmune diseases such as RA or SLE (Cutolo et al., 1998). As HIV patients but also in our neoLCMV model display chronic viral infection together with bacterial translocation, it is expected to see different types of immune responses involved in disease development but also clearance of bacteria and virus. We therefore looked both Th1 and Th2 response in neoLCMV $TLR2^{-/-}$ mice and we found no significant changes in IFNγ expression in different organs (Fig 11 A). But we observed significantly less $Ly6C^{low}$ monocytes but not $Ly6C^{hi}$ monocytes in the spleen of $TLR2^{-/-}$ mice (Fig 11 B) together with decreased IL-6 and IL-4 expression (Fig 11 C) which

shows their involvement in the host defense because it is known that Ly6C^{hi} monocytes exhibited activated inflammatory lysosome activation whereas Ly6C^{low} monocytes presented features of lymphocyte immunity pathways. These findings shows the ability of Ly6C^{low} monocytes to adapt to lymphocyte subsets lead them to involve in various changes of cytokines such as IL6, attributed to increased T/B cell activation, host defense or anti-inflammatory response (Yang et al., 2021). We then looked at Treg and Tfh numbers in the spleen of WT neoLCMV and TLR2$^{-/-}$ neoLCMV mice and we did not observe any significant difference (Fig 11 D).

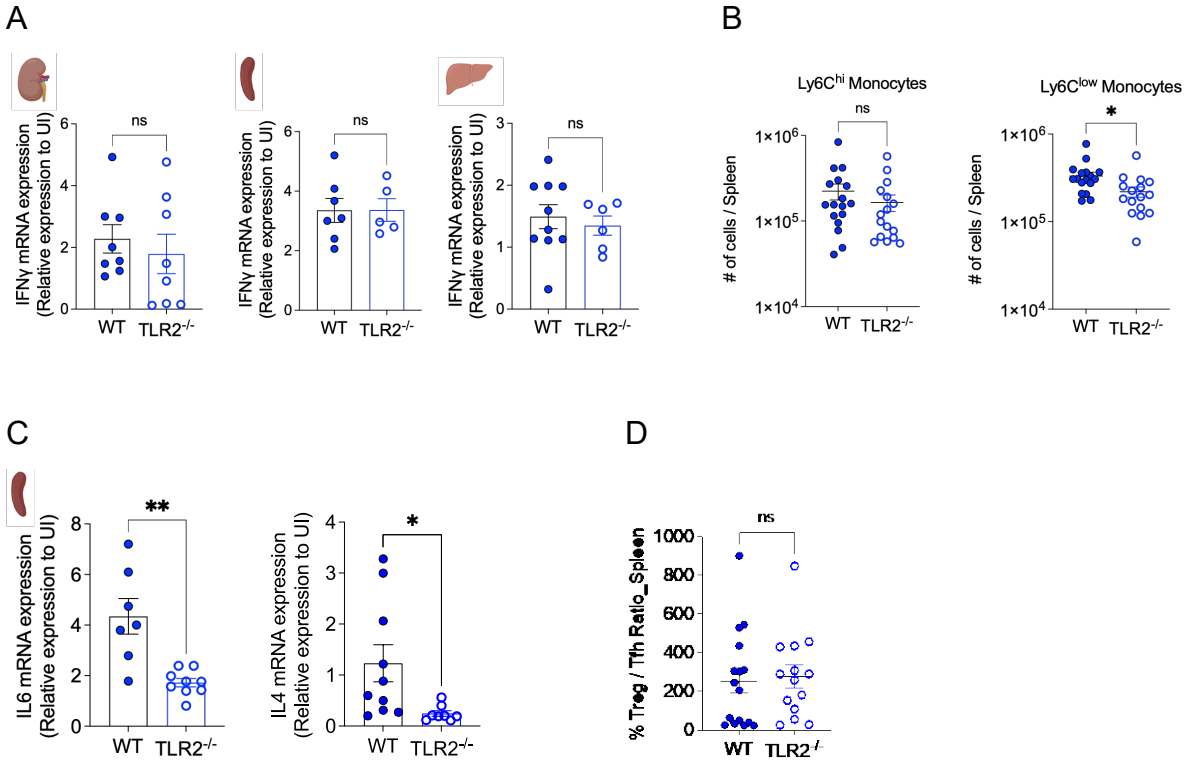

Fig 11: Involvement of TLR2 in Th2 response during neoLCMV infection.

(A) mRNA expression of IFNγ measured by QPCR from kidney, spleen and liver of WT neoLCMV (n=7-10) and neoLCMV TLR2$^{-/-}$ (n=5-8) mice at 16–18-week p.i. (B) Surface staining of Ly6C^{hi} and Ly6C^{low} Monoyctes (CD11b^{+}, Ly6C$^{hi\ or\ low}$) in spleen of WT neoLCMV (n=17) and neoLCMV TLR2$^{-/-}$ (n=16-17) mice at 16–18-week p.i by flow cytometry. (C) mRNA expression of IL-6 and IL-4 measured by QPCR from spleen of WT neoLCMV (n=7-10) and neoLCMV TLR2$^{-/-}$ (n=8-9) mice at 16–18-week p.i. (D) Surface staining of Tregs (CD4^{+} CD25^{+} Foxp3^{+}) and Tfh (CD4^{+} PD1^{+} Bcl6^{+} CXCR5^{+}) in spleen of WT neoLCMV (n=16) and neoLCMV TLR2$^{-/-}$ (n=14) mice at 16–18-week p.i by flow cytometry. Statistics were assessed by unpaired *t*-test (two groups) or one-way ANOVA with ordinary multiple comparisons test (three and more groups), ns not significant, *p<0.05, **p<0.01, ***p<0.001, ****p<0.001.

3.9 Chronic neoLCMV infection leads recruitment of neutrophils via Cxcl2 in liver and NETosis lead the recruitment of B cells to the infection area via Cxcl10

It is known that, infection can drive tissue resident B cells to migrate to the infection zone and differentiate into PC to boost antibody secretion at infected sites in lung (MacLean et al., 2022). Chemokines like Cxcl9 and Cxcl10 are known to recruit B cells to infected regions and increase local antibody levels (MacLean et al., 2022) whereas, chemokines like Cxcl1 and Cxcl2 known to recruit neutrophils to inflammatory sites (Herrero-Cervera et al., 2022). Since we observed increased antigen availability via NETosis in the liver, we therefore determined PC numbers and chemokine levels in liver. Total B cell numbers were not altered (Fig 12 A) but significantly less memory B cells (MBCs) (Fig 12 B) and PCs (Fig 12 C) were observed in TLR2$^{-/-}$ neoLCMV mice compared to WT neoLCMV mice. IgA and IgG antigen-specific B cells did not show significant differences between TLR2$^{-/-}$ neoLCMV mice and WT neoLCMV mice although there was a slight trend towards increase in TLR2$^{-/-}$ neoLCMV mice (Fig 12 D). Decreased levels of Cxcl2 but not Cxcl1 (Fig 12 E) together with decreased Cxcl10 (Fig 12 F) showed that TLR2 signaling might play a role in the recruitment of neutrophils and B cells to the inflammatory site.

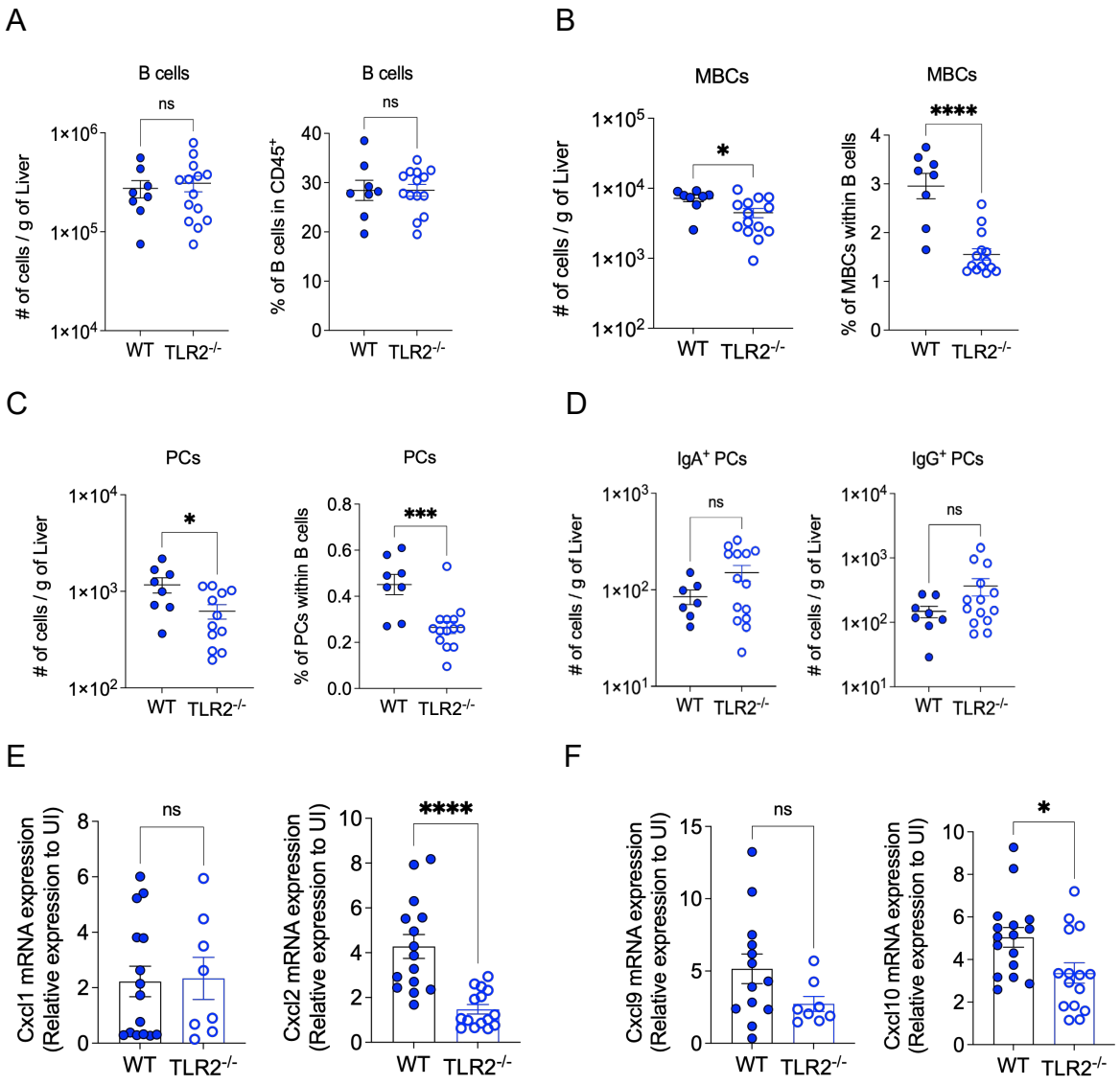

Fig 12: Recruitment of neutrophils via CXCL2 and B cells via CXCL10 during chronic neoLCMV infection.
(A) Surface staining of B cells ($CD19^+$ $B220^+$) in liver of WT neoLCMV (n=8) and neoLCMV $TLR2^{-/-}$ (n=14) mice at 16–18-week p.i by flow cytometry. (B) Surface staining of MBCs ($CD19^+B220^+IgM^-CD38^+CD138^-CD95^-IgD^-$) in liver of WT neoLCMV (n=8) and neoLCMV $TLR2^{-/-}$ (n=14) mice at 16–18-week p.i by flow cytometry. (C) Surface staining of PCs ($CD19^+B220^+CD38^{low}CD138^+CD98^+$) in liver of WT neoLCMV (n=8) and neoLCMV $TLR2^{-/-}$ (n=12-15) mice at 16–18-week p.i by flow cytometry. (D) Surface staining of antigen specific PCs ($CD19^+B220^+CD138^+CD98^+IgG^+$ or IgA^+) in liver of WT neoLCMV (n=7-8) and neoLCMV $TLR2^{-/-}$ (n=14) mice at 16–18-week p.i by flow cytometry. (E) mRNA expression of Cxcl1, Cxcl2 and (F) Cxcl9 and Cxcl10 measured by QPCR from liver of WT neoLCMV (n=12-16) and neoLCMV $TLR2^{-/-}$ (n=8-15) mice at 16–18-week p.i. Statistics were assessed by unpaired *t*-test (two groups) or one-way ANOVA with ordinary multiple comparisons test (three and more groups), ns not significant, *p<0.05, **p<0.01, ***p<0.001, ****p<0.001.

In summary, we found that Cxcl2 abundance might recruits neutrophils to infection site. Although we do not know exactly which cell type is producing Cxcl2, KC and hepatic macrophages known to produce Cxcl2 which needs to be further proved by another experiment. These neutrophils presumably undergo NETosis via TLR2 signaling in the liver. Increased antigen availability via NETosis might lead to recruitment of B cells to the NETosis area via Cxcl10 gradients. Furthermore, decreased Ly6C^{low} monocytes in the spleen together with decreased IL-6 production showed a role of Th2 response in the development of GN in the neoLCMV model.

4. Discussion

In the last century, HIV infection has become a manageable chronic disorder with cART, rather than an acute condition that can rapidly progress towards death or AIDS. Although these patients are treated with cART, 10 to 15 % of infected individuals still experience diverse form of renal diseases. These diseases can be directly associated with the virus which was first reported in 1984, or with some medications that are used to treat HIV infection such as tenofovir and atazanavir, that can also induce nephrotoxicity (Nobakht et al., 2016). One of the first idea in those years was that perhaps the medications caused the kidney damage but not the virus itself. But several studies showed that, HIV-infected subjects that are not undergoing cART had HIVAN. For instance, a study conducted in Nigeria showed that, 40 % of HIV-infected subject without cART, had proteinuria or reduction in creatinine clearance (Emem et al., 2007). Or, another study in South Africa showed that, in 83.3 % of patients with kidney disease who had not been treated with cART showed HIVAN (Han et al., 2006). All together these findings highlight the direct association of the virus and kidney diseases. With the help of Vivette D D'Agati from the Columbia University, Department of Pathology and Cell Biology, New York, we were able to detect increased immunoglobulin deposits in the kidney of five patient case from US. This showed that, distinct cohort of HIV infected individuals shows "lupus-like" glomerulonephritis as it is known type of HIVAN.

In fact, the renal biopsies are important to distinguish kidney diseases in HIV patients. Previous studies have described high prevalences of autoantibodies in HIV patients that contributes to the development of kidney diseases (Baranova et al., 2020; Lackner et al., 2010; Wang et al., 2020). Our human cohort helped us to show the contribution of autoantibodies in development of kidney diseases with increased levels of anti-DNA and anti-nucleosome IgGs in the plasma of HIV patients with kidney diseases group (CKD^+ HIV^+). Increased cfDNA but not the CIC levels in this group compared to healthy donors indicates immune system activation although these patients are all under cART. Elevated levels of IFNAR-stimulated genes (ISGs) such as MX1, IFIT1, ISG15, IRF3 and IRF7 as well as a slight increase in pro-inflammatory cytokines also indicates ongoing autoimmune reactions in HIV-infected individuals. Collectively, these data strongly implicate chronic

activation of innate immunity contributes to the disease development in HIV-infected adults. Altogether, the link between HIV infection, inflammation and glomerular disorders have been investigated in last two decades, the lack of appropriate animal models of HIV infection has hindered more sophisticated studies on HIVAN or HIVICD (Nobakht et al., 2016).

Early studies have reported the development of GN later in life in outbred Swiss mice chronically infected with the RNA virus lymphocytic choriomeningitis virus (LCMV). IC-GN development in these mice was attributable to circulating immune complexes (deposition in glomerular capillary walls) (Oldstone and Dixon, 1970)5/22/2024 1:09:00 PM and correlated with the levels of type I IFN (IFN-I) and circulating IC in the serum (Woodrow et al., 1982). Later studies tried to model IC-GN in HIV- and HCV-infected humans by using neonatal intracerebral LCMV infection in mouse strains from other backgrounds for which genetically modified mice and reagents are available such as C57BL/6, Balb/C and SER/J mice. However, these mice exhibited only low levels of circulating IC and did not show kidney disorders (Tishon et al., 1991). Another well-characterized model of chronic viral infection utilizes the clone 13 LCMV (C13-LCMV) in adult mice. Despite the existence of high levels of anti-virus IC, adult mice infected with C13-LCMV lack autoantibody formation and neither elicit a TNF signature nor develops GN.

In this thesis, we have adopted a murine model of chronic WE-LCMV infection (neoLCMV) in which we infected C57BL/6 mice with $2x10^6$ PFU subcutaneously between 18-24 hours after birth (Nobakht et al., 2016). The neoLCMV model mirrors most aspects of HIV and HCV infections in human like viral persistence, chronic IFN-I and TNF-α signatures, prevalence of immune complexes and autoantibodies and development of renal disorders. Despite the fact that, our neoLCMV model cannot mimic exactly a like HIV infection due to the difference between human and mouse, it represents a useful tool to understand the underlying molecular mechanisms during chronic viral infection. In this thesis, kidney histology of neoLCMV infected mice showed increased immunoglobulins IgG, IgA and IgM together with C3c deposits accompanied with increased Ki67-positive cells in the glomerular tuft and increased immune cell infiltration identified by CD45 staining. This shows that, LCMV infection leads to immune cell activation in kidney. The entry of HIV

into kidney cells through nonconventional receptors like, C-type lectins, macrophages mannose receptor (MMR) or dendritic cell-specific ICAM-3-grabbing nonintegrin (DCSIGN) is potential to serve as a reservoir that is an interesting topic (Mikulak and Singhal, 2010). While much is known about HIV infection and HIV-associated diseases, the mechanism by which HIV enters kidney cells is an ongoing area of research.

Increased anti-DNA and anti-nucleosome antibody levels together with higher cfDNA in the plasma of neoLCMV mice manifested an autoimmune feature of these mice that might lead to autoimmunity. These increased autoantibodies might also contribute to the immune complex formation. Although, circulating immune complex (CIC) levels did not show a significant difference between C13 and neoLCMV infection, the levels were higher compared to UI and it might contribute to the disease development. In line with the observed autoimmunity phenotype, neoLCMV mice showed increased levels of IFNAR-stimulated genes (ISGs) in spleen, kidney and liver and elevated levels of proinflammatory cytokines in the circulation. Taken together this demonstrates that, the neoLCMV-infected mice but not the C13-infected mice are a suitable model to study the mechanisms of HIV infection in mice. It also shows that, the disease is mainly driven by autoantibodies rather than immune complexes which is in line with autoimmune phenotype called “lupus like” mesangioproliferative glomerulonephritis consistent with “HIV-like” GN.

HIV is known to target $CD4^+$ T cells and the virus rapidly spreads throughout the gut-associated lymphoid tissue (GALT), leading directly to the loss of $CD4^+$ T cells and indirectly to epithelial injury (Vujkovic-Cvijin and Somsouk, 2019). Increased intestinal permeability leads to a leakage of microbial products first from gut to the liver and eventually to the blood stream. Elevated levels of LPS and LBP in the plasma of HIV patients showed that, these patients still suffer from leaky gut and cART is not able to restore full health. Detection of LBP, FABP2 and Claudin 2 in the plasma of neoLCMV mice proves bacterial translocation in our model and therefore our mouse model can be used for deeper analysis of the leaky gut syndrome in human HIV infection. To see the direct effect of microbiota in this mouse model, antibiotic treatment could be introduced as a future approach. Disruption of the gut microbiota might lead to the enrichment of bacterial species that have the ability to catabolize tryptophan through the kynurenine

pathway. This metabolic pathway can contribute to the loss of Th17 cells that can have an impact on immune responses (Vujkovic-Cvijin and Somsouk, 2019). The microbial products resulting from this disruption can reach the liver and they contribute to liver dysfunction, including clearance of various microbial products. These cumulative effects of liver dysfunction and presence of these microbial products can over time contribute to the development of end-organ disease like liver fibrosis (Duarte et al., 2023).

Since cART cannot restore the healthy microbiome, there are other therapies to improve the gut microbiome of HIV-infected people. For instance, vitamin C supplementation has been previously suggested to have a protective effect in HIV patients or fecal microbiota transplantation (FMT) that has also affect to increases alpha diversity in these infected individuals (Dubourg et al., 2016; Serrano-Villar et al., 2021). Other studies indicated that plant-based diets and dietary modifications may not effectively improve dysbiosis in these patients. Probiotics are suggested as a more promising dietary adjustment. While the data on effectiveness of probiotics in the context of HIV remains controversial (Duarte et al., 2023), they are believed to have a role in decreasing the levels of LBP and IL-6 levels and increasing Th17 cell numbers. The increase in Th17 cells is thought to improve the integrity of the gut epithelial barrier (Kuller et al., 2008).

Given that HIV is a viral infection that can trigger the immune system, these patients show distinct immunodeficiency, dysregulation of immunoglobulin responses and T-cell function. This viral infection activates the innate and adaptive immune system via TLRs or DNA sensors. Since, HIV patients but also neoLCMV mouse model showed increased cfDNA in their plasma, we analysed single KO mice of cGAS and STING upon neoLCMV infection to understand the role of DNA sensors. Kidney histology and serological analysis of $cGAS^{-/-}$ and $STING^{-/-}$ neoLCMV mice showed no protection from GN development. Although $cGAS^{-/-}$ mice had slightly less autoantibodies and ureacreatinine levels, the cGAS/STING pathway might not play a major role in the disease development. But, in response to binding to dsDNA, cGAS produces a dinucleotide product, cGAMP. This binding shows that the response to HIV infection is suppressed when cells are treated with a reverse transcriptase inhibitor. When they are treated with inhibitors of later stage HIV-1 enzymatic activities, infection is not suppressed, which indicates that DNA products

of HIV-1 reverse transcriptase serve as PAMPs for cGAS binding and activity (Altfeld and Gale Jr, 2015). However, the specific HIV-1 DNA ligands of cGAS are not yet defined.

Not only bacterial or host DNA are elevated in HIV patients and neoLCMV mouse model, but also bacterial products released to the circulation as an indicator for a leaky gut. These microbial products can be pathogen-associated molecular patterns (PAMPs) including, lipopolysaccharide (LPS), peptidoglycan, flagellin, and microbial nucleic acids and damage-associated molecular patterns (DAMPs). Furthermore, endogenous molecules released from dying host cells molecules upon cellular stress or tissue damage, such as oxidative stress and heat shock proteins that can be recognized by TLRs. We therefore, aimed to determine the role of a TLRs like TLR2, TLR4 and TLR9 by using single KO mouse models. Surprisingly, only $TLR2^{-/-}$ neoLCMV mice showed a partial protection from GN meaning significantly less IgG and C3c deposits in kidney compared to WT neoLCMV mice. Studies with TLR2-deficient mice showed decreased autoantibody levels and amelioration in different disease development such as glomerulonephritis, diabetes or autoimmune arthritis by using different models like B6-$Fas^{lpr/lpr}$ murine lupus model or pristine-induced lupus model (Marks et al., 2021). In line with these observations, $TLR2^{-/-}$ neoLCMV mice showed better kidney function with decreased albuminuria, proteinuria and ureacreatinine. Considering that, TLR2 and TLR4 are important in the pathogenesis of autoimmune diseases (Liu et al., 2014) which are characterized by the production of autoantibodies. Significantly less autoantibodies like, anti-Nuc IgG, anti-DNA IgG and anti-smRNP IgG in $TLR2^{-/-}$ neoLCMV mice demonstrated the contribution of TLR2 in autoimmunity. cfDNA and CIC levels did not change between WT and $TLR2^{-/-}$ neoLCMV mice. Arguably, this might be explained by the fact that TLR2 may not play a direct role in forming of CIC. However, viral titers that measured in the plasma of both WT and $TLR2^{-/-}$ neoLCMV mice showed similar levels which shows that the effects that were observed upon the deletion of TLR2 was not because of a difference in the clearance of virus.

Seeing that TLR2 is playing a role in disease development, we also aimed to check which ligand is triggered the downstream pathway. Although further experiments need to be conducted, we observed no differences in serum amyloid A (SAA) levels, which is another endogenous ligand of TLR2, of WT and $TLR2^{-/-}$ neoLCMV mice (data not shown).

Indicating, other ligands like human β-defensin-3, hyaluronan fragments or high mobility group box 1 (HMGB1), need to be considered for activating TLR2.

In HIV infection, the leaky gut is the main source of antigen and these microbes are likely playing a substantial role in contributing to HIV pathogenesis. In addition to that, other processes like apoptosis, necrosis or NETosis can also play an important role as an antigen provider in different autoimmune diseases like SLE or IBD or infections (Celec et al., 2018). NETosis is a cell death type that mainly occurs in activated neutrophils. Upon activation they release NETs characterized by net-like complexes composed of cell-free DNA, histones and neutrophil granule proteins. Knowing that HIV patients but also the neoLCMV mouse model showed increased levels of cfDNA in plasma, we then hypothesized that increased cell free DNA that is detected with PicoGreen assay, can be related to or released during NETosis (Yan et al., 2020). Indeed, spontaneous NETosis assays in human showed that, neutrophils from the HIV^{+} CKD^{+} group are more prone to undergo NETosis than neutrophils derived from other two groups. These data were then confirmed with mouse neutrophils in compared to WT and $TLR2^{-/-}$ neoLCMV. Collectively, NETosis is playing an antigen-providing role in HIV and neoLCMV infection and in mouse NETosis is regulated by TLR2 signaling.

To understand the specific role of TLR2 in providing antigen for the disease development, we aimed to perform adaptive transfer experiments. Previous experiment showed the role of TLR2 in neutrophils that lead NETosis. We therefore, isolated neutrophils from CD45.1 mice transferred into CD45.2 $TLR2^{-/-}$ neoLCMV mice and waited until week 16 to 18 to have full development of GN. However, technical complications of this setup did not allow us to conclude any information (data not shown). Since the experimental set up is too long, the cells that are transferred did not survived until the experiment day given the fact that neutrophils have really short life time. As an alternative way, we aimed to used TLR2 blocking antibodies, but in the long term, this mouse might also develop autoantibodies against the blocking antibodies which might worsen the disease. Also, the lack TLR2 flox mice in the time of the project did not allow us to perform in vivo experiments. Future research needed to investigate the role of TLR2 in specific cell manner by using flox-cre system like, TLR2fl x Mrp8.cre which can specifically delete the TLR2 on neutrophils.

Furthermore, we aimed to investigate the localization of NETosis during GN. The first hypothesis was that NETosis occurs in kidneys since GN is a kidney-related disease. MPO and citH3 staining in the kidney of WT neoLCMV mice showed that, NETosis might not occur in the kidney. But still, increased levels of MPO in the tubular epithelium and also weak signals in the bowmans capsule in projection to the glomerular tuft might originate from monocytes as monocytes are significantly increased in kidney. But presence of MPO alone is not sufficient to determine NETosis. NETs are a complex form of proteins that include histones or NE. We therefore hypothesize that NETosis might occur in the liver as bacterial translocation occurs from gut to the liver. Indeed, IF staining of NETs in the liver of neoLCMV mice revealed increased MPO and citH3 colocalization, which is indicative of NETosis, compared to C13-infected or the UI group. The same results were also observed for the liver of TLR2$^{-/-}$ neoLCMV indicating that, NETosis occurs in the liver via TLR2 signaling. To elucidate the effect of less cell count of neutrophils in liver we performed flow cytometric analysis and indeed, neutrophil numbers were similar between WT neoLCMV and TLR2$^{-/-}$ neoLCMV mice. This demonstrates, that decreased NETosis in TLR2$^{-/-}$ neoLCMV mice was not due to the reduced neutrophil numbers. Moreover, we confirmed with the IF staining of NETs in the liver of other TLR KO models like TLR4 or TLR9, that this cell death type was specific only for TLR2. But TLR2-dependent neutrophil activation is not unique for LCMV or HIV infection. There are other infections that involve the contribution of TLR2 in neutrophils such as airway prevotella infection (Horn et al., 2022), in bacterial sepsis (Roger and Calandra, 2009) or in *Candida albicans* infection (Tessarolli et al., 2010).

TLR2 is a key receptor in the immune system that is recognizes microbial pathogens, protects from pathogens and is implicated in innate and adaptive immune system to produce specific responses via B cells. The total splenic B cell numbers did not differ between WT and TLR2$^{-/-}$ neoLCMV mice but PCs and antigen-specific PCs IgG and IgA were significantly decreased in the absence of TLR2. Thus, the lack of TLR2 did not affect the total B cell numbers but affects antigen specific PCs. In line with this, ELISPOT assays revealed that TLR2$^{-/-}$ neoLCMV mice displayed decreased anti-nuc IgG and anti-DNA IgG in spleen and BM. Although BM PCs did not show significancy, there is a trend towards

decreased PCs in TLR2$^{-/-}$ neoLCMV mice. Indicates the role of TLR2 in BM PCs, which is known to be a niche for long lived PCs.

It is known that TLR2 signaling is an adaptable receptor that can affect both Th1 and Th2 responses via different types of proinflammatory cytokines. These cytokines have various functions in the immune system like, i.e., to protect the host from infections and defending it against a wide range of pathogens (Oliveira-Nascimento et al., 2012). While IL-12 triggers the differentiation of Th1 cells, IL-4 and IL-6 can be produced by macrophages, DCs or monocytes, is able to polarize naïve CD4^{+} T cells to effector Th2 cells and under some conditions also to Th17 cells that are responsible for humoral immunity, contributing to the production of antibody-producing B cells (Cutolo et al., 1998; Figueiredo and Schumacher, 2016). Also, different patterns of cytokine production affect different types of autoimmune diseases such as RA, which is considered to be Th1-cytokine driven disease, whereas SLE is considered to be Th2 or mixed Th1 and Th2 dependent disease (Lourenço, 2013). Significantly less Ly6C^{low} monocytes but not Ly6C^{hi} monocytes in the spleen of neoLCMV TLR2$^{-/-}$ mice together with decreased IL-6 expression showed the involvement of TLR2 mediated Th2 response in GN. Ly6C^{low} monocytes play a crucial role in various immune responses, including cytokine regulation and host defense and IL-6 is known to influence these factors together with T and B cell activation (Yang et al., 2021). Not only in GN but also in other diseases like RA, HIV or SIV, TLR2 expression on monocytes play a role in diseases pathogenesis. For instance, in patients with RA, TLR2 expression is upregulated on synovial monocytes and these monocytes showed increased sensitivity to TLR2 ligation (Marks et al., 2021). Or elevated levels of activated monocytes have been found both, in untreated and treated HIV patients. This increased monocyte turnover and activation have a direct link to SIV and HIV pathogenesis (Burdo et al., 2011; Deeks et al., 2013). Another study showed that overexpression of TLR2 in monocytes in HIV-infected patients might favour HIV-1 cell entry and induce increased viral replication (Heggelund et al., 2004; Laplana et al., 2020). Collectively, these findings suggest that TLR2 expression on monocytes plays an important role in disease development in different contexts.

Plasma cells are known to play a critical role in the formation of secondary and tertiary lymphoid tissues for short-term and long-term generation of antibody responses. Different B cell types have indeed been the subject of research in the context of autoimmune diseases or in vaccination particularly in cases involving kidney-related issues. In these scenarios, they might be functionally impaired or reduced in number. For instance, long-lived plasma cells are crucial to prolonged protection after vaccination or infection and also secondary infection can force tissue-resident B cells to migrate to the infected areas and differentiate into PC to boost antibody-secretion at infected sites in lung (MacLean et al., 2022; Plotkin, 2010). Regulatory B cells (B_{reg}) have been implicated in different autoimmune diseases such as EAE (Marks et al., 2021; Oleinika et al., 2019). Regarding the important role of B cells contributing to different disease development, we aimed to investigate PC in the liver where they expose to auto-antigen via NETosis. Decreased PCs and MBCs in TLR2$^{-/-}$ neoLCMV mice together with decreased levels of *Cxcl2* and *Cxcl10* showed that, TLR2 signaling plays a role in recruitment of neutrophils and B cells to the inflammatory site. IgA and IgG PCs were not significantly different between WT neoLCMV and TLR2$^{-/-}$ neoLCMV. While our study shows the contribution of liver and spleen PCs to the local antibody production, it implies that there might be an additional protective mechanism involving IgA-producing plasma cells from the intestine migrating to the liver (Moro-Sibilot et al., 2016). This dual strategy could enhance the immune defence and provide another layer of protection.

The findings of my thesis demonstrated the importance of TLR2 in the pathogenesis of GN and its potential contribution to the theopathic approaches. Because TLR2 impacts various cell types, that makes this receptor involve in many different immune responses and contributing to the development of inflammatory conditions. Pharmaceutical inhibitors of TLR2 have been designed, but they did not progress beyond the phase II of development (Anwar et al., 2019; Mistry et al., 2015). The reason for this limitation is that that blocking TLR2 can increase the susceptibility to infection. Furthermore, inhibiting TLR2 can negatively affect TLR2-dependent anti-inflammatory activities in other cell populations, such as regulatory T and B cells. This, in turn, reduces the inflammatory potential of T cells (Lampropoulou et al., 2008). To address these limitations, researchers are advised to focus on targeting specific functional outcomes of TLR2 signaling in both

regulatory and inflammatory populations. This approach will allow more precise and tailored interventions, rather than a broad inhibition of the entire TLR2 pathway (Marks et al., 2021). This information underscores the complexity of modulating TLR2 and the importance of considering its diverse functions in different cell types when developing pharmaceutical inhibitors.

In conclusion, this thesis shows that TLR2 modulates the autoimmune manifestations of GN by participating in pathogenic autoantibody production and tissue injury through NETosis. These findings provide new insights into the mechanisms controlling the interplay between the innate immunity and the adaptative immune system in the context of autoimmune diseases.

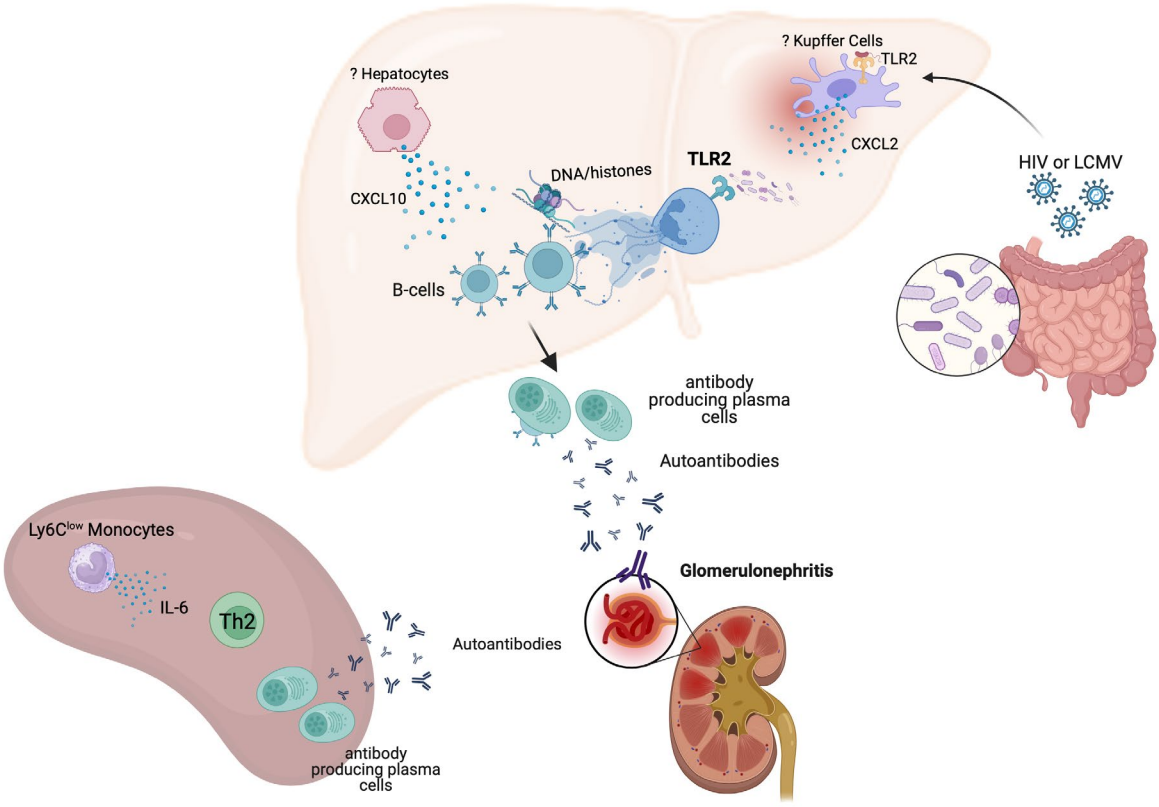

Fig 13: Schematic overview of pathological mechanisms that lead to the generation of autoantibodies and the formation of immune complexes that result in the onset of glomerulonephritis as a consequence of LCMV infection in the mouse as a model for HIV infection in humans (created with BioRender).

5. Abstract

Chronically infected patients with human immune deficiency virus (HIV) are at high risk of developing autoimmune diseases. Despite successful anti-retroviral therapy, autoimmune diseases and renal diseases affect 10–15 % of HIV-infected patients. Due to the lack of appropriate animal models, the pathophysiological mechanisms of HIV-associated glomerulonephritis (GN) remain elusive.

In my thesis, I characterized the murine neoLCMV infection model, which mimics the key hallmarks of HIV infection and allowed me investigating the cellular and molecular mechanisms of HIV-induced GN. Infection of neonatal C57BL/6 mice with the WE-LCMV strain resulted in GN, and reflected most aspects of HIV infection in humans such as, elevated levels of anti-DNA and anti-nucleosome auto-antibodies, cell free circulating DNA and a chronic type I interferons (IFNs) signature. HIV-infected patients suffer from the leaky gut syndrome, which is characterized by the translocation of gut microbiota into the liver, bacterial dissemination and increased inflammation. Clinical investigations in this thesis confirmed elevated levels of leaky gut indicators such as LBP and FABP2, in HIV patients with kidney disease group. These findings were confirmed in the murine neoLCMV infection model. Furthermore, loss of Kupffer cells together with elevated levels of claudin 2 in neoLCMV infected mouse further proved that this mouse model can mimic the leaky gut syndrome found in HIV-infected individuals.

To understand the underlying mechanisms of the leaky gut syndrome, I investigated the role of TLR2 and TLR4, which are known to sense translocated gut microbiota. Loss of TLR2, but not TLR4 resulted in partial protection from GN in neoLCMV-infected mice. TLR2 signaling in neutrophils triggered NETosis which can be the source of self-antigens and might therefore induce autoantibody formation that contributes to LCMV-induced GN. We further provided evidence that neutrophil-recruiting chemokines such as Cxcl2 were produced in a TLR2-dependent manner presumably by macrophages or Kupffer cells in the liver. Cxcl10 expression by hepatocytes, the dominant cell type producing this chemokine, might recruit B cells to the infection site where they encounter NETosis-derived autoantigens, leading to their activation and differentiation to auto-antibody

producing plasma cells. Decreased monocyte counts and IL-6 and IL-4 expression in the spleen further indicated the contribution of a Th2 response in LCMV virus-induced GN via TLR2 signaling.

In summary, I could demonstrate how nuclear autoantigens are released by NETosis in the liver of neoLCMV mice and how autoantibodies are induced that can later form deposits in the kidney and thereby contribute to the disease development as a consequence of LCMV infection. Moreover, TLR2 deficiency in the neoLCMV model ameliorated GN and resulted in decreased auto-antibody production. Hence, these findings revealed the importance of TLR2 in the pathogenesis of GN in murine LCMV infection that serves as a model for human HIV infection and its potential contribution to the therapeutic approaches.

6. List of figures

7. List of tables

8. References

Akira S, Uematsu S, Takeuchi O: Pathogen Recognition and Innate Immunity. Cell 2006; 124: 783–801.

Al-Ayadhi L, Zayed N, Bhat RS, Moubayed NMS, Al-Muammar MN, El-Ansary A: The use of biomarkers associated with leaky gut as a diagnostic tool for early intervention in autism spectrum disorder: a systematic review. Gut Pathog 2021; 13: 54.

Albariño CG, Palacios G, Khristova ML et al.: High Diversity and Ancient Common Ancestry of Lymphocytic Choriomeningitis Virus. Emerg Infect Dis 2010; 16: 1093–1100.
Altfeld M, Gale Jr M: Innate immunity against HIV-1 infection. Nat Immunol 2015; 16: 554–562.

Amoura Z, Piette J-C, Chabre H et al.: Circulating plasma levels of nucleosomes in patients with systemic lupus erythematosus. Correlation with serum antinucleosome antibody titers and absence of clear association with disease activity. Arthritis & Rheumatism 1997; 40: 2217–2225.

Anwar MA, Shah M, Kim J, Choi S: Recent clinical trends in Toll-like receptor targeting therapeutics. Medicinal Research Reviews 2019; 39: 1053–1090.

Armstrong C, Lillie RD: Experimental Lymphocytic Choriomeningitis of Monkeys and Mice Produced by a Virus Encountered in Studies of the 1933 St. Louis Encephalitis Epidemic. Public Health Reports (1896-1970) 1934; 49: 1019.

Azad MB, Konya T, Maughan H et al.: Gut microbiota of healthy Canadian infants: profiles by mode of delivery and infant diet at 4 months. CMAJ 2013; 185: 385–394.

Babu MM, Priya ML, Selvan AT et al.: A Database of Bacterial Lipoproteins (DOLOP) with Functional Assignments to Predicted Lipoproteins. J Bacteriol 2006; 188: 2761–2773.

Baranova SV, Dmitrienok PS, Buneva VN, Nevinsky GA: HIV-Infected Patients: Cross Site-Specific Hydrolysis of H2a and H2b Histones and Myelin Basic Protein with Antibodies against These Three Proteins. Biomolecules 2020; 10: 1501.

Benveniste O, Longuet P, Duval X, Le Moing V, Leport C, Vildé JL: Two Episodes of Acute Renal Failure, Rhabdomyolysis, and Severe Hepatitis in an AIDS Patient Successively Treated with Ritonavir and Indinavir. CLIN INFECT DIS 1999; 28: 1180–1181.

Bonthius DJ: Lymphocytic Choriomeningitis Virus: An Underrecognized Cause of Neurologic Disease in the Fetus, Child, and Adult. Seminars in Pediatric Neurology 2012; 19: 89–95.

Bowie A, O'Neill LAJ: The interleukin-1 receptor/Toll-like receptor superfamily: signal generators for pro-inflammatory interleukins and microbial products. Journal of Leukocyte Biology 2000; 67: 508–514.

Brenchley JM, Price DA, Schacker TW et al.: Microbial translocation is a cause of systemic immune activation in chronic HIV infection. Nat Med 2006; 12: 1365–1371.

Brooks WH: Viral Impact in Autoimmune Diseases: Expanding the "X Chromosome–Nucleolus Nexus" Hypothesis. Front Immunol 2017; 8: 1657.

Burdo TH, Lentz MR, Autissier P et al.: Soluble CD163 Made by Monocyte/Macrophages Is a Novel Marker of HIV Activity in Early and Chronic Infection Prior to and After Anti-retroviral Therapy. The Journal of Infectious Diseases 2011; 204: 154–163.

Cai X, Chiu Y-H, Chen ZJ: The cGAS-cGAMP-STING Pathway of Cytosolic DNA Sensing and Signaling. Molecular Cell 2014; 54: 289–296.

Carty M, Guy C, Bowie AG: Detection of Viral Infections by Innate Immunity. Biochemical Pharmacology 2021; 183: 114316.

Caza T, Oaks Z, Perl A: Interplay of Infections, Autoimmunity, and Immunosuppression in Systemic Lupus Erythematosus. International Reviews of Immunology 2014; 33: 330–363.

Celec P, Vlková B, Lauková L, Bábíčková J, Boor P: Cell-free DNA: the role in pathophysiology and as a biomarker in kidney diseases. Expert Rev Mol Med 2018; 20: e1.

Christabel Celia Kho CCK: “The role of NETosis in the pathogenesis of chronic kidney disease in HIV patients”, Master Thesis. University of Bonn, 2019.

Chun T-W, Stuyver L, Mizell SB et al.: Presence of an inducible HIV-1 latent reservoir during highly active antiretroviral therapy. Proc Natl Acad Sci USA 1997; 94: 13193–13197.

Cohen J: Back-to-Basics Push as HIV Prevention Struggles. Science 2008; 319: 888–888.

Cutolo M, Sulli A, Villaggio B, Seriolo B, Accardo S: Relations between steroid hormones and cytokines in rheumatoid arthritis and systemic lupus erythematosus. Annals of the Rheumatic Diseases 1998; 57: 573–577.

Deeks SG, Tracy R, Douek DC: Systemic Effects of Inflammation on Health during Chronic HIV Infection. Immunity 2013; 39: 633–645.

Delaloy C, Schuh W, Jäck H, Bonaud A, Espéli M: Single-cell resolution of plasma cell fate programming in health and disease. Eur J Immunol 2022; 52: 10–23.

Devarapu SK, Anders H-J: Toll-like receptors in lupus nephritis. J Biomed Sci 2018; 25: 35.

DiGiulio DB, Romero R, Amogan HP et al.: Microbial Prevalence, Diversity and Abundance in Amniotic Fluid During Preterm Labor: A Molecular and Culture-Based Investigation. PLoS ONE 2008; 3: e3056.

Duarte MJ, Tien PC, Somsouk M, Price JC: The human microbiome and gut–liver axis in people living with HIV. Curr HIV/AIDS Rep 2023; 20: 170–180.

Dubourg G, Lagier J-C, Hüe S et al.: Gut microbiota associated with HIV infection is significantly enriched in bacteria tolerant to oxygen. BMJ Open Gastroenterol 2016; 3: e000080.

Emem CP, Arogundade F, Sanusi A, Adelusola K, Wokoma F, Akinsola A: Renal disease in HIV-seropositive patients in Nigeria: an assessment of prevalence, clinical features and risk factors. Nephrology Dialysis Transplantation 2007; 23: 741–746.

Farhat K, Riekenberg S, Heine H et al.: Heterodimerization of TLR2 with TLR1 or TLR6 expands the ligand spectrum but does not lead to differential signaling. Journal of Leukocyte Biology 2008; 83: 692–701.

Fernando SK, Finkelstein FO, Moore BA, Weissman S: Prevalence of Chronic Kidney Disease in an Urban HIV Infected Population. The American Journal of the Medical Sciences 2008; 335: 89–94.

Figueiredo AS, Schumacher A: The T helper type 17/regulatory T cell paradigm in pregnancy. Immunology 2016; 148: 13–21.

Foy MC, Estrella MM, Lucas GM et al.: Comparison of Risk Factors and Outcomes in HIV Immune Complex Kidney Disease and HIV-Associated Nephropathy. Clinical Journal of the American Society of Nephrology 2013; 8: 1524–1532.

German Advisory Committee Blood (Arbeitskreis Blut), Subgroup ‘Assessment of Pathogens Transmissible by Blood’: Human Immunodeficiency Virus (HIV). Transfus Med Hemother 2016; 43: 203–222.

Han TM, Naicker S, Ramdial PK, Assounga AG: A cross-sectional study of HIV-seropositive patients with varying degrees of proteinuria in South Africa. Kidney International 2006; 69: 2243–2250.

Heggelund L, Muller F, Lien E et al.: Increased Expression of Toll-Like Receptor 2 on Monocytes in HIV Infection: Possible Roles in Inflammation and Viral Replication. Clinical Infectious Diseases 2004; 39: 264–269.

Herrero-Cervera A, Soehnlein O, Kenne E: Neutrophils in chronic inflammatory diseases. Cell Mol Immunol 2022; 19: 177–191.

Horn KJ, Schopper MA, Drigot ZG, Clark SE: Airway Prevotella promote TLR2-dependent neutrophil activation and rapid clearance of Streptococcus pneumoniae from the lung. Nat Commun 2022; 13: 3321.

Hotchin J: The Contamination of Laboratory Animals with Lymphocytic Choriomeningitis Virus 1971; 64.

Hsu CL, Schnabl B: The gut–liver axis and gut microbiota in health and liver disease. Nat Rev Microbiol 2023; 21: 719–733.

Hussein HM, Rahal EA: The role of viral infections in the development of autoimmune diseases. Critical Reviews in Microbiology 2019; 45: 394–412.

International Agency for Research on Cancer (ed.): Human immunodeficiency viruses and human T-cell lymphotropic viruses: this publication represents the views and expert opinions of an IARC Working Group on the Evaluation of Carcinogenic Risks to Humans, which met in Lyon, 11 - 18 June 1996. Lyon, IARC 1996.

Ishii KJ, Kawagoe T, Koyama S et al.: TANK-binding kinase-1 delineates innate and adaptive immune responses to DNA vaccines. Nature 2008; 451: 725–729.

Jara LJ, Medina G, Saavedra MA: Autoimmune manifestations of infections. Current Opinion in Rheumatology 2018; 30: 373–379.

Joshi MB, Baipadithaya G, Balakrishnan A et al.: Elevated homocysteine levels in type 2 diabetes induce constitutive neutrophil extracellular traps. Sci Rep 2016; 6: 36362.

Kamada N, Núñez G: Role of the Gut Microbiota in the Development and Function of Lymphoid Cells. The Journal of Immunology 2013; 190: 1389–1395.

Kato H, Sato S, Yoneyama M et al.: Cell Type-Specific Involvement of RIG-I in Antiviral Response. Immunity 2005; 23: 19–28.

Kenny EF, Herzig A, Krüger R et al.: Diverse stimuli engage different neutrophil extracellular trap pathways. eLife 2017; 6: e24437.

Khan A, Alsahli M, Rahmani A: Myeloperoxidase as an Active Disease Biomarker: Recent Biochemical and Pathological Perspectives. Medical Sciences 2018; 6: 33.

Kimmel PL, Barisoni L, Kopp JB: Pathogenesis and Treatment of HIV-Associated Renal Diseases: Lessons from Clinical and Animal Studies, Molecular Pathologic Correlations, and Genetic Investigations. Ann Intern Med 2003; 139: 214.

Klopf J, Brostjan C, Eilenberg W, Neumayer C: Neutrophil Extracellular Traps and Their Implications in Cardiovascular and Inflammatory Disease. IJMS 2021; 22: 559.

Konstantinos Symeonidis KS: “Identification of cellular and molecular markers in HIV patients with chronic kidney disease” Master Thesis, 2019. University of Bonn, 2019.

Kuller LH, Tracy R, Belloso W et al.: Inflammatory and Coagulation Biomarkers and Mortality in Patients with HIV Infection. PLoS Med 2008; 5: e203.

Lackner P, Kuenz B, Reindl M et al.: Antibodies to myelin oligodendrocyte glycoprotein in HIV-1 associated neurocognitive disorder: a cross-sectional cohort study. J Neuroinflammation 2010; 7: 79.

Lai J, Wang M, Huang C et al.: Infection with the dengue RNA virus activates TLR9 signaling in human dendritic cells. EMBO Reports 2018; 19: e46182.

Lampropoulou V, Hoehlig K, Roch T et al.: TLR-Activated B Cells Suppress T Cell-Mediated Autoimmunity. The Journal of Immunology 2008; 180: 4763–4773.

Laplana M, Bravo MJ, Fernández-Fuertes M et al.: Toll-Like Receptor 2 Promoter -196 to -174 Deletion Affects CD4 Levels Along Human Immunodeficiency Virus Infection Progression. The Journal of Infectious Diseases 2020; 222: 2007–2011.

Levisetti MG: Autoantibodies and CD4 T cells target a cell retroviral envelope protein in non-obese diabetic mice. International Immunology 2003; 15: 1473–1483.

Liu Y, Yin H, Zhao M, Lu Q: TLR2 and TLR4 in Autoimmune Diseases: a Comprehensive Review. Clinic Rev Allerg Immunol 2014; 47: 136–147.

Lood C, Blanco LP, Purmalek MM et al.: Neutrophil extracellular traps enriched in oxidized mitochondrial DNA are interferogenic and contribute to lupus-like disease. Nat Med 2016; 22: 146–153.

Lourenço EV: Cytokines in Systemic Lupus Erythematosus 2013.

Luecke S, Holleufer A, Christensen MH et al.: cGAS is activated by DNA in a length-dependent manner. EMBO Reports 2017; 18: 1707–1715.

Luettig J, Rosenthal R, Barmeyer C, Schulzke J: Claudin-2 as a mediator of leaky gut barrier during intestinal inflammation. Tissue Barriers 2015; 3: e977176.

Lukashevich IS, Rodas JD, Tikhonov II et al.: LCMV-mediated hepatitis in rhesus macaques: WE but not ARM strain activates hepatocytes and induces liver regeneration. Arch Virol 2004; 149: 2319–2336.

MacLean AJ, Richmond N, Koneva L et al.: Secondary influenza challenge triggers resident memory B cell migration and rapid relocation to boost antibody secretion at infected sites. Immunity 2022; 55: 718-733.e8.

Marks KE, Cho K, Stickling C, Reynolds JM: Toll-like Receptor 2 in Autoimmune Inflammation. Immune Netw 2021; 21: e18.

Márquez M: Gut epithelial barrier dysfunction in human immunodeficiency virus-hepatitis C virus coinfected patients: Influence on innate and acquired immunity. WJG 2016; 22: 1433.

Marshall JS, Warrington R, Watson W, Kim HL: An introduction to immunology and immunopathology. Allergy Asthma Clin Immunol 2018; 14: 49.

McIntyre J: What can we do to reduce mother to child transmission of HIV? BMJ 2002; 324: 218–221.

Mesin L, Ersching J, Victora GD: Germinal Center B Cell Dynamics. Immunity 2016; 45: 471–482.

Meylan F, De Smedt M, Leclercq G et al.: Negative thymocyte selection to HERV-K18 superantigens in humans. Blood 2005; 105: 4377–4382.

Miedema F, Hazenberg MD, Tesselaar K, Van Baarle D, De Boer RJ, Borghans JAM: Immune Activation and Collateral Damage in AIDS Pathogenesis. Front Immunol 2013; 4.

Mikulak J, Singhal PC: HIV-1 and Kidney Cells: Better Understanding of Viral Interaction. Nephron Exp Nephrol 2010; 115: e15–e21.

Mistry P, Laird MHW, Schwarz RS et al.: Inhibition of TLR2 signaling by small molecule inhibitors targeting a pocket within the TLR2 TIR domain. Proc Natl Acad Sci USA 2015; 112: 5455–5460.

Monsalve DM, Pacheco Y, Acosta-Ampudia Y, Rodríguez Y, Ramírez-Santana C, Anaya J-M: Zika virus and autoimmunity. One-step forward. Autoimmunity Reviews 2017; 16: 1237–1245.

Morgan XC, Segata N, Huttenhower C: Biodiversity and functional genomics in the human microbiome. Trends in Genetics 2013; 29: 51–58.

Moro-Sibilot L, Blanc P, Taillardet M et al.: Mouse and Human Liver Contain Immunoglobulin A–Secreting Cells Originating From Peyer's Patches and Directed Against Intestinal Antigens. Gastroenterology 2016; 151: 311–323.

Motwani M, Pesiridis S, Fitzgerald KA: DNA sensing by the cGAS–STING pathway in health and disease. Nat Rev Genet 2019; 20: 657–674.

Nobakht E, Cohen SD, Rosenberg AZ, Kimmel PL: HIV-associated immune complex kidney disease. Nat Rev Nephrol 2016; 12: 291–300.

Oldstone MBA, Dixon FJ: Persistent Lymphocytic Choriomeningitis Viral Infection. The Journal of Immunology 1970; 105: 829–837.

Oleinika K, Mauri C, Salama AD: Effector and regulatory B cells in immune-mediated kidney disease. Nat Rev Nephrol 2019; 15: 11–26.

Oliveira-Nascimento L, Massari P, Wetzler LM: The Role of TLR2 in Infection and Immunity. Front Immun 2012; 3.

Oracki SA, Walker JA, Hibbs ML, Corcoran LM, Tarlinton DM: Plasma cell development and survival. Immunological Reviews 2010; 237: 140–159.

Pacheco Y, Barahona-Correa J, Monsalve DM et al.: Cytokine and autoantibody clusters interaction in systemic lupus erythematosus. J Transl Med 2017; 15: 239.

Papayannopoulos V: Neutrophil extracellular traps in immunity and disease. Nat Rev Immunol 2018; 18: 134–147.

Plotkin SA: Correlates of Protection Induced by Vaccination. Clin Vaccine Immunol 2010; 17: 1055–1065.

Rautava S, Luoto R, Salminen S, Isolauri E: Microbial contact during pregnancy, intestinal colonization and human disease. Nat Rev Gastroenterol Hepatol 2012; 9: 565–576.

Roger T, Calandra T: TLR2-mediated neutrophil depletion exacerbates bacterial sepsis. Proc Natl Acad Sci USA 2009; 106: 6889–6890.

Rojas M, Rodríguez Y, Leon KJ et al.: Cytokines and Inflammatory Mediators in Systemic Lupus Erythematosus. EMJ Rheumatol 2018: 83–92.

Rosenberg AZ, Naicker S, Winkler CA, Kopp JB: HIV-associated nephropathies: epidemiology, pathology, mechanisms and treatment. Nat Rev Nephrol 2015; 11: 150–160.

Rother N, Pieterse E, Lubbers J, Hilbrands L, Van Der Vlag J: Acetylated Histones in Apoptotic Microparticles Drive the Formation of Neutrophil Extracellular Traps in Active Lupus Nephritis. Front Immunol 2017; 8: 1136.

Sanz I, Wei C, Jenks SA et al.: Challenges and Opportunities for Consistent Classification of Human B Cell and Plasma Cell Populations. Front Immunol 2019; 10: 2458.

Sauter D, Unterweger D, Vogl M et al.: Human Tetherin Exerts Strong Selection Pressure on the HIV-1 Group N Vpu Protein. PLoS Pathog 2012; 8: e1003093.

Schaub B, Bellou A, Gibbons FK et al.: TLR2 and TLR4 Stimulation Differentially Induce Cytokine Secretion in Human Neonatal, Adult, and Murine Mononuclear Cells 2007.

Schultheiß C, Steinmann S, Lohse AW, Binder M: B cells in autoimmune hepatitis: bystanders or central players? Semin Immunopathol 2022; 44: 411–427.

Serrano-Villar S, Talavera-Rodríguez A, Gosalbes MJ et al.: Fecal microbiota transplantation in HIV: A pilot placebo-controlled study. Nat Commun 2021; 12: 1139.

Shen S, Shao Y, Li C: Different types of cell death and their shift in shaping disease. Cell Death Discov 2023; 9: 284.

Silvestre-Roig C, Hidalgo A, Soehnlein O: Neutrophil heterogeneity: implications for homeostasis and pathogenesis. Blood 2016; 127: 2173–2181.

Smatti MK, Cyprian FS, Nasrallah GK, Al Thani AA, Almishal RO, Yassine HM: Viruses and Autoimmunity: A Review on the Potential Interaction and Molecular Mechanisms. Viruses 2019; 11: 762.

Smith PM, Howitt MR, Panikov N et al.: The Microbial Metabolites, Short-Chain Fatty Acids, Regulate Colonic T_{reg} Cell Homeostasis. Science 2013; 341: 569–573.

Sutkowski N, Conrad B, Thorley-Lawson DA, Huber BT: Epstein-Barr Virus Transactivates the Human Endogenous Retrovirus HERV-K18 that Encodes a Superantigen. Immunity 2001; 15: 579–589.

Taiwo B, Barcena L, Tressler R: Understanding and Controlling Chronic Immune Activation in the HIV-Infected Patients Suppressed on Combination Antiretroviral Therapy. Curr HIV/AIDS Rep 2013; 10: 21–32.

Takeuchi O, Akira S: Pattern Recognition Receptors and Inflammation. Cell 2010; 140: 805–820.

Tecklenborg J, Clayton D, Siebert S, Coley SM: The role of the immune system in kidney disease. Clinical and Experimental Immunology 2018; 192: 142–150.

Tessarolli V, Gasparoto TH, Lima HR et al.: Absence of TLR2 influences survival of neutrophils after infection with *Candida albicans*. Med Mycol 2010; 48: 129–140.

Tishon A, Salmi A, Ahmed R, Oldstone MBA: Role of Viral Strains and Host Genes in Determining Levels of Immune Complexes in a Model System: Implications for HIV Infection. AIDS Research and Human Retroviruses 1991; 7: 963–969.

Turvey SE, Broide DH: Innate immunity. Journal of Allergy and Clinical Immunology 2010; 125: S24–S32.

Vaure C, Liu Y: A Comparative Review of Toll-Like Receptor 4 Expression and Functionality in Different Animal Species. Front Immunol 2014; 5.

Vega LE, Espinoza LR: HIV infection and its effects on the development of autoimmune disorders. Pharmacological Research 2018; 129: 1–9.

Villanueva-Millán MJ, Pérez-Matute P, Oteo JA: Gut microbiota: a key player in health and disease. A review focused on obesity. J Physiol Biochem 2015; 71: 509–525.

Virgin HW, Wherry EJ, Ahmed R: Redefining Chronic Viral Infection. Cell 2009; 138: 30–50.

Vivier E, Malissen B: Innate and adaptive immunity: specificities and signaling hierarchies revisited. Nat Immunol 2005; 6: 17–21.

Vujkovic-Cvijin I, Somsouk M: HIV and the Gut Microbiota: Composition, Consequences, and Avenues for Amelioration. Curr HIV/AIDS Rep 2019; 16: 204–213.

Wang H, Li T, Chen S, Gu Y, Ye S: Neutrophil Extracellular Trap Mitochondrial DNA and Its Autoantibody in Systemic Lupus Erythematosus and a Proof-of-Concept Trial of Metformin. Arthritis & Rheumatology 2015; 67: 3190–3200.

Wang Wen-jing, Jia X, Cui Z et al.: The prevalence and immunological features of anti-glomerular basement membrane antibody in patients with HIV. BMC Nephrol 2020; 21: 429.

Wang-Johanning F, Radvanyi L, Rycaj K et al.: Human Endogenous Retrovirus K Triggers an Antigen-Specific Immune Response in Breast Cancer Patients. Cancer Research 2008; 68: 5869–5877.

Weiner NJ, Goodman JW, Kimmel PL: The HIV-associated renal diseases: Current insight into pathogenesis and treatment. Kidney International 2003; 63: 1618–1631.

Wong SL, Demers M, Martinod K et al.: Diabetes primes neutrophils to undergo NETosis, which impairs wound healing. Nat Med 2015; 21: 815–819.

Woodrow D, Ronco P, Riviere Y et al.: Severity of glomerulonephritis induced in different strains of suckling mice by infection with lymphocytic choriomeningitis virus: Correlation with amounts of endogenous interferon and circulating immune complexes. J Pathol 1982; 138: 325–336.

Yan G, Elbadawi M, Efferth T: Multiple cell death modalities and their key features (Review). World Acad Sci J 2020. DOI: 10.3892/wasj.2020.40.

Yang P, Liu L, Sun L et al.: Immunological Feature and Transcriptional Signaling of Ly6C Monocyte Subsets From Transcriptome Analysis in Control and Hyperhomocysteinemic Mice. Front Immunol 2021; 12: 632333.

Zandman-Goddard G, Shoenfeld Y: HIV and autoimmunity. Autoimmunity Reviews 2002; 1: 329–337.

Zhou X, Ramachandran S, Mann M, Popkin D: Role of Lymphocytic Choriomeningitis Virus (LCMV) in Understanding Viral Immunology: Past, Present and Future. Viruses 2012; 4: 2650–2669.

Zinkernagel MS, Bolinger B, Krebs P, Onder L, Miller S, Ludewig B: Immunopathological Basis of Lymphocytic Choriomeningitis Virus-Induced Chorioretinitis and Keratitis. J Virol 2009; 83: 159–166.

9. Acknowledgements

I would like to first thank to Prof. Dr. med. Christian Kurts and Prof. Dr. Zeinab Abdullah for giving me the opportunity to do my PhD and their supervision for my practical and written work. This work has been conducted in the laboratories of Prof. Zeinab Abdullah and Christian Kurts, with co-supervision by both.

I would like to also thank to Prof. Dr. Jürgen Ruland, who reviewed my thesis and Prof. Dr. Hiroki Kato for their support as being member of my thesis committee.

Special thanks to Moritz Blankart, the technician who worked with me long days in the lab. With his help my PhD life was much easier. And I cannot thank enough to Celia Kho, PhD student who worked with me day and night regardless of the time. We've been through so many things during our PhD. I was lucky to have her by myside.

I would like to also thank our collaboration partners from different countries. First, many thanks to Patrick Droste from University Clinic of Aachen who helped me with kidney stainings. Second big thanks to Vivette D D'Agati from Columbia University, Department of Pathology and Cell Biology in New York, who helped us with IF staining of HIV patient biopsies. Third, many thanks to Dr. rer. medic. Hella Luksch from TUD Dresden University of Technology, Department of Pediatrics, Faculty of Medicine and University Hospital Carl Gustav Carus who helped us with quantification of ISGs in different tissues of neoLCMV mouse. Fourth, I would like to thank to PD Dr. med. Carolynne Schwarzer-Zander who helped us with the measurement of anti-Nuc and anti-DNA in the plasma of HIV patients.

Thank you to all the members of Institute of Molecular Medicine and Experimental Immunology (IMMEI), who made my daily life in the lab happier.

Most importantly, I want to thank my partner PD Dr. rer. nat. Dr. habil. med. Wolfgang Schuh and my sister Dilruba Ertugrul for supporting me and being there for me all the time when I need them. I could not make it without your support.
Thanks a lot!